UNIVERSITÀ
DI PAVIA

PhD IN BIOMEDICAL SCIENCES

DEPARTMENT OF BRAIN AND BEHAVIORAL SCIENCES

UNIT OF NEUROPHYSIOLOGY

DEVELOPMENT OF A CEREBELLAR MEAN FIELD MODEL:
THE THEORETICAL FRAMEWORK, THE IMPLEMENTATION AND THE FIRST APPLICATION

PhD Tutor: Prof. Egidio D'Angelo

Prof. Claudia Casellato

Prof. Fulvia Palesi

PhD dissertation of
Roberta Maria Lorenzi

a.a. 2022-2023

Preface

Brain modeling is a fast-growing trend in neuroscience and medicine because it leads to much more accurate prediction of brain activity with several applications, such as deepening the knowledge of neuronal networks dynamics and defining *ad-hoc* treatment paving the way for personalized medicine. To implement a digital counterpart of the brain, a so-called *brain digital twin*, the inclusion of constraints from connectivity and functions represents a crucial point. Thus, the development of region-specific models has taken hold and it currently represents a challenge in neuroscience still far to be completed. Furthermore, brain is a multiscale system whose dynamics can be approached from microscale (i.e., neuron activity) to macroscale (i.e., cerebral network activity). In the perspective of building up a *real* brain digital twin, these domains should inform each other, integrating microscale biology grounded features in whole-brain dynamics simulators (bottom-up strategy) and using whole-brain simulated activity to infer underlying neuronal states (top-down strategy).

The present thesis introduces the first biology grounded model of the cerebellum that integrates a strong knowledge of its specific biological and physiological features. Mean field formalism, based on mean field approximation, was chosen to build up a mesoscale model of the cerebellum bridging the gap between micro and macroscale. This thesis aimed to provide a reliable model for a deep insight into cerebellar activity and enough flexible to be easily integrated into already validated whole-brain simulators improving the simulations of experimental large-scale recordings, such as electroencephalography and functional magnetic resonance imaging.

The aim of this **Preface** is to provide a key to drive readers through the many introduced themes, in order to contextualize our mean field model of the cerebellum, which is intended to be part of the new generation region-specific models developed with a bottom-up approach.

Chapter 1 provides an overview of the biology, anatomy, and functions of the cerebellum with a focus on its multi-layer organization addressed from the microscale domain, i.e., the specific neurons type, to the macroscale with the outline of the cerebro-cerebellar loops, also clarifying why an accurate model of the cerebellum must be included into a brain digital twin. The biological background is contextualized in the computational one, introducing modeling strategies from virtual neurons to virtual brains. Furthermore, Chapter 1 includes a mini review of the simulators with their technical specifics and simulation targets to explain how to address practically the multiscale complex issue of the construction of a brain digital twin. Mean field modeling strategy is mentioned as an advantageous approach to link microscale to macroscale, outlining the rationale of the choice of this reliable formalism to develop our multi-layer model of the cerebellum.

This represents the introduction for **Chapter 2** which addresses the complex mean field formalism, providing a description at-a-glance of the physics theory, and of some applications to tackle decision making challenges in very different domain, ranging from economy to analyze the trade markets, to the epidemiology to predict the evolution of the COVID-19 outbreak. Further, the focus is moved on the master equation of mean field approach, as explained in El Boustani and Destexhe, 2009, which provides an effective way to use mean field formalism for neural network simulations. Our work

relied on this formalism and took inspiration from the heuristic approach to the master equation explained by Zerlaut et al., 2016, 2018. The core of this formalism is the semi-analytic approach to compute a transfer function, which is a mathematical construct taking as input the presynaptic activity and providing in output the postsynaptic activity. This semi-analytic approach presents high complexity and cannot be analytically solvable. A heuristic approach explained in Zerlaut et al. 2018 allows to translate microscale properties to the mean field domain in an effective way, as demonstrated by already implemented generical cortical mean field. We adopted this formalism as basis for the development of the multi-layer MF of the cerebellum to provide an accurate insight on cerebellar activity and a model that can be easily integrated in whole-brain dynamics simulators, replacing current generic mean field models with region-specific ones.

Chapter 3 is the core of the work. The development of our MF model is detailed from conceptualization to implementation, towards to the first applications. It is to note that the master formalism and the heuristic approach were the starting points from which some changes were implemented to tailor the formalism on the specific characteristics of the cerebellum, such as the multi-layer structure of its cortex. Furthermore, our pipeline could be seen as a general framework that could be extended to cortical and subcortical regions whose activity can be simulated more accurately with a multi-layer network.

Chapter 4 takes the stock of the entire work and points out the limits and the relevance of the multi-layer cerebellar MF model. The impact of the cerebellum on whole-brain dynamics has been demonstrated in resting state functional networks, as presented in our previous work (Palesi F., Lorenzi R.M., Casellato C., et al., 2020)[1] Furthermore, with an ongoing preliminary study we assessed that the cerebellum influences the activity of other brain regions during task performance, demonstrating to be a causal direct influence on generating brain-dynamics. Taking together these results, it is crystal clear the need of a model specific for the cerebellum into whole-brain dynamics simulator. In parallel, we are working on a "pathological cerebellum", tailoring our model on pathological data to simulate altered activity with the perspective of tuning *digital* brain twin on specific pathologies to achieve *real* subject-specific treatments, making a definitive step ahead in personalized medicine.

---

[1]*Reference of our previous work: Palesi F., Lorenzi R.M., Casellato C., et al. (2020). The Importance of Cerebellar Connectivity on Simulated Brain Dynamics. Front. Cell. Neurosci. 14, 1–11. doi:10.3389/fncel.2020.00240.*

CONTENTS

List of Figures

List of Tables

List of Acronyms

AdEx	Adaptive Exponential (model)
BC	Basket Cells
BOLD	Blood Oxygenation Level Dependent (signal)
BSB	Brain Scaffold Builder
COBA	Conductance Based (model)
CUBA	Current Based (model)
DCM	Dynamic Causal Modelling
DCN	Deep Cerebellar Nucleus
E-GLIF	Extended Generalized Leaky Integrate and Fire (model)
EEG	Electroencephalogram
erfc	Error function
FC	Functional connectivity
fMRI	functional Magnetic Resonance Imaging
GoC	Golgi Cells
GrC	Granule Cells
HD MEA	High Density Multielectrode Array
I/O	Input/Output
IO	Inferior Olive
LC	Lugaro Cells
LFP	Local Field Potential
LIF	Linear Integrate and Fire (model)
MEG	Magnetoencephalogram
mf	mossy fibers
MF	Mean Field

MLI   Molecular Layer Interneurons

PC   Purkinje Cells

PCC   Pearson Correlation Coefficient

pf   parallel fibers

SC   Stellate Cells

SNN   Spiking Neural Network

TF   Transfer Function

TVB   The Virtual Brain

UBC   Unipolar Brush Cells

VSDI   Voltage Sensitive Dye Imaging

Abstract

Brain modeling constantly evolves to improve the accuracy of the simulated brain dynamics with the ambitious aim to build a digital twin of the brain. Specific models tuned on brain regions specific features empower the brain simulations introducing bottom-up physiology properties into data-driven simulators. Despite the cerebellum contains 80 % of the neurons and is deeply involved in a wide range of functions, from sensorimotor to cognitive ones, a specific cerebellar model is still missing. Furthermore, its quasi-crystalline multi-layer circuitry deeply differs from the cerebral cortical one, therefore is hard to imagine a unique general model suitable for the realistic simulation of both cerebellar and cerebral cortex.

The present thesis tackles the challenge of developing a specific model for the cerebellum. Specifically, multi-neuron multi-layer mean field (MF) model of the cerebellar network, including Granule Cells, Golgi Cells, Molecular Layer Interneurons, and Purkinje Cells, was implemented, and validated against experimental data and the corresponding spiking neural network microcircuit model. The cerebellar MF model was built using a system of interdependent equations, where the single neuronal populations and topological parameters were captured by neuron-specific inter-dependent Transfer Functions. The model time resolution was optimized using Local Field Potentials recorded experimentally with high-density multielectrode array from acute mouse cerebellar slices. The present MF model satisfactorily captured the average discharge of different microcircuit neuronal populations in response to various input patterns and was able to predict the changes in Purkinje Cells firing patterns occurring in specific behavioral conditions: cortical plasticity mapping, which drives learning in associative tasks, and Molecular Layer Interneurons feed-forward inhibition, which controls Purkinje Cells activity patterns.

The cerebellar multi-layer MF model thus provides a computationally efficient tool that will allow to investigate the causal relationship between microscopic neuronal properties and ensemble brain activity in health and pathological conditions. Furthermore, preliminary attempts to simulate a pathological cerebellum were done in the perspective of introducing our multi-layer cerebellar MF model in whole-brain simulators to realize patient-specific treatments, moving ahead towards personalized medicine. Two preliminary works assessed the relevant impact of the cerebellum on whole-brain dynamics and its role in modulating complex responses in causal connected cerebral regions, confirming that a specific model is required to further investigate the cerebellum-on-cerebrum influence.

The framework presented in this thesis allows to develop a multi-layer MF model depicting the features of a specific brain region (e.g., cerebellum, basal ganglia), in order to define a general strategy to build up a pool of biology grounded MF models for computationally feasible simulations. Interconnected bottom-up MF models integrated in large-scale simulators would capture specific features of different brain regions, while the applications of a *virtual brain* would have a substantial impact on the *reality* ranging from the characterization of neurobiological processes, subject-specific preoperative plans, and development of neuro-prosthetic devices.

Multi-scale insight into the Cerebellum for a multi-scale brain dynamic simulation

In humans the cerebral cortex represents 82% of total brain mass holding 16 billion neurons, while the cerebellum covers 10% of total brain mass holding 69 billion neurons (Herculano-Houzel, 2009). Thus, despite the volumetric preponderance of the cerebral cortex, 80% of all brain neurons in humans are in the cerebellum therefore the nickname "little brain" is broadly justified. Furthermore, the numerosity of neurons in the cerebral and cerebellar cortices varies proportionally, keeping a ratio of 3-4 neurons in the cerebellum for every neuron in the cerebral cortex (Herculano-Houzel, 2010). Despite the nickname "little brain", the anatomy of the cerebellum deeply differs from the cerebrum structures both in term of neuronal population and cortical circuitry. Moreover, the "little brain" and the brain are deeply interconnected in long-range cerebro-cerebellar loops to carry out sensorimotor and cognitive functions (Palesi et al., 2015, 2017, 2020; Castellazzi et al., 2018; Casiraghi et al., 2019).

1.1 The anatomy of the cerebellum and the cerebro-cerebellar loop
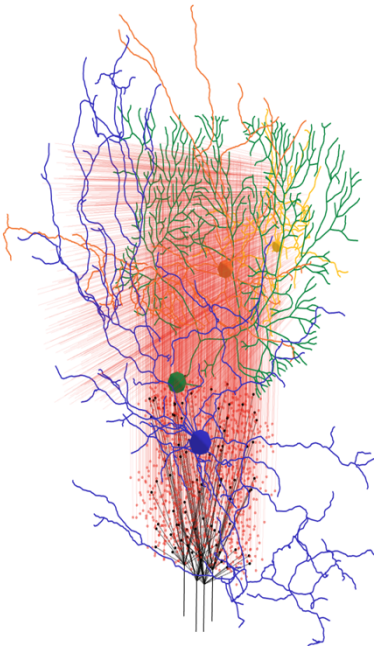
In this chapter, the anatomy of the cerebellum is described at different scales following a bottom-up approach, that is from micro- to macroscale:

- neuron types (microscale)
- cerebellar cortex circuitry (mesoscale)
- cerebellar cortex anatomy and connectivity with cerebrum (macroscale).

1.1.1 Neurons of the cerebellar cortex

The main neurons constituting the cerebellar cortex are Granule Cells (GrC), Unipolar Brush Cells (UBC), Golgi Cells (GoC), Lugaro Cells (LC), Basket Cells (BC), Stellate Cells (SC), and Purkinje Cells (PC). Their main features are reported in Table 1.1.

Table 1. 1) Features of cerebellar neuronal populations

Cerebellar cortex network	Neurons type	Soma diameter [μm]	Autorhythmic [Hz]	Synaptic connections
	GrC D'Angelo 2011, Masoli et al., 2017, Palay and Chan-Palay, 1974a	5 - 8	--	mfs (e), UBC (e), GoC (i)
	UBC Kim et al., 2012; Mugnaini et al., 2011	10	--	mf (e), BC (i)
	GoC Solinas et al., 2007; D'Angelo et al., 2013, Palay and Chan-Palay, 1974c	10 - 30	5 - 15	mfs (e), GrC (e), LC (e), GoC (i)
	LC Melik-Musyan and Fanardzhyan, 2011 Ito, 2014, Palay and Chan-Palay, 1974d	16 and 9 (elliptic soma)	5 - 15	BC (i)
	BC Galliano et al., 2013; Lennon et al., 2014, Palay and Chan-Palay, 1974b	10-15	7 - 10	GrC pfs (e), LC (e), BC (i)
	SC Galliano et al., 2013; Lennon et al., 2014, Palay and Chan-Palay, 1974f	5-10	7 - 10	GrC pfs (e), LC (e), SC (i)
	PC Lennon et al., 2014; Masoli and D'Angelo, 2017, Palay and Chan-Palay, 1974e	35 - 60	40 - 80	GrC (e), SC (i), BC (i)

GrC = granule cells (red), GoC = Golgi cells (blu), BC = basket cells (yellow), SC = stellate cells (orange), PC = Purkinje cells (green), UBC = unipolar brush cells, LC = lugaro cells; mfs = mossy fibers (black); LC and UBC are not shown in the graphics. pf = parallel fibers from GrC to the other cells (see Figure 1.1); (e) and (i) indicates excitatory and inhibitory connections respectively.

GrCs are the smallest neurons (5–8 μm of soma diameter) and the most numerous cells in the brain (10^{10}–10^{11} in humans) (Palay and Chan-Palay, 1974a; Ito, 2014). GrCs axons ascend perpendicularly to the cerebellar cortical surface (ascending axons) and bifurcate into parallel fibers. GrCs are excitatory neurons using glutamate as excitatory neurotransmitter and they don't present autorhythmic (D'Angelo et al., 2001; Masoli et al., 2017).

GoCs present a peculiar structure with apical and basal dendrites (Masoli et al., 2020b) and a soma of about 10 – 30 μm (Palay and Chan-Palay, 1974c). They are inhibitory neurons using both GABA and glycine as neurotransmitter (Galliano et al., 2010). The GoCs autorhythmic is 5-15 Hz (Solinas et al., 2007; D'Angelo et al., 2013).

UBCs are named after a single dendrite forming a "brush" connected to mossy fibers with a soma of about 10 μm (Kim et al., 2012). They are excitatory neurons expressing calretinin that is a calcium driving protein involved in calcium signals (Mugnaini and Floris, 1994; Mugnaini et al., 2011).

LCs have a cigar-shaped cell body with a elliptic soma with diameters of 16 μm and 9 μm (Palay and Chan-Palay, 1974d), and long dendrites, emerging from its poles (Lainé and Axelrad, 1998; Melik-Musyan and Fanardzhyan, 2004). They co-localize GABA and glycine and represent the main target of the serotoninergic plexus in the cerebellar cortex. They discharge spikes regularly at 5–15 Hz (Ito, 2014).

SCs and **BCs** are GABAergic neurons, namely producing the inhibitory transmitter GABA. SCs soma diameter is about 5-10 μm (Palay and Chan-Palay, 1974f), while BCs 10-15 μm (Palay and Chan-Palay, 1974b). Despite the morphological difference, they are functionally similar, therefore they are grouped together forming the Molecular Layer Interneurons (MLIs). MLIs have an autorhythmic of about 8 Hz (Galliano et al., 2013; Lennon et al., 2014).

PCs are the largest cells of the central nervous system in vertebrate. The soma diameter is about 30 - 40 μm, namely 4 - 8 times the GrC one (Palay and Chan-Palay, 1974e). Their dendrites are flat and lay in the cortex looking like a *pressed leaf*. They are inhibitory GABA neurons with an autorhythmic at high frequencies of 40 – 80 Hz and they carry out the activity from the cerebellar cortex to deep cerebellar nuclei (McKay and Turner, 2005; Molineux et al., 2006; Lennon et al., 2014; Masoli and D'Angelo, 2017).

Neurons are interconnected constituting the multi-layer organization of the cerebellar cortex shown in Figure 1.1 and detailed in the next section.

1.1.2 Multi-layer circuit of the cerebellar cortex

The cerebellar cortex is characterized by a quasi-crystalline geometry with a multi-layer organization (D'Angelo et al., 2016; D'Angelo, 2018). Three layers are clearly identifiable as shown in Figure 1.1A: Granular layer (1), Molecular layer (2), and Purkinje layer (3). These three layers are interconnected building up the cerebellar multi-layer circuit schematized in Figure 1.1B.

1. Granular layer. Made up of GrCs, GoCs, UBCs and LCs, it is the input stage of the cerebellum. Granular layer acts as a spatial-temporal filter of sensory inputs thanks to GoCs and GrCs oscillatory

and resonant dynamics (Solinas et al., 2010; Prestori and Person, 2013). GrCs and GoCs receive input signals coming from mossy fibers. UBCs act as a booster system for the mossy fiber input to the GrCs. Inhibitory input is provided to GrCs by GoCs, both in feedforward and feedback loop. GoCs self-inhibited each other through gap junctions (Simões de Souza and De Schutter, 2011; Szoboszlay et al., 2016). Their activity can be modulated by LCs that are mainly silent, but they are the main target of the serotoninergic plexus in the cerebellar cortex, thus in presence of serotonin they shape not only the activity of GoCs, but also MLIs and PCs as well (Prestori et al., 2019). GrCs axons ascend to the Purkinje layer and Molecular layer where they bifurcate into parallel fibers conveying the excitatory input from the Granular layer to Purkinje layer and Molecular layer. Both ascending axons and parallel fibers make synaptic contact with PCs while only parallel fibers intercept MLIs.

2. Molecular layer. It is populated by SCs in the upper part and by BCs in the deepest part at the edge of Purkinje layer. MLIs (SCs and BCs) are connected each other in a self-inhibitory loop. MLIs make synapses also with PCs, inhibiting PCs activity as follows: axons of SCs terminate on a single PC dendrite while BCs axon forms an axonal *basket* surrounding the soma of a series of PCs (D'Angelo, 2018).

3. Purkinje layer. It is the sole output channel of the cerebellar cortex projecting the activity towards the deep cerebellar nuclei and it is spatially located in the middle of the circuit, between granular and molecular layer. In addition to the excitatory connections from GrCs and inhibitory input carried by MLIs, PCs are connected to the inferior olive cells located in the brainstem through a single climbing fiber that makes excitatory synapsis climbing around the extended arborization of PC dendritic tree (D'Angelo, 2011).
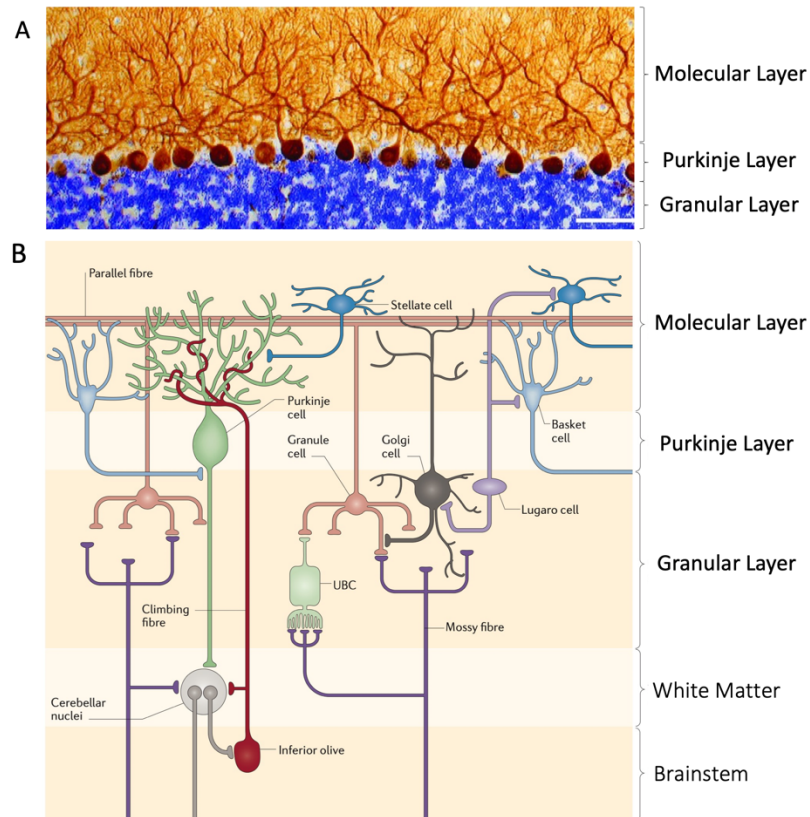
Figure 1. 1) Multi-layer organization of the cerebellar cortex. A) Sagittal histological view of a mouse cerebellar slice (Lackey et al., 2018). Cell bodies in Granular Layer was labeled using a Nissl stain (blue-violet) and Purkinje cells with calbindin immunohistochemistry (brown). The geometry of mouse and human cerebellar is the same. **B**) Multi-layer cerebellar circuit (Cerminara et al., 2015) . Schematic view of the multi-layer cerebellar cortex circuitry and the connections with deep cerebellar nuclei and brainstem through inferior olive cells. UBC = Unipolar Brush Cell.

1.1.3 Anatomical parcellation of the cerebellar cortex

The cerebellum is part of the brain located in the posterior cranial fossa (Figure 1.2 A, B, C) and it is connected to the brainstem through three pairs of peduncles: inferior, middle, and superior peduncles (Figure 1.2 E, F).

The cerebellum is organized with an outer layer of gray matter constituting the cerebellar cortex, overlying a dense core of white matter embedding four deep cerebellar nuclei (DCN), i.e., the fastigial, globose, emboliform, and dentate (Figure 1.2 F). Dorsal view (Figure 1.2 F) shows two large hemispheres united by the midline vermis and the paravermis. The cortex is highly convoluted, forming narrow ridges (folia), and intervening sulci and fissures (Figure 1.2 A, D). The fissures divide the cerebellum in ten lobules commonly labeled with Roman numbers (I-X Figure 1.3 A). Primary fissure and posterolateral fissure are deepest two fissures (Figure 1.2 D) which divide the cerebellum into three lobes: the anterior, the posterior, and the flocculonodular lobe.
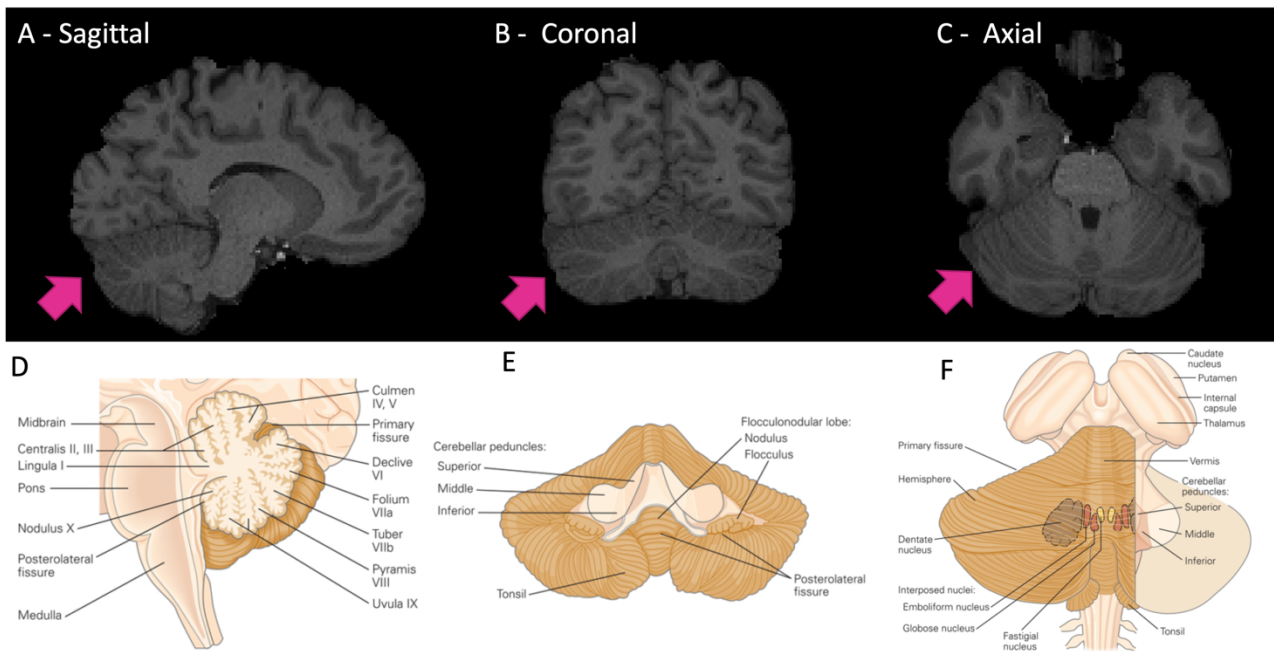
Figure 1. 2) Cerebellar anatomy in a nutshell. Top: Brain T1-weighted image from randomly chosen subject of the Human Connectome Project (https://www.humanconnectome.org/). **A** = sagittal view, **B** = coronal view, **C** = axial view. Cerebellum is located in the posterior cranial fossa and indicated with the pink arrow. **Bottom:** Anatomic chart of the cerebellum adapted from (Kandel et al., 2013): **D** = midsagittal view schematizes the folia and the primary fissure. **E** = ventral view showing the posterolateral fissure separating the flocculonodular lobe. The cerebellar peduncles are shown located in the middle part. **F** = dorsal view showing the vermis in the midline that divides the cerebellum in left and right hemispheres. Deep cerebellar nuclei (dentate in brown, interposed in red and fastigial in yellow) are highlighted, showing the different morphologies.

1.1.4 Functional parcellation of the cerebellar cortex

For many years the cerebellum owes its fame to its motor function but considering only this role became a narrow view of its impact on brain functions. Even the motor functional parcellation cannot be overlook, a functional division including also sensorimotor and cognitive function should be consider for a complete overview of the cerebellar functions. The most part of the afferent connections, i.e., those coming from the cerebral cortex and from the spine, terminates in the cerebellar cortex and is made up of climbing fibers targeting PCs or mossy fibers connected with the granular layer. Hemispheres, vermis and paravermis receive different afferent projections, so that they are not only anatomical but also functionally different. Based on the segregation of the input, the cerebellum could be divided into three main different functional areas: the vestibulocerebellum, the spinocerebellum, and the cerebrocerebellum (Figure 1.3 B).

The vestibulocerebellum (or archicerebellum) is the phylogenetically oldest part of the cerebellum and it corresponds to the flocculonodular lobe (Li et al., 2019). Vestibulocerebellum receives inputs from the vestibular nuclei of the brainstem and its main functions are related to balance maintenance, eyes movement control and coordination of head-eye movements (Barmack and Yakhnitsa, 2013).

Vermis and paravermis constitute the spinocerebellum (or paleocerebellum) that controls the movement executions and the muscle tone. It receives input directly from the spinal cord through the spinocerebellar tract, but also from the head and face through the trigeminocerebellar tract (Roostaei

et al., 2014). These two tracts contact different cerebellar areas: the spinocerebellar tract contacts lobule VIII, and the trigeminocerebellar tract primarily projects to lobule V and VI (Stoodley, 2012).

The cerebellar hemispheres constitute the cerebrocerebellum (or neocerebellum) involved in planning and sensory guidance of the movements. Inputs are sent by many different cerebral areas including the sensory-motor, premotor and parietal cortices via pontine nuclei by forming the so called corticopontine tract.
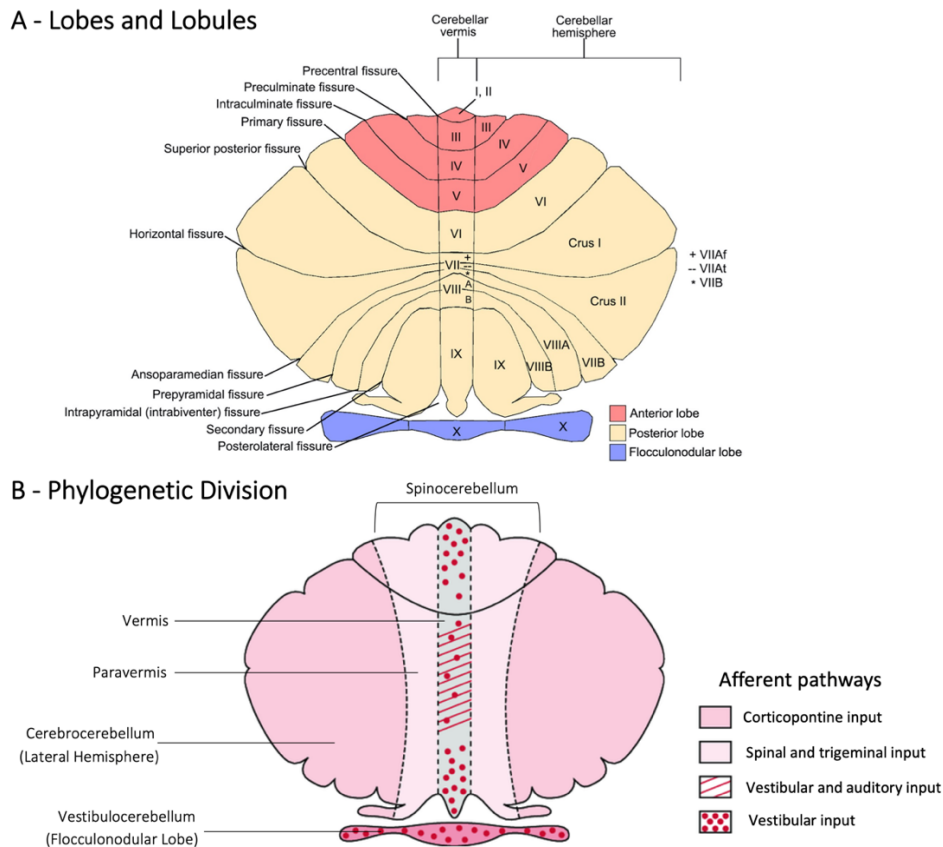
Figure 1. 3) Cerebellar lobes, lobules, and functional regions. **A)** Unfolded view of the cerebellum with lobules labelled with romans numbers from I to X (D'Mello and Stoodley, 2015). Vermis in the midline divides the cerebellum into two hemispheres. Primary fissure separates anterior lobe (red) and posterior lobe (yellow). Flocculonodular lobe (violet) is separated by posterior (or posterolateral) fissure. **B)** Phylogenetic division of the cerebellum. Three main cerebellar regions are defined according to different functions and afferent pathways: vestibulocerebellum (flocculonodular lobe – dark pink) that receives vestibular input, spinocerebellum (vermis – gray, paravermis – light pink) that receives spinal, trigeminal, and vestibular inputs, cerebrocerebellum (lateral hemispheres – pink) that receives input carried by the corticopontine tract. Figure adapted from (Marsden, 2018).

The division in vestibulocerebellum, spinocerebellum and cerebrocerebellum is not the sole functional parcellation of the cerebellum. Generally, sensory functions distribution can be schematized with a gradient map showing sensorimotor functions located mainly in the midline of the cerebellum and cognitive ones that become more prominent moving towards the lateral and

posterior hemispheres (Figure 1.4 A). Specifically, considering the associative learning, which is the ability to learn how different events are related each other, the vermis is more involved in emotional processing while the hemispheres in cognition (Figure 1.4 B) (Klein et al., 2016). Thus, the cerebellum results involved in many non-motor functions like sensorial, emotional, and high-cognitive tasks, such as action selection and behavioral switching. Functional Magnetic Resonance Imaging (fMRI) studies on the cognitive processes have unveiled cluster of activated cerebellar regions as lobules I-VI and Crus I-II (Castellazzi et al., 2018). Furthermore, lobule VI and Crus I-II resulted activated also in mirroring processes during action observation tasks (Casiraghi et al., 2019).
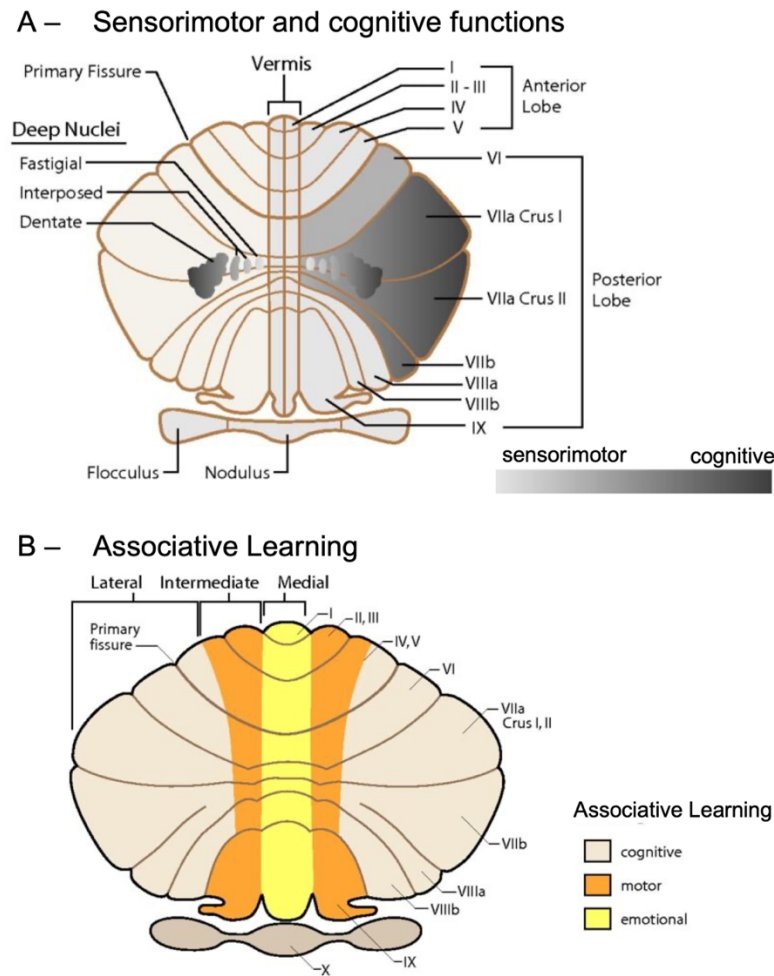
Figure 1. 4) Multi-skilled Cerebellum. Unfolded maps of the functional parcellation (Klein et al., 2016) **A)** Map of sensorimotor-to-cognitive function distribution. For clarity, only right cerebellum is colored. Sensorimotor areas (lighter gray) are located mainly in the vermis, right hemisphere (lobules I, II-III, IV), while cognitive functions (dark gray) are distributed in the posterior lobe (lobule VIIa, Crus I, Crus II). Also the cerebellar nuclei present a functional gradient with fastigial and interposed (Emboliform + Globose) nuclei more involved in sensorimotor function, and dentate nuclei more involved in cognition. **B)** – Associative learning in the cerebellum. Vermis (medial part) acts as emotional processor, paravermis (intermediate part) in motor functions and hemispheres (lateral part) in cognition.

On top of the afferent connections, also the efferent cerebellar pathways suggested a multifaceted role of the cerebellum. The output from the cerebellar cortex, are carried solely by the axons of cortical PCs that terminate into the deep cerebellar nuclei which project, in turn, directly towards

thalamus or towards red nucleus and then thalamus. The target of the cerebellar output is not only the motor and premotor cerebral area but also the prefrontal and associative regions.

According to these physiological evidences, the cerebellum acts as a multi-skilled processor receiving input from different afferent pathways and sending output to many cortical regions. This role is made possible because the cerebellum results embedded into several loops with the cerebrum, playing an important role in whole-brain dynamics modulation.

1.1.5 Cerebro-cerebellar loops

In the past, the cerebellum was studied integrated in cerebro-cerebellar loops solely as a co-processor of the movement but over the years this narrow view has been gradually abandoned thanks to the evidence about the wide range of functions executed by the cerebellum (see **section 1.1.4**). Therefore, not only the motor loop is in the spotlight, but also emotional and cognitive loops have gained more and more popularity amongst the neuroscientists to investigate the cerebellar role in health and neurodegenerative pathologies (Rogers et al., 2011; Castellazzi et al., 2014; Palesi et al., 2015, 2020; Pizzarotti et al., 2020). The cerebro-cerebellar loops are detailed below to give a structural and functional overview of such long-range connections.

Motor and somatosensory loop. Cerebellum projects both to motor and somatosensory cerebral areas. Cerebellar outputs project to the primary motor area passing through the ventrolateral thalamic nucleus, while outputs to the primary somatosensory area are conveyed through the intralaminar nuclei projecting to intragranular and superficial layers. Cerebellum impacts on motor cortex activity by assisting the cerebral cortex in transforming the sensory input into motor-oriented through the cerebello-thalamo-cortical projection (Luft et al., 2005). Furthermore the posterior cerebellum modulates the motor cortex excitability in response to emotional stimuli (Ferrari et al., 2021). In addition, embedded in this loop, cerebellum acts as a machine for the fast spatio-temporal integration of the inputs perceiving the reality continuously. It is interconnected with premotor and supplementary motor areas proving to be involved into motor planning as a forward controller (Rouiller et al., 1994; Dum and Strick, 2003).

Oculomotor loop. Oculomotor regulation involves several cortical and subcortical areas participating in automatic and cognitive control processes. The cerebellum is involved in the control of saccadic (to search a static target) and smooth pursuit (to track moving targets) eye movements which are thought to be the outcomes of a single sensory-motor process to orient the visual axis. Lateral and posterior cerebellum and the vermis are involved in control of ocular saccades (Doron et al., 2010). Furthermore, the fastigial oculomotor region resulted to be deeply involved in both saccades and smooth pursuit eye movements. It has been recently demonstrated that the cerebellum is strongly connected with the precentral gyrus and the superior frontal gyrus which take part in motor and oculomotor processes as well as the processing of spatial working memory (du Boisgueheneuc et al., 2006). Hence, the cerebellum resulted to be deeply integrated in processes controlling both the motor and cognitive components of eye movements.

Parietal loop. Embedded in the parietal loop, the cerebellum is involved in visuo-motor and visuo-attentional control. It is closely connected to the parietal lobe, directly sending input to the inferior

parietal lobe through the dentate nucleus. Further, secondary cerebellar afferents to the anterior intraparietal area are sent by motor and premotor areas (Clower et al., 2005). The anterior intraparietal area becomes activated in response to the sight of an object, as well as in reach-to-grasp arm movements (Tunik et al., 2005), and in the creation of cross modal sensorial representations of objects (Grefkes et al., 2002). Cerebellum also targets the ventral lateral intraparietal area crucial for visual attentional control, and medial intraparietal area involved in visuo-motor coordinate transformation (Prevosto et al., 2010). Medial intraparietal area sends strong projections to parahippocampal regions and, together with the cerebellum, is also included in complex loops with subcortical areas as the thalamus and basal ganglia (Grefkes et al., 2004).

Prefrontal loop. The cerebellum takes part in cognitive and working memory control and procedural learning. It is reciprocally connected through the thalamus (Middleton and Strick, 2001) with the medial prefrontal cortex, which is involved in saccades and cognitive control (Watson et al., 2009), and the dorsolateral prefrontal cortex that is responsible of working memory control, mental preparation of imminent actions (Pochon et al., 2001), and procedural learning (Kelly and Strick, 2003). Furthermore, cerebellum is also connected to the anterior prefrontal cortex whose functions are not completely understood yet, but it might be involved in the integration of multiple distinct cognitive processes during goal-directed complex behaviors (Krienen and Buckner, 2009).

Temporal loop. The connections between cerebellum and temporal areas, including the hippocampus and amygdala, are not still completely clarified. Negligible contribution to the corticopontine fiber tract has been found (Ramnani et al., 2006) suggesting that the cerebellum is unlikely to receive strong direct afferents from temporal areas. Nevertheless, cerebellar fastigial nuclei in monkeys and cats seem to project to several temporal areas, like the hippocampus and amygdala. A dynamic causal modeling proved a strong and bidirectional connection between the cerebellum and the lateral anterior temporal lobe during the execution of a cognitive task (Booth et al., 2007). More extensive studies are required to elucidate the pattern of connectivity, but it is reasonable to speculate on a functional interplay between cerebellum and temporal areas.

Loops with basal ganglia and limbic system. The cerebellum has recently been shown to form bidirectional connections with the basal ganglia. The cerebellar efferent pathway starts from the dentate nucleus, goes through the thalamus, and reaches the striatum. Backward pathway starts from the subthalamic nucleus and ends in the cerebellar cortex, through the pontine nuclei (Bostan et al., 2010). The cerebellar-limbic system loop is still under investigation. Evidence from anatomical studies suggests cerebellar connections with cortical and subcortical areas of the limbic system, i.e., amygdala, hippocampus, septal nuclei, and hypothalamus. Furthermore, meta-analytic studies on functional neuroimaging delineated distinct regions of the so-called "limbic" cerebellum, pointing at medial (vermis and para-vermis) and posterior lateral cerebellar portions (Crus I and Crus II – see Figure 3 A) as relevant parts activated during the emotional processing (Stoodley, 2012). Interestingly, cerebellar functional activation is not recorded only for the regulation of mood and emotion, but also in emotive information processing that is a mechanism required for appropriate behavioral responses (D'Angelo, 2019).

Given all these considerations, the integration of the cerebellum in several loops deeply different in terms of functions supports that the view of the cerebellum as co-processor of movement is reductive.

Hence, it is limiting to think about brain activity without embedding the cerebro-cerebellar loop in brain network.

1.2 The brain as a multiscale problem

Studying the activity of the brain is an ongoing and remarkable challenge due to all the biological features that play a role in generating dynamics. These features can be described at different levels of detail: single cell features (e.g., membrane capacitance and membrane time constant) operate at microscale, synaptic connectivity parameters (e.g., synaptic time decay and synaptic convergence) refer to mesoscale, and long-range connectivity parameters (e.g., directionality and causality of connections) between different brain regions are defined at macroscale. Since the brain presents this multiscale organization, the challenge of studying the multifaceted brain dynamics should be addressed with a multiscale approach. The following sections provide a description of the main multiscale approaches, i.e., bottom-up and top-down ones (**section 1.2.1**), together with the models **(section 1.2.2)** developed and integrated with simulation software (**section 1.2.3**).

1.2.1 Bottom-up and top-down approaches

Bottom-up approaches start from physiological and biological knowledge of the elementary mechanisms that are responsible of a certain observation (e.g., from the knowledge of neuronal microcircuitry physiology to the overall brain activity), whereas top-down approaches are aimed at inferring the hidden causes starting from recorded data that characterize, structurally and/or functionally, the neural system (e.g., from fMRI recordings to underlying neuronal dynamics) (Figure 1.5). At a first sight, bottom-up and top-down might seem dichotomic approaches because top-down approach is focused on the overall brain behavior, while the bottom-up on neural dynamics. However, their integration could lead to an effective brain dynamic simulation that would be achieve by combining the physiological knowledge about the neuronal microcircuit with whole-brain data in large-scale simulators, such as The Virtual Brain (TVB) and Dynamic Causal Modelling (DCM) (see **section 1.2.3**). An effective way to bring the bottom-up knowledge in top-down simulators could be the integration of biologically validated mesoscale models that provide a link between microscale and macroscale dynamics. This strategy merges knowledge of different scales by combining different approaches. For example, mean field (MF) models, which will be introduced in **section 1.2.3** and formally described in **section 2.1,** are used in whole-brain simulators, and describe mesoscale brain activity by averaging microscopic structural and functional properties, hence partially bridging the gap between micro/mesoscale spiking dynamics and macroscale activity. Developing a biology grounded MF model with a bottom-up approach and plugging it into whole-brain dynamic simulators would permit to integrate bottom-up with top-down approaches.

Constructing a reliable *virtual* brain trying to capture its polyhedric faces, is an active research field aimed at studying brain dynamics at different scales. To ensure the biological reliability of the digital dynamics, the underlying models should capture the physiological peculiarities of the target brain regions. In this context, first attempts to specify models for the subcortical structure have been implemented (van Albada and Robinson, 2009; van Wijk et al., 2018), but a MF model specifically tailored on the cerebellum is missing. Once the models are integrated in the simulators, they will

13

capture the peculiarities of the different brain regions and the applications of a digital brain would have a substantial impact on the *reality* ranging from the characterization of neurobiological processes, subject-specific preoperative plans, and development of neuro-prosthetic devices.
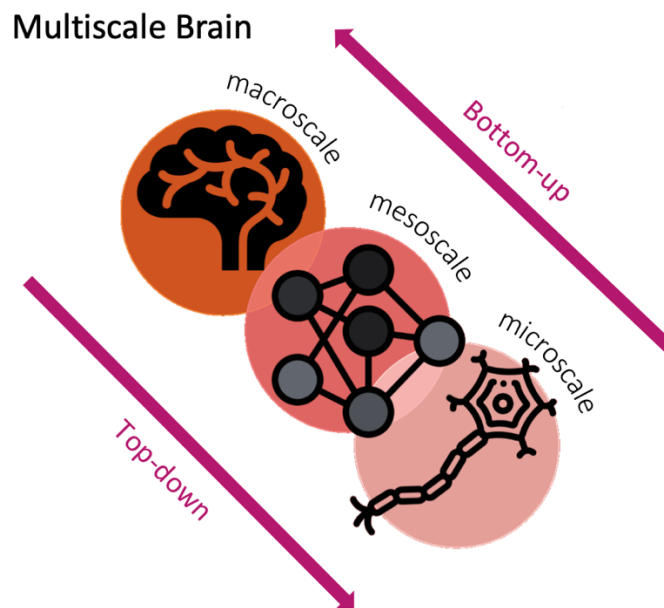
Figure 1. 5) Multiscale Brain, bottom-up & top-down approaches. The bottom-up approach starts from the knowledge of the elementary causes (e.g., neuron dynamic) that are responsible of a certain observation (e.g., simulated whole-brain dynamic), whereas the top-down pathway aims to infer the hidden causes (e.g., underlying neuron dynamic) of the ensemble observation (e.g., whole-brain activity). Bringing the bottom-up knowledge in top-down simulators as TVB is of crucial importance for the simulation of an effective virtual brain, and MF models are an effective way to bridge the gap between micro and macroscale

1.2.2 Modelling: the theory from *virtual neurons* to *virtual brains*

Neurons are the *unit* of the brain, thus in the context of whole-brain dynamics simulation, neuron models represent the microscale. At this level of detail, the simulation of single neuron activity reproduces neurons dynamics and how the connections among neurons influence those dynamics. A fundamental aspect that cannot be neglected is that, as for a biological neuron, also a *virtual* neuron should account for the presynaptic influence, i.e., the presynaptic currents, since virtual neurons embedded in a network communicate through synapses as the biological ones (Figure 1.6). In biology, synapses enable the information exchange between two neuronal cells. Specifically, the axonal terminal of one cell is separated from the postsynaptic receptors by the synaptic cleft. According to receptors position, synapsis can be differently classified as axodentric, axosomatic or axoaxonic synapses, in which postsynaptic receptors are localized on dendrites, on the cell body or on the axon, respectively. Despite this morphological distinction, the interneuronal communication is the same: the presynaptic terminal releases vesicles of neurotransmitters that cross the synaptic cleft and bind postsynaptic receptors, determining a current influx into the postsynaptic neuron. Consequently, the postsynaptic neuron voltage changes rely on the sum of synaptic currents, and it may reach the spiking voltage threshold determining the postsynaptic neuronal firing. Importantly, the synaptic activity can be described with mathematical models and, along with virtual neurons equations, they can be classified in current-based (CUBA) and conductance-based (COBA) models.

CUBA model describes a single synaptic current, while COBA is an advanced approach to compute the synaptic current using conductance equations that can be specific for each type of synaptic receptor, enabling to separate different contributions. Thus, the difference between CUBA and COBA models is in the definitions of the synaptic current I_{syn}.

For CUBA, I_{syn} is proportional to the synaptic connection strength yielding (Cavallari et al., 2014):

$$I_{syn}(t) = J_{syn}s_{syn}(t)$$

$$(1)$$

With J_{syn} = synaptic efficacy (pA), i.e., the strength of synaptic connection, and $s_{syn}(t)$ = time-dependent function of the synapsis activity. For COBA model, s_{syn} is still included to model the synapsis kinetics but I_{syn} expression is written in term of the driving force (Cavallari et al., 2014):

$$I_{syn}(t) = g_{syn}s_{syn}(t)(E(t) - E_{rev})$$

$$(2)$$

Where g_{syn} = conductance (nS), and $E(t) – E_{rev}$ = driving force (mV) of the synaptic current including $E(t)$ = membrane potential and E_{rev} = reversal potential of that synapsis.

Generally, CUBA models are largely used thanks to the relative simplicity of their mathematical formulation that admits an analytical closed form. COBA models have a more complicated mathematical expression that is difficult to treat analytically, requiring an approximated analytical approach. On the other hands, COBA are more biophysically-grounded (Kuhn et al., 2004) since they can reproduce more complex dynamics that are similar to intracellular in-vivo recordings (Destexhe et al., 2003).(Destexhe et al., 2003). Which is the best choice between COBA and CUBA is a query without a unique answer because it is a design choice depending on the final goal of the simulation.
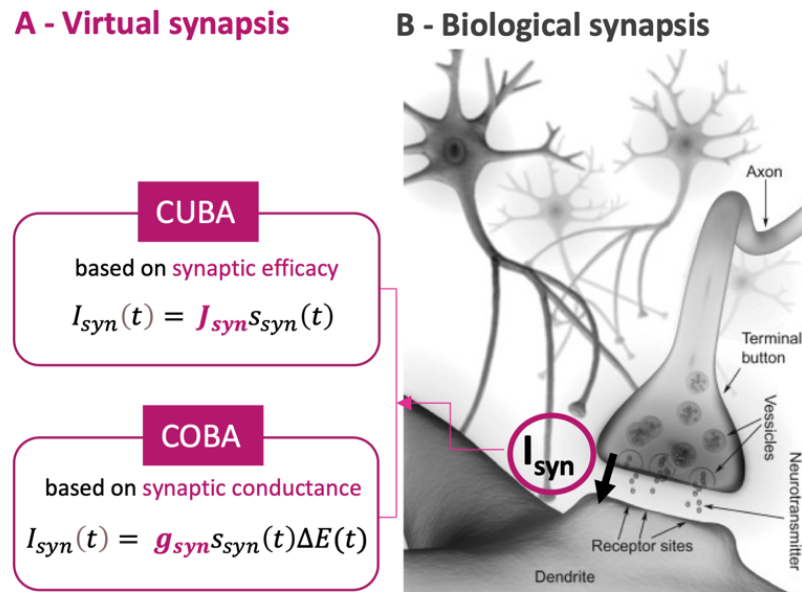
Figure 1. 6) Virtual and biological synapses. A) COBA and CUBA models representing virtual synapses. I_{syn} = synaptic current, $s_{syn}(t)$ = synaptic kinetics function. CUBA: I_{syn} is proportional to the synaptic efficacy J_{syn} (pA). COBA: I_{syn} is proportional to the conductance g_{syn} (nS) and to the driving force ΔE (mV). **B)** Biological synapsis (modified from (Kapalka, 2010)). The synaptic clef is the gap that separates the axon terminal button of the presynaptic neuron from receptors of the postsynaptic neuron. The vesicles in the presynaptic button release the neurotransmitter that flows through the synaptic clef towards the postsynaptic receptors determining a current influx I_{syn} into the postsynaptic neuron.

Over the years, many COBA and CUBA models have been developed considering the neuron at different level of granularity. The multicompartmental strategy includes specific morphological features of each compartment and endows biology grounded models with high complexity. On the other hand, monocompartimental strategy collapses the morphological characteristic in a unique single compartment simplifying the model. In 1952 the popular Hodgkin-Huxley model was developed by A. L. Hodgkin and A. F. Huxley to describe the action potential propagation along nerves with a very fine resolution. Starting from the recordings in an axon of a giant squid, they developed a model that separated the membrane current into three components: the sodium, the potassium and the calcium current, considering the respective ionic channels as different compartment with specific parameters (Hodgkin and Huxley, 1952). Furthermore, the model was developed as COBA, with one driving force for each ionic current, achieving a higher level of realism that made the Hodgkin-Huxley model widely used in neuroscience even seventy years after (Brown, 2022; Giannari and Astolfi, 2022). Moving to a lower level of granularity, the neuron morphology considering only the soma and the axon can be simplified with the so-called *ball and stick* model (Pettersen et al., 2011; Aspart et al., 2016). This bi-compartmental approach reduced the number of equations and parameters resulting in a convenient model for the computational implementation but still making possible to separate specific parameters that account for the different morphology of the soma and the dendrites (e.g., the diameter). This bi-compartmental design can be specified both with Leaky Integrate and Fire (LIF) models, which are developed as COBA or CUBA (Cavallari et al., 2014; Peterson et al., 2015), but also with non-linear models like the COBA Adaptive Exponential (AdEx) (Cakan and Obermayer, 2020a).

Losing any morphological reference, a neuron can be simplified with a single compartment. This design strategy is at the basis of single-point neuron models that, despite at first sight it might seem an oversimplification, provide effective simulations including physiological parameters (e.g., the quantal synapses conductance and the synaptic time decay). Furthermore, this strategy leads to a significant reduction of the computational load required to reconstruct a neurons network, resulting in an advantageous balance between physiological properties and computational time. As for the bicompartmental strategy, single point neurons can be specified as single-point AdEx (Brette and Gerstner, 2005; Depannemaecker et al., 2020) or LIF neurons (Nordlie et al., 2010) but also as Extended-Generalized Leaky Integrate and Fire (E-GLIF) neurons, with COBA synapses (see **section 3.2.1 (Neuron model)**) commonly used to model cerebellar neuron types (Geminiani et al., 2018, 2019a).

So far, an overview of the modeling strategies has been provided to underline that each strategy can be implemented with different models. Wondering which approach is the best it is an ill-posed problem because it depends on the level of details required by the specific study. As an example, multicompartmental neuron models are a powerful tool but if the goal is to simulate mesoscale dynamics of a spiking network (order of nm or mm) they might be not the best choice because the computational load might be unaffordable, thus point neurons represent a more convenient strategy. When the goal of the simulation is to provide whole-brain dynamics, the computational load increases due to the complexity of the system made up of interconnected networks. In this framework, spiking networks made of spiking neuron led to a still too high computational complexity. Additionally, the recorded brain signals with in vivo non-invasive techniques, like electroencephalography (EEG), magnetoencephalography (MEG) and functional magnetic resonance imaging (fMRI), are time-continuous series, therefore a formalism producing a signal in the same domain allows direct comparison with these recordings. On top of these considerations, the biophysical properties expressed by single neurons and spiking network models should be considered to construct effective *virtual brains*. From the need to link the microscale of the single neuron model to the macroscale of whole-brain dynamics, mean field strategy represents an effective mesoscale tool. The principle is to construct a brain network in which each node is represented with MF. This strategy finds its root in physics (see **section 2.1**) and it is widely used in brain dynamics because it permits to bridge the gap between micro/mesoscale spiking dynamics and macroscale activity. MFs, indeed, underpin the simulation of whole-brain dynamics after being optimized on the spiking network activity, plugging the information from higher-resolution models into macroscale simulators.

1.2.3 Simulation of *virtual neurons* and *virtual brains*

The computational models developed so far are specialized in reproducing the brain dynamics at a certain scale. At microscale the goal is to simulate the firing rate of a single neuron, for mesoscale the target is the activity of a network representing a microcircuit, and macroscale aims to reproduce brain signals such as the recordings from electroencephalograph or the Blood Oxygenation Level Dependent (BOLD) signal from fMRI. Due to the different scales of the signals target of the simulation, simulators integrating computational models at different levels of granularity have been developed to address the challenge of reproducing such a rich pool of dynamics (Table 1.2).
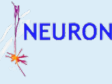
Microscale simulators. NEURON (Hines and Carnevale, 1997; Carnevale and Hines, 2006) is the premier simulator used since the 1990s in the neurocomputational sciences (Magkanaris et al., 2022). It reproduces the activity of a morphologically detailed multicompartment cell model, with the soma, the axon, and the dendrites (and their parts) modelled as different compartments with their ionic channels and membrane voltage dynamics. Through the years it has been extended with updates as CoreNeuron to exploit parallel computing and improve computational cost of simulations (Kumbhar et al., 2019). GENESIS (GEneral NEural SImulation System) (Bower and Beeman, 1998) is an object-oriented environment. It is "GEneral" because the user can extend the environment by adding a new "object" (class), i.e., a new neuron model. The simulations are constructed by building blocks (GENESIS elements) which communicates during the simulation. Each block contains its own variables and functions (methods) to perform computations. Although the programming strategy is different from NEURON, it is intended to reach the same level of resolution and an extension compatible with parallel computing (PGENESIS) was implemented. Recently, a new simulator for multi-compartmental models has been developed: ARBOR (Akar et al., 2019) provides an high level of morphological resolution as GENESIS and NEURON and it doesn't required update for parallel computing. ARBOR is ready to be integrated with high-performing computing technologies to tackle the issue of the heavy computational load.

Mesoscale simulators. Considering a lower level of resolution, NEST (NEural Simulation Technology Initiative) (Plesser et al., 2015) allows to reproduce the activity of one single neuron simplified as a mono-compartmental point neuron (e.g. AdEx, LIF; E-GLIF – see **section 1.2.2**) by solving a set of few ordinary differential equations, representing the membrane voltage dynamics and additional currents. The extension NEST 4G is developed to run NEST with parallel computing technology. BRIAN (Stimberg et al., 2019) is developed for fast prototyping. Compared to NEST, it has the same rich pool of pre-defined point models, but with the additional option to implement bi-compartmental *ball and stick* neurons. Depending on the mathematical model and the mono or-multicompartmental resolution required, the user has to specify cellular parameters such as the membrane capacitance, the membrane time decay constant, and the reversal potential. Additionally, these simulators permit to reproduce the activity of a neuronal network, combining different models of different type single cell by adding synaptic connectivity parameters (e.g., the mean synaptic convergence) to the neuronal ones. NEURON, for instance, combined morphological-detailed single cell models building up high resolution spiking circuits by defining connectivity parameters proper for axon-dendrite, axosomatic and axoaxonic synapses. NEST, instead, provides the option to define lower resolution networks made up of interconnected point neurons, by collapsing the different type of synapses (**section 1.2.2**) into a single connectivity parameter. An example of the usage of NEST to address a mesoscale simulation, is the reconstruction of a module of the cerebellar spiking network where the and GrC, GoC, MLI and PC were simulated with E-GLIF models (Geminiani et al., 2019b). To improve the placement of the neurons embedded in a spiking network, the Brain Scaffold Builder (BSB) (De Schepper et al., 2022) has been developed as a bottom-up open source framework. BSB is a tool that permits to construct a network topology (neuron position and connectivity) with *ad-hoc* algorithms by specifying rules ranging from simple random placement of neurons as particles, regular placement in grid, probabilistic connectivity to intersection of ultra-detailed cell morphologies (e.g. touch-detection algorithm). BSB interfaces with NEURON or NEST according to the required level of granularity of the simulation (Figure 1.7 A, B).

Macroscale simulators. Moving up to the macroscale, frameworks tailored on the simulation of subject-specific whole-brain dynamics have been implemented with the option to specify a large-scale connectome, i.e., the long-range connections between all pairs of different brain regions. In this context, Dynamic Causal Modeling (DCM) and The Virtual Brain (TVB) are reliable tools to infer on subject-specific brain dynamics (Figure 1.7 C, D).

DCM (Friston et al., 2003, 2019; Marreiros et al., 2008) is a Bayesian framework to investigate the effective connectivity, i.e., the direct mutual influence between brain regions embedded in a network either in resting-state or during a task execution. The source-data can be different types of in vivo recordings such as: rest fMRI (Friston et al., 2014), task fMRI (Havlicek et al., 2017; Rothkirch et al., 2018; Van Overwalle et al., 2020), or EEG (Murta et al., 2012). The concept behind DCM is independent from the source data: it is based on a generative model that aims to estimate parameters set representative of the effective connectivity and informed with *prior* knowledge from structural (anatomical) and functional connectivity. To achieve this purpose, it reproduces the network activity and generates the *posterior* effective connectome by maximizing the similarity between the predicted activity and the experimental recordings (Friston and Stephan, 2007; Friston et al., 2007). DCM provides an estimate of the effective connectivity accounting for the directionality of the connections, allowing to understand the causal influence of one region to another one. As a direct consequence, DCM enables an interpretation of the hierarchical organization of the brain understanding for instance which region is the driving source during a task execution and whether the information propagate in the network following backward or forward loop. DCM was developed as an inference method to compute effective connectivity assuming neural activity to be governed by the same model for all the brain (Friston et al., 2003), but recently new options allow to replace the standard neural dynamics approximation with region-specific models (Friston et al., 2019). This improvement endows more flexibility in DCM framework, enabling to perform Bayesian model comparison of physiologically plausible synaptic effects at the origins. As an example, DCM was used to infer the effective connectivity at the basis of altered oscillations recorded in Parkinson's disease by specifying different models for basal ganglia and thalamus, deeply affected by the neurodegeneration (van Wijk et al., 2018). Further, like DCM, TVB is a framework for simulating subject-specific brain dynamics starting from experimental recordings (Deco et al., 2013; Sanz Leon et al., 2013; Sanz-Leon et al., 2015). Nevertheless, the target is no more the effective connectivity, but the resting-state functional connectome. Different brain regions are remapped onto nodes and a network is reconstructed through the subject-specific structural connectome extracted from Diffusion-Weighted MRI (Schirner et al., 2015). Brain activity is reproduced through using mean field models (**section 2.2.4**) that reproduce excitatory and inhibitory oscillating activity in each node (Wong and Wang, 2006; Deco et al., 2014b). The simulated activity is converted into a functional connectivity matrix that can then be compared with the empirical functional data to assess the predictive power of the model. The model inversion mechanism to achieve this goal is designed to maximize the similarity, assessed with the Pearson Correlation Coefficient (PCC) and/or with cost functions such as the Kolmogorov distance, between the predicted and experimental activity, by tuning biophysical parameters.

Table 1. 2) Simulators pool: technical specifics and targets

	Software	First release	Programming language	Parallel computing	Mathematical models	Simulation target
Micro	**NEURON** Hines and Carnevale, 1997	1980	Core in FORTRAN, C, C++ with Python interface	Extension: CoreNeuron	Multicompartmental neurons with detailed synaptic models	Subcellular mechanisms of single neuron (microscale with high level of resolution); Detailed neuronal networks activity (mesoscale with high level of resolution)
	GENESIS Bower and Beeman, 1998	1990	Core in FORTRAN, C, C++ with Python interface	Extension: PGENESIS		
	ARBOR Akar et al., 2019	2019	Core in C++ with Python interface	Integrated		
Meso	**BRIAN** Stimberg et al., 2019	2016	Core in C++ with Python interface	Integrated	Mono/Bi-compartmental with COBA and CUBA synapses	Single point /ball and stick neuron (microscale); Spiking networks (mesoscale)
	NEST Plesser et al., 2015	1994	Core in C++ with Python interfaces (pyNEST, pyNN)	Extension: NEST 4G	Monocompartmental with COBA and CUBA synapses	Single point /ball and stick neuron (microscale); Spiking networks activity (mesoscale)
Macro	**DCM** Friston et al., 2003	2003	MATLAB SPM12 and Python	Possible integration (MATLAB and Python libraries)	Region specific MF model	Large-scale networks activity
	TVB Sanz Leon et al., 2013	2013	Python	Possible integration (Python libraries)	Generic MF model	Large-scale networks and whole-brain activity
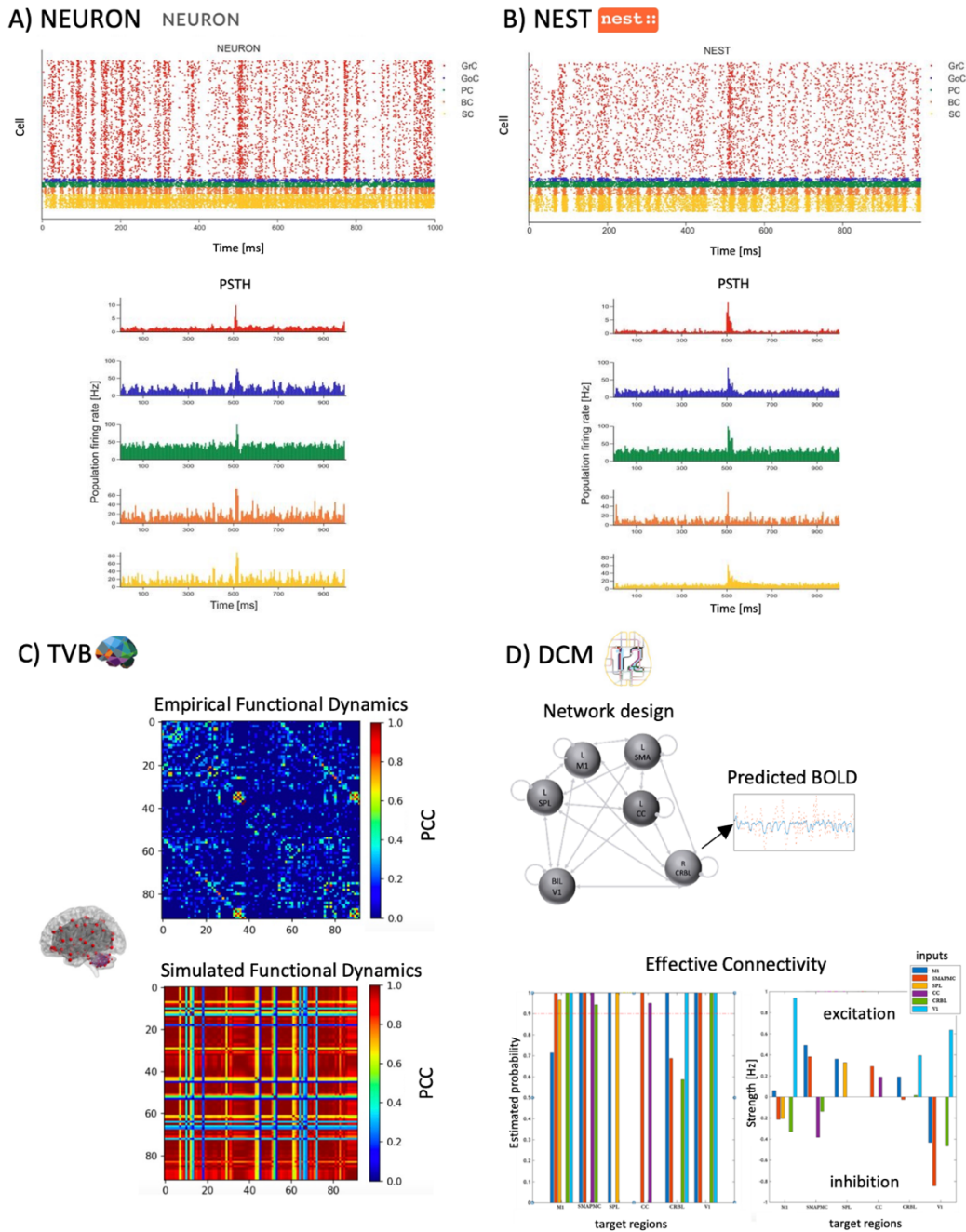
Figure 1. 7) Simulations at different scales. Mesoscale (A and B adapted form De Schepper et al., 2022) and macroscale simulations (C adapted from Palesi et al., 2020, and D). **A)** NEURON-based simulation. Mesoscale network built up with multicompartmental cells. **B)** NEST-based simulation. Mesoscale network as in A, with single point neurons. The dendritic compartments determined the differences in Peristimulus Time Histogram (PSTH) of A and B. **C)** TVB-based simulation. Whole-brain experimental and simulated functional connectivity matrices weighted by Pearson Correlation Coefficient (PCC). The similarity is assessed via global PCC. **D)** DCM-based simulation. Effective connectivity estimated with Bayesian inference in a visuomotor network. The estimate probability and its strength (positive=excitation, negative=inhibition) maximize the log-likelihood between experimental and predicted BOLD.

The polyhedric Mean Field formalism

Mean field (MF) theory has its roots in physics and statistics (Kadanoff, 2009; Parr et al., 2020) but it is widely used in many other disciplines such as mathematics to explain macroeconomics with mean field games theory (Nourian and Caines, 2013; Barreiro-Gomez and Tembine, 2019; Cardaliaguet and Porretta, 2020; Carmona, 2021), artificial intelligence from the origins to the nowadays sophisticate deep learning algorithms (Gabrié, 2020), epidemiology with a large application to study COVID-19 outbreaks (Tembine, 2020; Gao et al., 2021; Lee et al., 2022; Olmez et al., 2022; Petrakova and Krivorotko, 2022), and neuroscience to model brain network activity (Destexhe and Sejnowski, 2009; El Boustani and Destexhe, 2009; Coombes and Byrne, 2019; Bick et al., 2020; Parr et al., 2020; Byrne et al., 2022). The present chapter reports the basics of MF theory (**section 2.1**), some examples of applications in different fields to underline the polyhedric attitude of this formalism (**section 2.2**), and an extensive overview of the formalism used in neuroscience to investigate neuronal activity (**section 2.3**).

2.1 Mean field theory at-a-glance

The rationale at the basis of MF theory is to simplify the dynamic of a complex system, which arises from the activities of several different elements, by assuming it equal to the mean activity of *many particles*. The practical advantage is the reduction of a so called many-body problem into a one-body problem by replacing the one-to-one interactions between the *particles* with an average interaction. The many-body problem is usually described with the Hamiltonian form:

$$H_N = \sum_j^N F_j + \frac{1}{N} \sum_{j,k}^N S_j \cdot S_k$$

(3)

With F_j = free energy of particles j, S = interactions force between particles j and k, and N = total number of particles in the system. In the MF approximation, the interaction of a certain particle j with each of the others k particles (with k = [1, N]) is replaced by the interaction with the *mean field* of forces generated by all the k particles (⟨S⟩).

Therefore, the MF theory neglects the microscopic details (i.e., the between-*particles* fluctuations) yielding the MF Hamiltonian (H_{MF}):

$$H_{MF} = \sum_{j}^{N} F_j + S_j\langle S\rangle$$

(4)

2.1.1 The Ising Model

Considering the *particles* as the molecules, and a ferromagnet as a complex system where the spins can interact in different configurations, MF theory could be used to describe the macroscopic states of ferromagnets, i.e., the magnetization, in relation to variation of temperature. Analogy between this state transitions and brain dynamics has been widely studied with a multidisciplinary approach both by physicist and neuroscientists (Tkacik et al., 2006). The Ising model relies on MF approximations and it has been already exploited to provide a statistical descriptions of spiking neural networks (Schaub and Schultz, 2012; Spreemann et al., 2018). Ferromagnets molecules, as the neuron in the brain, can interact each other, or being influenced by an external magnetic field. The Hamiltonian of the Ising model is:

$$H = -\frac{1}{2}\sum_{i\neq j=1}^{N} JS_iS_j - \sum_{i=1}^{N} h_iS_i$$

(5)

With S_i is the spin of the i-th molecule (e.g., Si = +1 for spin oriented upwards), J is a constant modeling the force and h_i is the external magnetic field that acts on the molecule i. The first term considers the spin-spin interactions between different molecules while the second the interactions with the external magnetic field h_i. It is worth notice that, due to the first term, it is not a one-body problem. Indeed, to study ferromagnet states, it is essential to understand how the microscopic phenomena as the spin-spin interactions result in a magnetization which can be observed at a macroscopic level. Spin-spin interactions leading to ferromagnet states changes can be considered analogue to the neuronal mechanisms that occurs at a microscale and impact onto the whole-brain dynamics recorded in vivo.

Ferromagnets magnetization can be computed with a partition function. Considering a null external magnetic field for the sake of simplicity, the Hamiltonian is reduced to the spin-spin interaction term, and the partition function of the resulting Ising model at a certain temperature T is:

$$Z = \sum_{C} e^{-\beta H(C)}$$

(6)

Where $e^{-\beta H(C)}$ is the Boltzmann factor with $\beta = 1/kT$ (k = Boltzmann' constant, T = Temperature) and H(C) is the Hamiltonian that depends on the spin configurations C. The index C indeed, includes all the possible configuration of the spin orientation (e.g., one spin up and the others down, two spin

up and the others down,....., all spin up,....all spin down – Figure 2.1), resulting in 2^N number of configuration with N = molecules number with an order of 10^{23} (as Avogadro number) or higher.
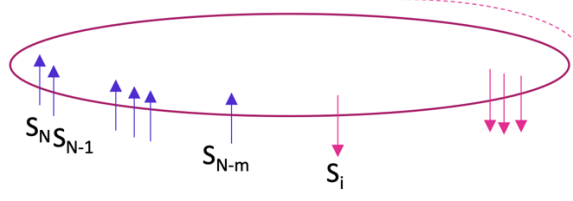
Figure 2. 1) 1D Ising Model. S_i is the spin of the molecule i which can be +1 or -1. All possible configurations with the interacting spins should be considered resulting in 2^N possibilities with N = number of molecules. Ising model for magnetization, based on mean field approximation, consists in replacing spin-spin interactions with spin-mean field interactions.

Therefore, it is very complicate to handle the partition function in equation (6) and using a MF approximation simplifies this problem. Under the MF approximation, the spin fluctuations around the mean are assumed to be negligible, resulting in the local mean magnetization:

$$m_i = \langle S_i \rangle = \frac{1}{N} \sum_i^N S_i$$

(7)

Under the MF hypothesis it is possible to replace the spin-spin interaction with the interaction between each spin and the mean of the magnetic field. Therefore, the Hamiltonian, considering the hypothesis of a null external magnetic field, can be written as:

$$H_{MF} = -\frac{1}{2} \sum_{i,j}^N J\big(S_i \langle S_i \rangle + S_j \langle S_j \rangle \big)$$

(8)

This H_{MF} is of one-body type and plugged into equation (6) allows to compute the mean total magnetization:

$$M = \frac{1}{N} \sum_C S_i e^{-\beta H_{MF}(C)}$$

(9)

MF approximation simplifies the computation of the macroscopic state changes (i.e., the magnetization) caused by microscopic mechanism (i.e., the (dis)alignment of the spins) with a mathematically and computationally advantageous strategy, by reducing the one-one interactions, to a one-vs-mean field interactions. Applied to brain networks, where the activity of each neuron is regulated by a differential equation in the simplified case of point neurons, MF approximation

replaces the neuron-neuron interaction, with neuron-mean field ones, making computationally feasible the simulations of large-scale brain dynamics (Ruffini and Deco, 2021).

2.2 Mean field applications

The Ising model to derive the magnetization of a ferromagnet has been explained in **section 2.1** pointing out the analogy between spin interactions in a ferromagnet and neuron interactions in the brain. However, MF theory has a widespread application in cross-cutting fields (Figure 2.2), whenever an effective approximation of a complex system is needed.

2.2.1 MF game theory: macroeconomics

Game theory is a mathematical framework that models a competition with the strategic interactions among many players whose influence on the overall system is neglectable. These players are indistinguishable in the system because they are identical meaning that they compete with symmetrical payoffs (equal probabilities of win or lose)(Petrosjan and Zenkevich, 1996; Greif, 2010). Considering the players as the molecules of a ferromagnet, the analogy between MF and game theory results clear (**section 2.1**). Thus, MF has been integrated with game theory for studying the strategic decision making and used to tackle many issues in different topics (Achdou et al., 2012; Cardaliaguet and Porretta, 2020). As an example, MF integrated with game theory has found a widely spread application in economy to study markets and price evolution as well as in finance to address issues such as the systemic risk and bank runs (Carmona, 2021). Going into detail, MF game theory is suitable for study macroeconomics that deals with large-scale economy (e.g., the economy of an entire country). Firms are heterogenous characters but can be approximated as identical players within microstates in the global system represented by the world trading scenario. With this hypothesis, a MF game model can be constructed based on statistics that describe the evolution of a market fluctuation. Consequently, the world-wide trend of a specific market can be analyzed with MF game theory to predict for instance the risk of certain investments or the growth opportunities.

2.2.2 MF in technology: smart approach to the artificial intelligence

Artificial intelligence allows a computer to learn information from input data and to answer to a certain question, without an *ad hoc* program written for an *ad hoc* issue. Machine learning exploits the computational capability to address the so-called learning problems such as classification or object identification. The mathematical description of a learning query includes a lot of interacting random variables. This description of the learning variables recalls the one of the molecules (**section 2.1**), thus MF strategies could extend to learning topics (Gabrié, 2020). Since MF is an approximation theory, learning procedures integrating MF assumptions requires a lower number of epoch with respect to techniques as the back propagation learning (Peterson and Hartman, 1989). Hence, MF have been conveniently applied to reinforcement learning to solve tracking problem of multi-agent interaction, by considering the average of the influences of the neighbors on the target agent (Zhou et al., 2021). Furthermore, MF-based training algorithms could be used to train shallow neural network (Wojtowytsch and E, 2021) and, going more into technical details, to analyze the dynamic behind the learning by approximating the Stochastic Gradient Descent[2] with the mean field

---

[2] Stochastic Gradient Descent (SGD) is an optimization methods that replace the gradient descent with a stochastic approximation computed on a randomly chosen subset of data (Bottou, 2012).

distribution of neural network parameters (Mei et al., 2018). This approximation is insensitive to the number of hidden units (i.e., hidden neurons of a neural network) and considers the statistical distribution of the neural network parameters rather than their specific value, with the advantage of focusing on global aspect such as the global convergence (Mei et al., 2019).

2.2.3 MF in epidemiology: the fight against COVID-19

Corona Virus Disease 2019 (COVID-19) is a severe acute respiratory syndrome caused by the coronavirus SARS-CoV-2 (Severe Acute Respiratory Syndrome CoronaVirus). The pandemic affected not only people health but also the social rules and the habits of the entire world, forcing the authority to take prompt decisions about the healthcare but also the economy and the local migration (Petrakova and Krivorotko, 2022). In this difficult and uncertain context, modeling strategies represented an effective way to predict the outline of the complicated situation. Compartmental models have been suggested in literature to simplify the complexity of infectious diseases by assuming homogeneous populations and neglecting the characteristics of individual factors (Gao et al., 2021; Lee et al., 2021; Olmez et al., 2022). The homogeneity assumption makes the MF theory suitable and useful to build up effective models in short time to investigate different aspects of COVID-19. MF theory, indeed, was exploited to predict the evolution of COVID-19 adapting the formalism from physics and the evolution of particles state to the society and the factors that affect people decision. MF theory was integrated with game theory (**section 2.2.1**) transforming the evolving-states into payoffs for the decision-making concerning the security during the pandemic. (Tembine, 2020). The same strategy was applied to tackle the issue on vaccine distribution to optimize the transportation considering the cold-chain, the cost and the limited vaccine supply (Lee et al., 2022).
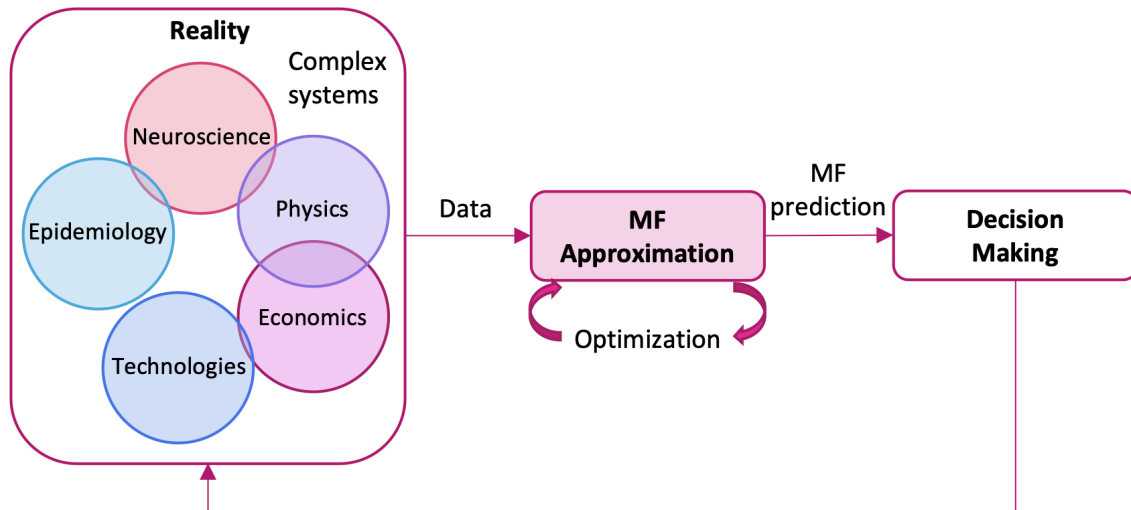
Figure 2. 2) MF applications in cross-cutting fields. Reality is built up by complex system that are suitable for the MF approximations. Data about the states transitions of the complex system of the reality could constitute an input base for MF model (e.g., Economics: interactions between orthopedic companies). The MF prediction (e.g., Economics: the trend of the planned surgeries) can be used in decision making processes (e.g., Economics: how many prostheses to be produced) that in turn influence the reality (e.g. Economics: the price of the orthopedic prostheses, influencing the interaction between orthopedic companies) and its complex system in a closed loop configurations.

2.2.4 MF in neurosciences: simulate the brain

The same approach linking molecules microscopic properties to the macroscopic states has been applied to neurosciences to derive a model based on single neuron activity and to plug it into whole-brain dynamics simulator, bridging the gap between micro and macroscale. Moreover, experimental signals could be recorded with a mesoscale resolution ranging from nanometers to millimeters. Local field potential measured in mice specimens, for instance, are recorded using a multielectrode array, calcium imaging, voltage-sensitive dye signals that have a nanometric resolution, as well as the voxel (3D pixel) of a volumetric image obtained with MRI (Figure 2.3). The signal extracted from pixel/voxel of these imaging techniques represents the averaged activity over an ensemble of neurons, therefore a mesoscale model represents the most appropriate formalism to simulate that kind of signals avoiding slowing down the simulations with an extra-resolution that is not required by the nature of the experimental data. Thus, MF allows a direct comparison with studies based on different imaging techniques. Taken together the analogy between physics particles with neurons and the mesoscale resolution of many kinds of the experiments, MF models perfectly fit with the goal of simulate those signals, providing a powerful tool to investigate brain dynamics.
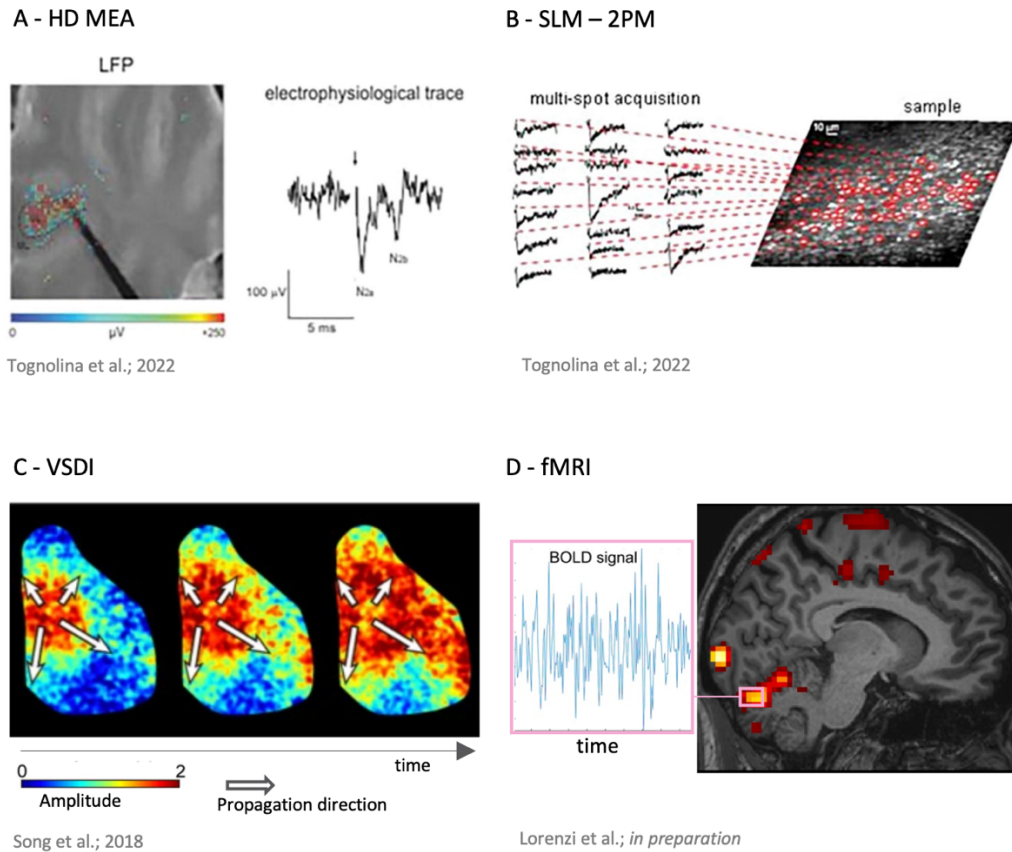
Figure 2. 3) Experimental recordings at mesoscale. Mean field models allow a direct comparison with signals recorded at mesoscale with different techniques. **A)** Local Field Potential (LFP) recorded with High Density Multielectrode array (HD-MEA) from acute cerebellar slice evoked with a stimulus on mossy fibers. **B)** Stimulus-induced calcium signals recorded with two-photon spatial light modulator microscopy (SLM-2PM) from mice granular layer. **C)** Spatiotemporal map of the spontaneous neural activity recorded with Voltage sensitive-dye imaging (VSDI) *in vivo* from mice. **D)** BOLD signal acquired with fMRI in a human brain. Mean field predictions can be directly compared with the BOLD extracted from few voxels and different mean field modules can be connected to reproduce the activity of a large-scale network.

Furthermore, MF as generative models have been already integrated into TVB and DCM frameworks (**section 1.2.3**), where a single module of the cortex is represented with a single MF, hence different cortical partitions, i.e., different MFs, are connected each other with long-range connections reproducing large-scale connectome. In practice, the regions considered in a certain simulation are schematized as network nodes behaving as coupled oscillators (Bick et al., 2020). It is worth mentioning that these large-scale simulations are computationally demanding, with computational load that increases proportionally to the level of resolution. MF approximation represents a convenient formalism because it describes the collective dynamics of neuronal populations embedded in oscillator network with only few collective variables. Although these variables take into account the single neuron biological features, the resulting equations are sufficiently simple to analyze brain dynamics without great computational effort (Bick et al., 2020). A widely used MF model integrated in TVB is the Wong-Wang model that simplifies a network of 7200 neurons into a two nodes network (one excitatory and one inhibitory) (Wong and Wang, 2006; Deco et al., 2014b). TVB with Wong-

29

Wang as generative model was used to have an insight on physiological brain dynamics, assessing the importance of the cerebellar impact in cerebral activity of healthy volunteers, (Palesi et al., 2020) (**see section 4.2.3** for an insight into the method), but also in pathological dynamics as for the investigation of limbic network changes in dementia (Zimmermann et al., 2018) or the excitation/inhibition profile in Alzheimer's patients (Monteverdi et al., 2022). Furthermore, a MF model has been developed specifically to investigate epileptic seizures, based on bifurcations analysis and tuned on epilepsy features (Jirsa et al., 2017; Houssaini et al., 2020) confirming the high impact of modelling in personalized medicine. More sophisticate MF models have been embedded in TVB, to provide a clear link with neuronal spiking activity (Deco et al., 2008; Di Volo et al., 2019). As an example, the TVB-AdEx (Figure 2.4) uses a MF formalism whose functional reference is represented by Adaptive Exponential (AdEx) point neuron model explained in detail in **section 2.3.3** and includes complex phenomena as the adaptation (Di Volo et al., 2019).
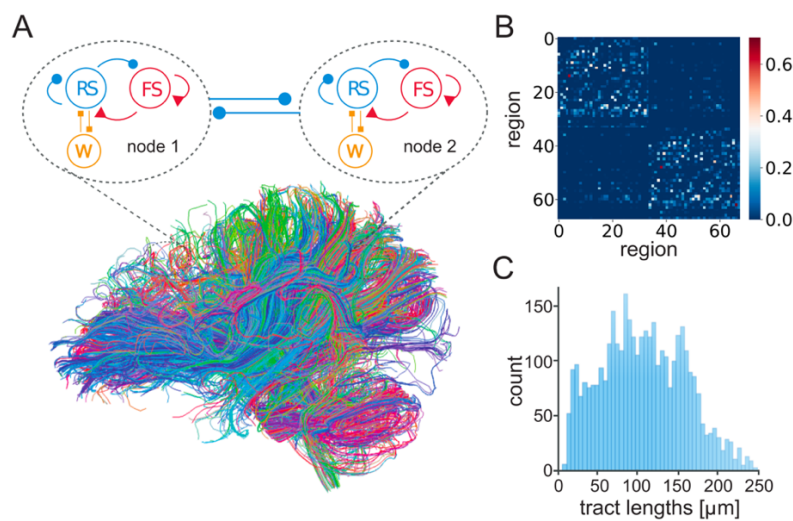
Figure 2. 4) TVB-AdEx (Goldman et al., 2021). The nodes of the network were represented as MF modules **(A)** including an inhibitory fast spiking (FS in red) population and an excitatory regular spiking (RS in blue) whose activity is modulated by adaptation (W in orange). The connections between MF modules were set up based on the large-scale connectome. The number of fibers connecting different brain regions was extracted from tractography data and normalized on cortical gray matter region **(B)**. To enrich the model with transmission, delay distribution has been inferred based on tract lengths between interconnected nodes **(C)**.

TVB-AdEx reproduced asynchronous irregular state seen experimentally in wakefulness as well as up-down states that characterize slow-wave sleep (Goldman et al., 2020, 2021).

MF modeling approach used in the present thesis relies on the work of El Boustani and Destexhe which was developed for conductance-based networks to design a MF model by deriving a Master Equation for the activity of the network (El Boustani and Destexhe, 2009). As proof of the effectiveness of MF approximations applied to the brain, this formalism is not the only MF technique but many other MF formalisms have been developed with the same goal of simplifying the complexity of the brain with comparable reliability (Montbrió et al., 2015; Devalle et al., 2017; Coombes and Byrne, 2019). The present work is inspired by El Boustani and Destexhe 2009 for consistency with what has been already done for TVB-AdEx (Di Volo et al., 2019; Goldman et al., 2020) in the perspective of creating a pool of region-specific MFs ready to be integrated in whole-brain dynamics simulator.

MF approximation up to the second order is detailed in the following section, reporting the Master Equation formalism explained in El Boustani and Destexhe 2009, aiming at clarifying how the mean and the covariance of a system can provide a reliable description of the complex state resulting from Spiking Neural Network (SNN) built up with highly stochastic excitatory and inhibitory neurons

2.3 Master Equation formalism

A master equation is a mathematical formalism to describe the time evolution of a system. In this context, the master equation framework presented by El Boustani and Destexhe (El Boustani and Destexhe, 2009) is summarized to explain the mathematical ground used for the present thesis. The target of this kind of formalism is the evolution of a neuronal population dynamics, and the statistical approach of mean field theory aims to write a master equation to describe the time evolution of the neuronal activity expressed in terms of probability to spike. From master equation, a mean field model has been derived in term of second order differential equations modeling the time evolution of the mean activity of the network accounting for its standard deviation and autocorrelation (**section 2.3.1**). The core of the theory is the Transfer Function (TF), which is a mathematical construct to map the output firing rate of the neuron as a function of the presynaptic input rates with the advantage of a continuous description of the network activity related to the neurons spiking activity. Furthermore, a master equation is a flexible formalism applicable to any type of neurons with a mathematically characterizable TF. To proceed with the description of the master equation formalism, some assumptions should be clarified. The macroscopic dynamics is assumed to be Markovian, meaning that the state of the system at time t depend only on the state at time t-1, i.e., the system is memoryless (i). The firing rates of neurons belonging to a certain population are Gaussian-distributed (ii) and the system reaches the steady-state within a period T (adiabatic hypothesis in physics) (iii).

Even though the flexibility of the master equation formalism reported here, some issues still exist. A still open challenge is the definition of a timing period T which should be either appropriate to simulate biological dynamic and to fulfill the assumptions (i) and (ii) (**section 2.3.2**). On top of that, the TF is a complex mathematical construct that is analytically known only for CUBA model (**section 1.2.2**). Here a heuristic approach developed by Zerlaut and colleagues (Zerlaut et al., 2016, 2018) to determine an analytical TF with a semi-analytic framework is presented (**section 2.3.3**) as mathematical and computational ground for the multi-layer cerebellar model developed and presented in **Chapter 3.**

2.3.1 From the master equation to the second order mean field

The goal of the formalism developed by El Boustani and Destexhe is to write a master equation that provides a statistical summary of a spiking activity, assuming the network constituted by K homogeneous populations. Therefore, the first *ingredient* needed is an equation that models the behavior of a spiking population (i.e., the state of a population in the network):

$$m_\gamma(t) = \lim_{\Delta t \to 0} \frac{n_\gamma(t - \Delta t, t)}{\Delta t N_\gamma}$$

(10)

31

Where ɣ is one of the K population and ranges from 1 to K, m is the spiking activity of the population ɣ at time t, n_γ is the number of spikes in the time interval t-Δt, N_γ is the number of neurons in population the ɣ. The spiking activity (equation 10) can be interpreted as the number of neurons that fire at least one time in a short period of fixed duration T. Therefore, T has to be large enough to guarantee at least one spike and shorter enough to avoid signal correlation in two adjacent time windows, i.e., the memoryless system. The probability of firing can be written as marginal probability given the network state in the time interval t-T. Assuming time invariance of the system, the conditional probability of firing depends only on T:

$$P\big(\{m_\gamma(t)\}\big|\{m'_\gamma(t - T)\}\big) = P_T\big(\{m_\gamma\}\big|\{m'_\gamma\}\big)$$

(11)

Where P_T is the probability of the system to be in a certain state m within a time window T, given the state in the precedent T.

According to MF approximation the pairwise correlation could be neglected, therefore equation (11) can be split as the product of marginal probabilities describing each variable exclusively.

$$P_T\big(\{m_1\}\big|\{m'_\gamma\}\big) * P_T\big(\{m_2\}\big|\{m'_\gamma\}\big) * \dots * P_T\big(\{m_K\}\big|\{m'_\gamma\}\big)$$

(12)

The Markov transition (W) under the assumption of a memoryless system is defined as the rate of transition from m_γ to m'_γ, and using the conditional probability density in equation (12) results in:

$$W\big(\{m_\gamma\}\big|\{m'_\gamma\}\big) = \lim_{T\to 0}\frac{P_T\big(\{m_\gamma\}\big|\{m'_\gamma\}\big)}{T} = \lim_{T\to 0}\frac{\prod_{\alpha=1}^{K} P_T\big(\{m_\alpha\}\big|\{m'_\gamma\}\big)}{T} = \frac{\prod_{\alpha=1}^{K} P_T\big(\{m_\alpha\}\big|\{m'_\gamma\}\big)}{T}$$

(13)

With α index denotes a population and it ranges from 1 to K as ɣ. The computation of $P_T\big(\{m_\alpha\}\big|\{m'_\gamma\}\big)$ leads to a fully-specification of the model and, to achieve this goal, it was assumed the quasi-stationary evolution of the network as for the adiabatic transformation in physics. This means that during the time interval T the system reaches a stationary state that is determined only by the previous state at a time T earlier. Therefore, T has to be small enough to satisfy the adiabatic approximation, but large enough to ensure the independency of signals in two adjacent time windows to split $P_T\big(\{m_\gamma\}\big|\{m'_\gamma\}\big)$ into products of marginal probabilities. By merging equations (12) and (13), the master equation has been defined to describe the population activity describing its evolution with a differential equation modelling the firing probability distribution density:

$$\partial t P_t\big(\{m_\gamma\}\big) = \prod_{\alpha=1}^{K}\int_0^{\frac{1}{T}} dm'_\alpha \big(P_t\big(\{m'_\gamma\}\big)W\big(\{m_\gamma\}\big|\{m'_\gamma\}\big) - P_t\big(\{m_\gamma\}\big)W\big(\{m'_\gamma\}\big|\{m_\gamma\}\big)\big)$$

(14)

The master equation is not exactly solvable, but it is possible to derive a description of equation 14 through the mean, the variance, and the correlation of the network activity.

The following second order differential equation system was yielded:

$$\begin{cases} \partial_t \langle m_\gamma \rangle = a_\mu(\{\langle m_\gamma \rangle\}) + \dfrac{1}{2}\partial_\lambda \partial_\eta a_\mu(\{\langle m_\gamma \rangle\})c_{\lambda\eta} \\ \partial_t c_{\mu\nu} = a_{\mu\nu}(\{\langle m_\gamma \rangle\}) + \partial_\lambda a_\mu(\{\langle m_\gamma \rangle\})c_{\nu\lambda} + \partial_\lambda a_\mu(\{\langle m_\gamma \rangle\})c_{\mu\lambda} \end{cases}$$

(15)

Where:
$\langle m_\gamma \rangle$ = mean population activity
$c_{\mu\nu} = (m_\gamma - \langle m_\gamma \rangle)(m_\nu - \langle m_\nu \rangle)$ = covariance of population activity (variance when μ=ν)
$a_\mu(\{\langle m_\gamma \rangle\})$ and $a_{\mu\nu}(\{\langle m_\gamma \rangle\})$ = step moment functions for the population activity and for the interactions between populations respectively. They are defined as:

$$a_\mu(\{\langle m_\gamma \rangle\}) = \int_0^{\frac{1}{T}} dm'_\mu (m'_\mu - \langle m_\mu \rangle)\frac{P(m'_\mu|\{\langle m_\gamma \rangle\})}{T}$$

(16)

$$a_{\mu\nu}(\{\langle m_\gamma \rangle\}) = \int_0^{\frac{1}{T}} dm'_\mu \int_0^{\frac{1}{T}} dm'_\nu (m'_\mu - \langle m_\mu \rangle)(m'_\nu - \langle m_\nu \rangle)\frac{P(m'_\mu|\{\langle m_\gamma \rangle\})P(m'_\nu|\{\langle m_\nu \rangle\})}{T}$$

(17)

The second-order system (15) is completed by including the correlation (*Corr*), that for the steady state results:

$$\partial_\tau Corr_{\mu\nu}(\tau) = \partial_\lambda \alpha_\nu(\{\langle m_\gamma^{stat} \rangle\})Corr_{\mu\lambda}(\tau)$$

(18)

With α_ν computed according to equation (16) and $\langle m_\gamma^{stat} \rangle$ is the solution at the stationary state of the first equation of system (15).

So far, the master equation (14) has been derived assuming a network with gaussian distributed firing rate of the embedded neurons, and Markov process (memoryless system) that reaches the quasi-steady state within T (adiabatic approximation). Then, thanks to these assumptions, the differential equations for the statistical moments have been derived (mean, and covariance in equation (15) and correlation in equation (18)). What is still missing is a specification of the transition operator W that is obtained by the definition of $P_T(\{m_\alpha\}|\{m'_\gamma\})$. Since W models the transition between two states of the neuronal network, it depends directly on the neuron properties. It is known that a neuron embedded in a network is exposed to a synaptic bombing from the other neuronal populations, therefore the

transition can be described by using a Transfer Function (TF)(Kuhn et al., 2004). This mathematical construct maps the neuron output activity taking in input the activity of the other presynaptic populations. As consequence of the adiabatic hypothesis and assuming to know the stationary TF of a population α, the probability of firing during a period T can be written as:

$$p_\alpha(\{m'_\gamma\}) \cong \nu_\alpha(\{m'_\gamma\})T \le 1$$

(19)

Furthermore, since during the period T a neuron can fire only one time, the binomial distribution describes well the conditional probability. In the case of a very strong interneurons correlations, the binomial distribution is no more appropriate, therefore it should be chosen another function to model the conditional probability. The number of neurons in population α was assumed large enough to ensure the gaussian distribution of the firing rate. With these considerations, the moments step function and its differentials can be written as:

$$a_\mu(\{\langle m_\gamma \rangle\}) = \frac{1}{T}(\nu_\mu - \langle m_\mu \rangle)$$

$$\partial_\lambda a_\mu(\{\langle m_\gamma \rangle\}) = \frac{1}{T}(\partial_\lambda \nu_\mu - \delta_{\mu\lambda})$$

$$\partial_\lambda \partial_\eta a_\mu(\{\langle m_\gamma \rangle\}) = \frac{1}{T}\partial_\lambda \partial_\eta \nu_\mu$$

(20)

Where $\nu_\mu = \nu_\mu(\{\langle m_\gamma \rangle\})$ is the TF of the neuron in population μ which depends on the mean of the activity of each population (ɣ = [1, K])

Equations of the system (20) provide a complete description of the master equation formalism, resulting in a set of differential equations that are the mean field system to describe the behavior of a spiking neural network in a continuous time domain:

$$\begin{cases} T\partial_t \langle m_\gamma \rangle = (\nu_\mu - \langle m_\gamma \rangle) + \frac{1}{2}\partial_\lambda \partial_\eta \nu_\mu c_{\lambda\eta} \\ T\partial_t c_{\mu\nu} = \delta_{\mu\nu} A_{\mu\mu}^{-1}(\nu_\mu - \langle m_\gamma \rangle)(\nu_\nu - \langle m_\nu \rangle) + \partial_\lambda \nu_\mu c_{\nu\lambda} + \partial_\lambda \nu_\nu c_{\mu\lambda} - 2c_{\mu\nu} \\ T\partial_\tau Corr_{\mu\nu}(\tau) = (\partial_\lambda \nu_\nu(\{\langle m_\gamma^{stat} \rangle\}) - \delta_{\lambda\nu})Corr_{\mu\lambda}(\tau) \end{cases}$$

(21)

2.3.2: The choice of the time constant T: an open challenge

A sensitive issue for this formalism is represented by the choice of the value T that in line of principle could be arbitrarily chose within the constrain of Markov hypothesis. For a memoryless system one neuron produces at most one spike in a time window of length T. With an increasing size of the

network, the time constant T can take smaller values because the temporal finite-size effect[3] in the autocorrelation vanishes because of sparse connectivity (Brunel, 2000). The formalism described in **section 2.3.1** addresses this issue for sparsely connected networks, that are large enough to avoid temporal correlation finite-size effects and, at the same time, small enough to require second-order statistics to describe its population dynamics. However, T value should be chosen considering that a too large value might lead to an underestimation of the firing rate in high activity regimes, while a too small value could overestimate the second-order statistics, i.e., the correlation between different population.

It is crystal-clear that the choice of T is critical for the MF formalism. Based on literature T ranges from 5 to 20 ms (Zerlaut et al., 2018; Di Volo et al., 2019). The firing rate of one neuron is 1/T, therefore for a choice of T = 20 ms, the MF dynamic is not very fast with a maximum firing rate of 50 Hz, resulting in a MF that addresses to slow dynamics as the cerebral ones. Hence, the choice of T is essential for the nature of this formalism, and it should also consider the speed that characterized the dynamics of the region(s) target for the simulation.

2.3.3 Heuristic approach: AdEx mean field model

The choice of an optimal value of T is not the only challenge of the master equation formalism explained in **section 2.3**. The limit of the master equation (14) is that TF is a function analytically known only for very simple systems like a network of leaky integrate and fire neurons with CUBA synapses (**section 1.2.2**). To overcome this drawback, a heuristic approach was developed by Zerlaut and colleagues (Zerlaut et al., 2016, 2018) making the formalism suitable also for more complex and conductance-based models. This formalism used a "semi-analytic" approach to get an analytic TF, which consists of computing a numerical template for the transfer function (i.e., a matrix) from other simulator tools as NEST or Brian and then fits the polynomial form on the numerical template (Zerlaut et al., 2016). As a result, a sort of analytical TF was obtained, even if its parameters were not general but specific to the neuron model used to compute the numerical template. Nevertheless, this approach allowed to get an analytically solvable simple system able to capture complex neuronal dynamics (Zerlaut et al., 2018; Di Volo et al., 2019; Carlu et al., 2020). Zerlaut and colleagues provided an effective pipeline (Figure 2.5) to build up a generic MF for the cortex. Specifically, the MF model built up following this heuristic approach was derived from a network of AdEx neurons as described in detail in the next sections.

---

[3] Finite size effects refer to a systematic error introduced by the approximations done to study system with many degrees of freedom

A - Single neuron

Neuron models:
AdEx, LIF, E-GLIF…

Parameters:
Membrane voltage,
Membrane capacitance
….

B - Spiking network

Conductance models:
Exponential, alpha …

Parameters:
Synaptic convergence,
Quantal conductance
….

C - Mean Field model

Mean Field equations

Transfer Function
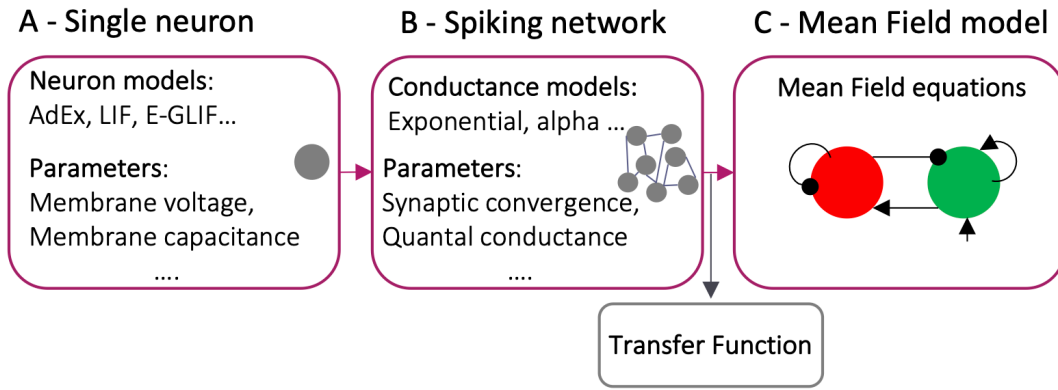
Figure 2. 5) Pipeline to design a generic cortical Mean Field model. A) The single neuron model is chosen (e.g., AdEx, LIF, E-GLIF) according to the single cell features of interest for the target region of the mean field. **B)** A spiking network is constructed with single neurons. The synaptic model regulates the connections between single neurons embedded in the network (e.g., alpha synaptic model, exponential synaptic model). **C)** The MF network is designed using the spiking network as functional reference. Here, a single layer recurrent MF network is shown, with one excitatory population (green), which receives external input, and one inhibitory population (red).

AdEx model. AdEx is a point neuron conductance-based model which includes an exponential and an adaptive variable that improves the realism of the modelled activity, capturing a wide variety of intrinsic neural properties like regular spiking, bursting neurons and delayed firing. AdEx is an appropriate choice for simulating cerebral cortex dynamics because it reproduces excitatory regular spiking (RS) as well as inhibitory fast spiking (FS) that are commonly found in pyramidal neurons and inhibitory interneurons respectively (Zerlaut et al., 2018). The model is made up of two coupled equations (Brette and Gerstner, 2005):

$$
\begin{cases}
c_m \dfrac{dV}{dt} = g_L(E_L - V) + g_L k_a e^{\frac{V - V_{thre}}{k_a}} - I_w + I_{syn} \\
\tau_w \dfrac{dI_w}{dt} = -I_w + a(V - E_L) + \sum_{t_s \in \{t_{spike}\}} b\delta(t - t_s)
\end{cases}
$$

$$(22)$$

Where V = voltage of the AdEx neuron, C_m = membrane capacitance (pF), g_L = leakage conductance (nS), E_L= rest potential (mV), k_a = spike sharpness (mV), V_{thre} = threshold potential (mV), I_w = adaptation current, which evolution is modelled in the second equation, I_{syn} = synaptic current, τ_w = adaptation time constant (ms), a = adaptation conductance (nS), b = adaptation current increment (pA), δ = Dirac function. At time t_s, V reaches $V_{thre}+5k_a$ and a spike is triggered. For the refractory period set at 5 ms ,V is set at the value of E_L and I_w is incremented by b (Zerlaut et al., 2018).

The AdEx equations (22) were used to design a mono-layer network as a very simple construct collapsing neuron types into two populations, one excitatory (RS) and one inhibitory (FS) (Figure 3C). Although this network was a big simplification, without many physiological details specific for

a certain type of neurons, it accounted for the higher excitability of inhibitory neurons compared to the excitatory ones that is a relevant feature in brain cortical dynamics simulations.

Spiking Network. A network with AdEx point neurons was built up to be employed as functional reference for the TF formalism. The synaptic model used to regulate the connections between neurons embedded in the network was the exponential model:

$$I_{syn}(V,t) = \sum_{s \in \{e.i\}} \sum_{t_s \in \{t_{spike}\}} Q_s(E_s - V) \, e^{-\frac{t-t_s}{\tau_s}} \mathcal{H}(t - t_s)$$

(23)

Where s is the population index that can be e = excitatory (RS) or i = inhibitory (FS); Q = quantal synaptic conductance, E = reversal potential, τ_{syn} = synaptic time decay and $\mathcal{H}$ = Heaviside function. This equation models the synaptic trend with an exponential function and permits to specify different synaptic properties as Q and τ_{syn} tailored on the different populations included in the network.

MF model: Transfer Functional formalism. The mean field model implemented by Zerlaut and colleagues (Zerlaut et al., 2018) aiming at simulating the cortical activity by collapsing the different neurons type into two populations, one inhibitory and one excitatory (Figure 2.6).

Therefore, two different TFs, one for an inhibitory FS neuron and the other for excitatory RS neuron, were implemented with the same procedure but accounting for the different nature of these two categories. The heuristic approach to the TF computation relies on the fitting of the TF expression, indicated for sake of simplicity with F in the equations, and reads (Zerlaut et al., 2016):

$$\nu_{out} = F_p(\nu_s) = \frac{1}{2\tau_V} erfc\left(\frac{V_{thre}^{eff} - \mu_V}{\sqrt{2}\sigma_V}\right)$$

(24)

Where ν_{out} = output activity, i.e. the Transfer Function of a neuron embedded in the population p, and it is function of its presynaptic inputs; μ_V = average of membrane potential fluctuation, σ_V = standard deviation of membrane potential fluctuations, τ_V = autocorrelation time of membrane potential fluctuations; $erfc$ = Gaussian error function; V_{thre}^{eff} = phenomenological firing threshold modelling the single neuron non linearities, i.e., the deviation from its baseline behavior (Zerlaut et al., 2016).
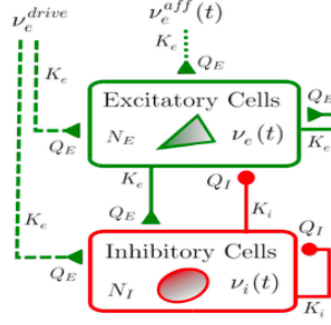
Figure 2. 6) Mean Field Network (Zerlaut et al., 2018). Excitatory population (green square) and Inhibitory population (red square) with excitatory (green arrows) and inhibitory connections (red arrows). Parameters shown are: ν_s = population activity [Hz], K_s = mean synaptic convergence, Q_s = quantal synaptic conductance [nS], N_s = number of neurons in population s. Index s indicated the population: s = [e, i]. External input is modeled as a constant input (ν^{drive} [Hz]) and a time-evolving input (ν^{aff}(t) [Hz]), targeting excitatory population.

The statistical moments μ_V, σ_V, τ_V were computed integrating the contribution of the average population-specific conductance, which includes the connectivity parameters as the mean synaptic convergence, together with the quantal synaptic conductance and synaptic time decay (section **Spiking Network**). Therefore, the average population-specific conductance was computed for excitatory (μ_{Ge}) and inhibitory (μ_{Gi}) populations and used to define the total average population conductance (μ_G) that also includes the leakage current ($I_L = g_L E_L$):

$$\mu_{Ge}(\nu_e, \nu_i) = K_e \tau_e Q_e \nu_e$$

$$\mu_{Gi}(\nu_e, \nu_i) = K_i \tau_i Q_i \nu_i$$

$$\mu_G(\nu_e, \nu_i) = \mu_{Ge} + \mu_{Gi} + g_L E_L$$

$$(25)$$

In addition to the synaptic parameters, the average population conductance μ_G depends directly on the presynaptic inputs transferring the presynaptic activity into the computation of the statistics μ_V, σ_V, τ_V, that results:

$$\mu_V(\nu_e, \nu_i) = \frac{\mu_{Ge} E_e + \mu_{Gi} E_i + g_L E_L}{\mu_G}$$

$$\sigma_V(\nu_e, \nu_i) = \sqrt{\sum_s K_s \nu_s \frac{U_s \tau_s}{2(\tau_m^{eff} + \tau_s)}}$$

$$\tau_V(\nu_e, \nu_i) = \frac{\sum_s K_s \nu_s (U_s \tau_s)^2}{\sum_s K_s \nu_s \ (U_s \tau_s)^2 / (\tau_s + \tau_m^{eff})}$$

$$(26)$$

With the effective membrane time constant defined as $\tau_m^{eff}(\nu_e, \nu_i) = \frac{C_m}{\mu_G}$ and $U_s = \frac{Q_s}{\mu_G}(E_s - \mu_V)$.

So far, the statistics included in the TF expression are defined, while here V_{thre}^{eff} must be defined to fully specify the TF equation. For the AdEx mean field described here, the V_{thre}^{eff} expression reads (Zerlaut et al., 2018):

$$V_{thre}^{eff}(\mu_V, \sigma_V, \tau_V, \mu_{G,}) =$$

$$P_0 + P_{\mu_G} log\left(\frac{\mu_G}{g_L}\right) + \sum_{x\in\{\mu_V,\sigma_V,\tau_V^N\}} P_x\left(\frac{x-x^0}{\delta x^0}\right) + \sum_{x,y\in\{\mu_V,\sigma_V,\tau_V^N\}^2} P_{xy}\left(\frac{x-x^0}{\delta x^0}\right)\times\left(\frac{y-y^0}{\delta y^0}\right)$$

$$(27)$$

Where P are the polynomial coefficients and the quantities μ_{0V}, $\delta_{\mu0V}$, σ_{0V}, $\delta\sigma_{0V}$, τ_V^N, and $\delta\tau_V^N$ are constant rescaling factors of the μ_V, σ_V, and τ_V^N, which indicates the normalized autocorrelation time. A simplified expression without the bilinear term can be used to model Linear Integrate and Fire or Extended Generalized Integrate and Fire neurons (E-GLIF neuron – see **Chapter 3**).

By inverting equation 24 an explicit expression of V_{thre}^{eff} is:

$$V_{thre}^{eff}(\nu_{out}, \mu_V, \sigma_V, \tau_V) = \sqrt{2}\sigma_V\ erfc^{-1}(2\ \tau_V\ \nu_{out}) + \mu_V \quad \forall \nu_{out} > 0$$

$$(28)$$

Where erfc[-1] is the inverse of the error function.

At this point all the *ingredients* to implement the fitting procedure of the TF have been defined. Thus, the fitting procedure is developed in two steps:

1) Computation of V_{thre}^{eff} using the activity of the spiking network as functional reference. In practice, spiking network simulations for different combinations of excitatory and inhibitory inputs are performed and the resulting ν_{out} values are collected in a matrix that represented a template for the output activity and it is formally called *numerical TF* (dots in Figure 2.7). Each value of the numerical TF is used as ν_{out} in equation (28) to compute V_{thre}^{eff} in different stimulating conditions.

2) Fitting of the polynomial coefficients of the TF using a non-linear least-squared algorithm that minimizes the difference between the computed values of V_{thre}^{eff} (see step **1**) and its polynomial expression in equation (27). Once the algorithm stops, the optimal P coefficients are identified and can be plugged into equation (28), yielding a polynomial expression of V_{thre}^{eff} generalizing its trend for the different stimulus conditions. The fitted expression is plugged into the equation (28) resulting in an analytical expression of the TF (lines in Figure 2.7) that represents the core of the MF model.

A - Excitatory population   **B - Inhibitory population**
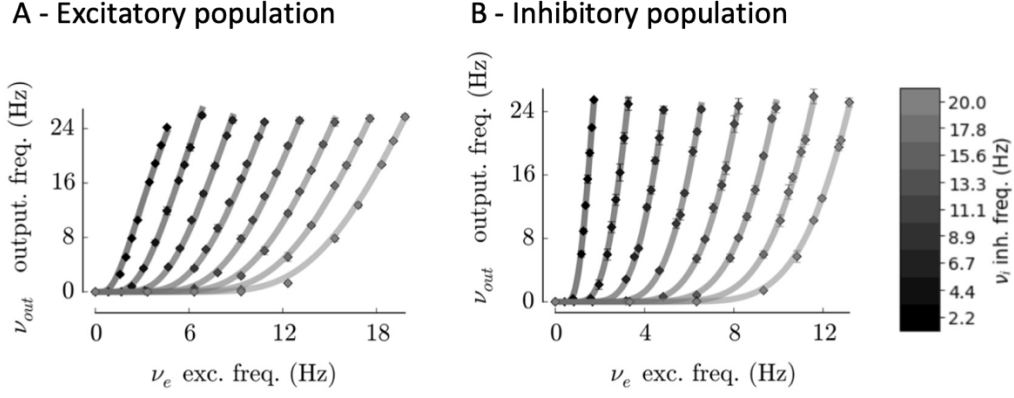
Figure 2. 7) Analytical Transfer Function (Zerlaut et al.; 2018). Y-axis = Transfer Function (ν_{out}) for excitatory RS **(A)** and inhibitory FS **(B)** populations. X-axis = excitatory input frequencies; Color bar = inhibitory input frequencies; Dots are the numerical Transfer Function computed with spiking network activity as functional reference; Lines are the result of the fitting procedure.

Once the TF is fitted, it is plugged into the MF model equation yielding:

$$\begin{cases} \text{T}\dfrac{d\nu_\mu}{dt} = \left(F_\mu - \nu_\mu\right) + \dfrac{1}{2}c_{\lambda\eta}\dfrac{\partial F_\mu}{\partial\nu_\lambda\partial\nu_\eta} \\[2ex] T\dfrac{dc_{\lambda\eta}}{dt} = \delta_{\lambda\eta}\dfrac{F_\lambda\left(1/T - F_\eta\right)}{N_\lambda} + (F_\lambda - \nu_\lambda)(F_\eta - \nu_\eta) + \dfrac{\partial F_\lambda}{\partial\nu_\mu}c_{\eta\mu} + \dfrac{\partial F_\eta}{\partial\nu_\mu}c_{\lambda\mu} - 2c_{\lambda\eta} \end{cases}$$

$$(29)$$

Where ν is the MF predicted activity and c is the covariance between populations; T is the MF model time constant; λ, η, μ denote the populations modelled, which are RS and FS in the present example; N_λ is the number of neurons in population λ and δ is the Dirac function that is 1 when $\lambda = \eta$. This model is a single layer MF model predicting the activity of RS and FS population (Figure 2.8).
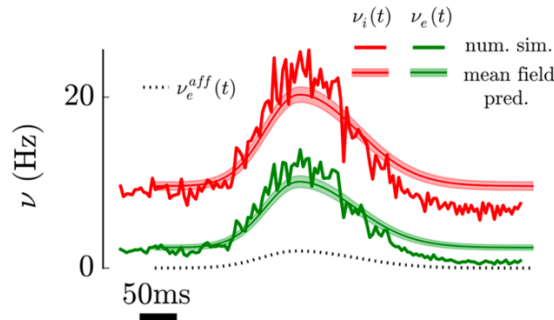
Figure 2. 8) Mean Field vs. Spiking Network prediction (Zerlaut et al.; 2018). Mean field prediction overlapped to the interpolation of numerical network output.

The heuristic approach to the TF computation summarized in this section represents a benchmark for the development of a more complex MF model including an extra equation to model adaptation (Di Volo et al, 2019). In the present work, the framework explained in this section was expanded to a multi-layer MF model that includes four different populations: Granule cells, Golgi cells, Molecular Layer Interneurons, and Purkinje cells (**section 1.1.1**) Spiking network was built up with E-GLIF

model instead of AdEx model, and for each population a specific transfer function was computed with the two-step procedure described above. Furthermore, all the synaptic connections were kept separated resulting in both bi-dimensional and tri-dimensional TF. Table 2.1 shows the main differences between the AdEx cortical MF (with and without adaptation) and the multi-layer cerebellar MF implemented in this work (**Chapter 3**), highlighting both the differences and the consistency of multi-layer cerebellar MF with adaptive cortical generic MF already included in TVB.

Table 2. 1) Multi-layer cerebellar MF model vs generic cortical MFs. Adaptive generic cortical MF is the MF currently integrate in TVB AdEx (see Figure 2.4).

	Generic cortical MF (Zerlaut et al., 2018)	Adaptive generic cortical MF (Di Volo et al., 2019)	Multi-layer cerebellar MF (Chapter 3)
Approach	**Bottom-up**	**Bottom-up**	**Bottom-up**
Neuron model	**AdEx** single point neurons with parameters for a generic excitatory and a generic inhibitory neuron (E, I)	**AdEx** single point neurons with parameters for a generic excitatory and a generic inhibitory neuron (E, I)	**E-GLIF** single point neurons with parameters tuned on each neuron type (GrC, GoC, MLI, PC)
Network design	**Mono-layer** network, collapsing neurons into a generic excitatory and a generic inhibitory population	**Mono-layer** network, collapsing neurons into a generic excitatory and a generic inhibitory population	**Multi-layer** network including the four specific neuronal population of the cerebellar cortex
Conductance model	**Exponential** function	**Exponential** function	**Alpha-shaped** function
TF formalism	**Semi-analytic TF** **2D TFs** collapsing all excitatory and inhibitory presynaptic frequencies into two inputs	**Semi-analytic TF** **2D TFs** with 2 inputs (excitatory and inhibitory), accounting for **adaptation**	**Semi-analytic TF**, fitted on actual working frequencies **2D or 3D TFs** according to the number of presynaptic inputs
Time constant	5 ms. Set according to **literature**	20 ms. Set according to **literature**	3.5 ms. Optimized with **experimental data**
Mean field model	**6** second-order differential equations	**7** second-order differential equations (6 for the activity + **1 for adaptation**)	**20** second-order differential equations

A multi-layer Mean Field model for the Cerebellum: design, validation, and prediction

In this Chapter a detailed explanation on how the mean field formalism described in **Chapter 2** was informed with the physiological knowledge described in **Chapter 1** to develop a multi-layer mean field model (MF) for the cerebellum. This Chapter introduce the multi-layer MF of the cerebellum to study the dynamics of the cerebellar cortex but it also explains a pipeline to implement advanced multi-layer MF specified for other brain regions.

Abstract

Mean-field (MF) models can be used to summarize in a few statistical parameters the salient properties of an inter-wired neuronal network incorporating different types of neurons and synapses along with their topological organization. MF are crucial to efficiently implement the modules of large-scale brain models maintaining the specificity of local microcircuits. While MFs have been generated for the isocortex, they are still missing for other parts of the brain. Here we have designed and simulated a multi-layer MF of the cerebellar network (including Granule Cells, Golgi Cells, Molecular Layer Interneurons, and Purkinje Cells) and validated it against experimental data and the corresponding spiking neural network (SNN) microcircuit model. The cerebellar MF was built using a system of equations, where properties of neuronal populations and topological parameters are embedded in inter-dependent transfer functions. The model time constant was optimised using local field potentials recorded experimentally from acute mouse cerebellar slices as a template. The MF satisfactorily reproduced the average dynamics of the different neuronal populations in response to various input patterns and predicted the modulation of Purkinje Cells firing depending on cortical plasticity, which drives learning in associative tasks, and the level of feedforward inhibition. The cerebellar MF provides a computationally efficient tool that will allow to investigate the causal relationship between microscopic neuronal properties and ensemble brain activity in virtual brain models addressing both physiological and pathological conditions.

3.1 Introduction

Brain modelling is opening new frontiers for experimental and clinical research toward personalised and precision medicine (Amunts et al., 2013; Schirner et al., 2015). Brain models can be developed

at different scale, ranging from microscopic properties of neurons and microcircuits to the ensemble behaviour of the whole brain. Arguably, a model spanning across scales would increase the fidelity in modelling single brain regions, improving the accuracy of whole-brain dynamics simulations (D'Angelo and Jirsa, 2022), but this clearly bears conceptual and practical drawbacks. At the microscale, Spiking Neural Networks (SNNs) reproduce neural circuits as a set of interconnected neurons (Plesser et al., 2015; Yavuz et al., 2016; Knight et al., 2021): the state of each neuron and synapse in the network is updated at each simulation step, allowing to investigate neural circuits functioning at a high level of granularity and biological plausibility. However, this degree of detail is hard to manage when simulating brain signals, like those derived from electroencephalography (EEG) or functional magnetic resonance imaging (fMRI). To manage the high complexity of brain signals, the dynamics of a neuronal population have been condensed into ensemble density models called neural masses. These provide a description of the expected values of neuronal activity states, under the assumption that the equilibrium density has a point mass (Wilson and Cowan, 1972; Jansen and Rit, 1995). Neural fields are obtained from neural mass models when considering spatial information: these can be used to model spatial propagation of activity throughout brain volumes (Deco et al., 2008). Despite being computationally efficient and easy to fit on brain signals data, neural mass and neural field models lack a direct link to the microscopic scale, a fact that limits their applicability in investigating the neuronal bases of brain dynamics and the causal relationships between neural mechanisms at different scales.

A different approach is based on the mean-field (MF) approximation. The MF theory provides a general formalism to approximate high-dimensional random models by averaging the original system properties over degrees of freedom, i.e., maintaining the first two statistical moments (mean and variance) of the system. In neuroscience, MFs have been used to provide a representation of neuronal population dynamics, by replacing multiple single-neuron input-output (I/O) relationship with one based on the MF of the interconnected populations. MFs thus summarize the neuronal and connectivity properties of an entire spiking microcircuit through *ad-hoc* transfer functions (TFs) (Amit and Brunel, 1997; Brunel and Sergi, 1998; Kumar et al., 2008) and capture the statistical properties of network activity by computing the probabilistic evolution of neuronal states at subsequent time intervals (Kuhn et al., 2004; El Boustani and Destexhe, 2009; Zerlaut et al., 2016).

MFs can be used to investigate macroscale phenomena, such as brain rhythms and coherent oscillations (Cakan and Obermayer, 2020b), and are computationally advantageous, with increased computational speed and low memory requirements compared to SNNs. Among current limitations, MFs do not capture in full the complex properties of specific neuronal populations and are valid only in certain firing regimes, e.g., at low frequency (Carlu et al., 2020).

Moreover, while a diversification of MFs for specific cortical regions has been proposed (Marreiros et al., 2008; Bastos et al., 2012; Deco et al., 2014; Auksztulewicz and Friston, 2015; Glomb et al., 2017; El Houssaini et al., 2020; Naskar et al., 2021), few attempts to develop MFs for subcortical regions have been performed (Moran et al., 2011; Saggar et al., 2015; van Wijk et al., 2018; Levenstein et al., 2019), despite their fundamental role in controlling brain dynamics and behavior (Schutter and van Honk, 2006; Castellazzi et al., 2014, 2018; Casiraghi et al., 2019; Andersen et al., 2020). In particular, the cerebellum has a dense connectivity with the cerebral cortex and remarkably impacts on whole-brain dynamics in resting-state and task-dependent fMRI (Casiraghi et al., 2019;

Palesi et al., 2020; Monteverdi et al., 2022) prompting for the development of specific MFs to be included into whole-brain simulators.

The cerebellar cortex receives inputs from mossy fibers and climbing fibers and sends outputs to the deep cerebellar nuclei. Granule Cells (GrC), Golgi Cells (GoC), Molecular Layer Interneuron (MLI) and Purkinje Cells (PC) constitute the backbone of the cerebellar cortex, which shows a peculiar anisotropic geometry implementing a forward architecture with limited lateral connectivity and recurrent excitation. These properties, along with the neuronal types, differ remarkably from those of the cerebral cortex prompting for the definition of a specific MF. This operation represents both a challenge and an opportunity. All the neuron types of the cerebellar cortex, following a careful characterization in electrophysiology experiments in rodents *in vitro* and *in vivo* (D'Angelo et al., 2001; McKay and Turner, 2005; Molineux et al., 2006; Solinas et al., 2007; Lachamp et al., 2009), have been represented by detailed multicompartmental models (Masoli et al., 2015, 2020b, 2020a; Masoli and D'Angelo, 2017; Rizza et al., 2021), simplified into point-neuron models (Lennon et al., 2014; Geminiani et al., 2018, 2019a), and embedded in network models of the cerebellar microcircuit (Solinas et al., 2007; Geminiani et al., 2019b, 2019a; Casali et al., 2020; De Schepper et al., 2022). Thus, the cerebellum provides an ideal substrate for generating a MF, in which the internal dynamics can be remapped onto a precise physiological counterpart and validated against a rich and informative dataset.

In this work we have developed and validated a multi-layer MF of the cerebellar cortex, which maintains the salient properties of the inter-wired cerebellar neuronal populations. Indeed, the MF was derived from a biology-grounded model of the cerebellar microcircuit, which was used to define the topology and tune the parameters of the MF, and it was then validated against a rich set of SNN outputs. The perspective is to integrate the present mesoscopic cerebellar MF as a module of macroscale models, e.g. Dynamic Causal Modeling (DCM) (Friston et al., 2003, 2019; Parr et al., 2020) or The Virtual Brain (TVB)(Sanz Leon et al., 2013), to simulate the cerebellar contribution to brain activity in physiological and pathological conditions.

3.2 Methods

In this section we describe the development, tuning, validation, and application of a multi-layer MF of the cerebellar circuit (Figure 3.1). The MF formalism provides a statistical summary of a SNN activity through the first two statistical moments (i.e. average and variance) of the population firing rates (El Boustani and Destexhe, 2009) . Here the SNN bottom-up modelling approach is merged with the standard MF mathematical formalism to obtain a multi-layer MF of the cerebellar cortex. In order, we present the cerebellar SNN model used as the structural and functional reference of the MF (**section 3.2.1**), the design of the MF architecture based on cerebellar topology (**section 3.2.3 - Architecture**), the implementation of the MF equations derived with an heuristic approach (**section 3.2.2 - TF computation and Multi-layer Equation**) (Zerlaut et al., 2016, 2018; Carlu et al., 2020), the protocols used to optimise the MF time constant (**section 3.2.2 - Timing optimisation**) and to validate the MF (**section 3.2.3**), the applications of the MF to predict the activity modulation induced by different levels of synaptic plasticity and of inhibitory control (**section 3.2.4**).
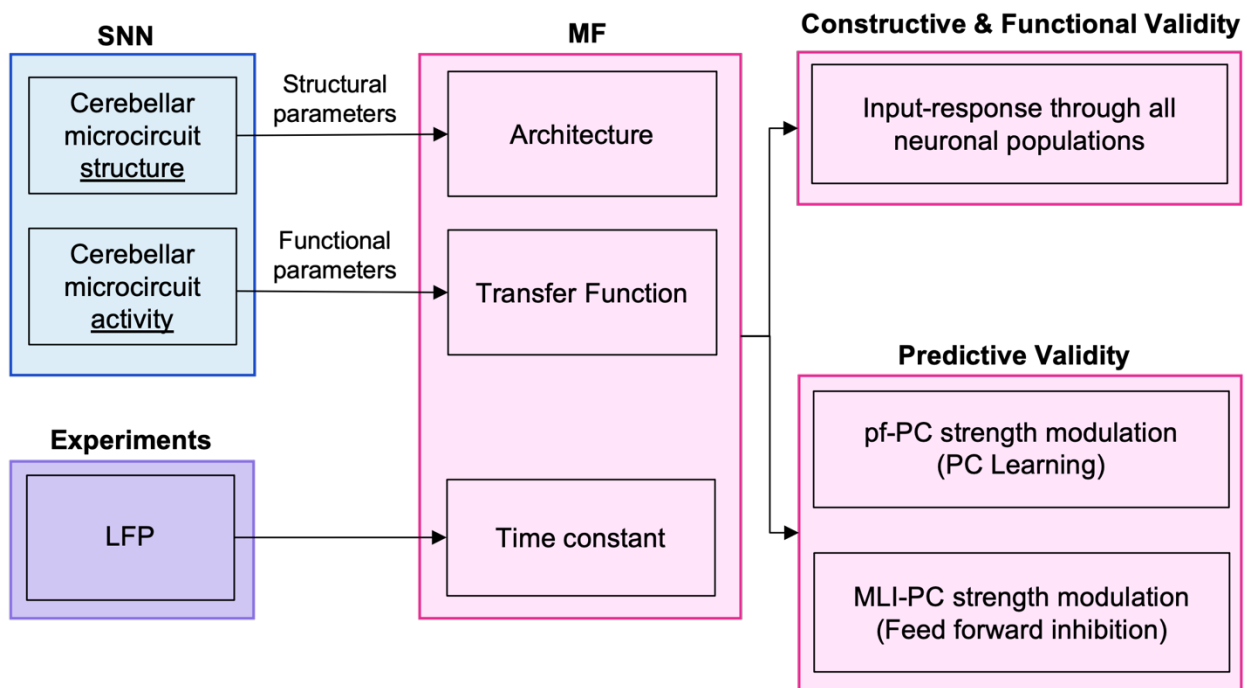
Figure 3. 1) Pipeline of the multi-layer cerebellar MF model. The workflow of the study is represented. MF was designed based on structural and functional parameters extracted from Spiking Neural Network (SNN) simulations. The time constant of the resulting MF was optimized against Local Field Potential (LFP) experimental data. The model was first validated against neural activity of SNN with different stimulation protocols and then used to reproduce the effect of synaptic plasticity in molecular layer interneurons.

3.2.1 SNN model

This cerebellar cortex model was built using the Brain Scaffold Builder (BSB) (https://bsb.readthedocs.io/en/latest/), a neuroinformatic framework allowing a detailed microcircuit reconstruction based on neuron morphologies and orientations and the incorporation of active neuronal and synaptic properties (De Schepper et al., 2022). The SNN was made of ~3x10⁴ extended-Generalised Leaky Integrate and Fire (E-GLIF) neurons (Geminiani et al., 2018, 2019a) and ~1.5x10⁶

alpha-shaped conductance-based synapses (Roth and van Rossum, 2013). The SNN simulations were performed using NEST (Plesser et al., 2015; Jordan et al., 2019)

Table 3. 1)Neuron parameters

Parameter	Name	unit	GrC	GoC	MLI	PC
g_L	Leak conductance	nS	0.29	3.30	1.60	7.10
C_m	Membrane capacitance	pF	7.00	145.00	14.60	334.00
τ_{ref}	Refractory time	ns	1.50	2.00	1.59	0.50
τ_m	Membrane time constant	ns	24.15	44.00	9.12	47.00
E_L	Resting potential	mV	-62.00	-62.00	-68.00	-59.00
V_{th}	Threshold potential	mV	-41.00	-55.00	-53.00	-43.00
V_r	Reset potential	mV	-70.00	-75.00	-78.00	-69.00
k_{adap}	Adaptation constant	MH^{-1}	0.02	0.22	2.03	1.50
$k2$	Adaptation constant	ms^{-1}	0.04	0.02	1.10	0.04
$k1$	Decay rate	ms^{-1}	0.31	0.03	1.89	0.19
$A2$	Update constant	pA	-0.94	170.01	5.86	172.62
$A1$	Update constant	pA	0.01	259.99	5.95	157.62
I_e	Endogenous current	pA	-0.89	16.21	4.45	891.04

Parameters specific of the type of neurons included in the multi-layer MF populations. The parameters in the top part are chosen according to literature (Table 2 of Geminiani et al., 2019a), while the parameters at the bottom were extracted from spiking neural network simulating the cerebellar cortex spiking activity (Geminiani et al., 2018, 2019a). mf = mossy fibers, GrC = Granule Cells, GoC = Golgi Cells, MLI = Molecular Layer Interneurons (Basket cells and Stellate cells)

Neuron model

The E-GLIF formalism describes the time evolution of membrane potential (V_m) depending on two intrinsic currents to generate slow adaptation (I_{adap}) and fast depolarisation (I_{dep}), using a the system of three ODEs (Geminiani et al., 2018)

$$\begin{cases} \dfrac{dV_m(t)}{dt} = \dfrac{1}{C_m}(\dfrac{C_m}{\tau_m}(V_m(t) - E_{rev}) - I_{adap}(t) + I_{dep}(t) + I_e + I_{syn} \\ \dfrac{dI_{adap}(t)}{dt} = k_{adap}(V_m(t) - E_{rev}) - k_2 I_{dep}(t) \\ \dfrac{dI_{dep}(t)}{dt} = k_1 I_{dep}(t) \end{cases}$$

(30)

where I_{syn} = synaptic current (it models the synaptic stimulus, see section 2.1.2); C_m = membrane capacitance; τ_m = membrane time constant; E_{rev} = reversal potential; I_e = endogenous current; k_{adap} and k_2 = adaptation constants; k_1 = decay rate of I_{dep}. When a spike occurs, state variables are updated as follows:

$$V_m(t_{spk}^+) = V_r$$

$$I_{adap}(t_{spk}^+) = I_{adap}t_{spk} + A_2$$

$$I_{dep}(t_{spk}^+) = A_1$$

(31)

where t_{spk}^+ = time instant immediately following the spike time t_{spk} ; V_r = reset potential; A_2, A_1 = model currents update constants. E-GLIF models were implemented using parameter sets specific for each neuronal population (Geminiani et al., 2019a) as shown in Table 3.1.

Synaptic model
Connections between neural populations were modelled as conductance-based synapses:

$$I_{syn}(t) = g_{syn}(t)(V_m(t) - E_{rev})$$

(32)

When a spike occurs, the conductance g_{syn} changes according to an alpha function:

$$g_{syn}(t) = G_{syn}\frac{t - t_{spk}}{\tau_{syn}}e^{1-\frac{t-t_{spk}}{\tau_{syn}}}$$

(33)

where G_{syn} is the maximum conductance change and τ_{syn} the synaptic time constant. E-GLIF neuron models and conductance-based synaptic models used in SNN simulations provided the functional reference of cerebellar spiking activity for MF development.

3.2.2 MF design
The design of the cerebellar multi-layer MF was based on the extensive knowledge of cerebellar anatomy and physiology summarized in previous cerebellar cortex network models (Geminiani et al., 2018, 2019c; De Schepper et al., 2021).

Architecture
The cerebellar MF included the main neuronal populations of the cerebellar cortex - GrC, GoC, MLI and PC (Figure 3.2) and the corresponding excitatory and inhibitory synapses. The MF network topology reproduced the multi-layer organisation of the cerebellar cortex. Granular layer at the cerebellar input stage includes GrC and GoC receiving external input (ν_{drive}) from mossy fibers. GrC excite GoC, which, in turn, inhibit themselves and GrC forming recurrent loops. GrC represent the excitatory input for the molecular layer constituted by MLI and PC. MLI inhibit PC, which are the sole output of the cerebellar cortex and shape the deep cerebellar nuclei activity through inhibition.

Although other neurons have been reported to play a role in the cerebellar microcircuit (e.g. Lugaro cells (Melik-Musyan and Fanardzhyan, 2004), and unipolar brush cells (Mugnaini et al., 2011) for the sake of simplicity we have limited the present model to the canonical architecture that is thought to generate core network computations.

To connect the nodes of the MF network, synaptic parameters were set according to those of the reference SNN (Table 3.2). The connection probability for each connection type (K) was derived from the convergence ratio in a cerebellar cortical volume (De Schepper et al., 2022). The quantal synaptic conductance and synaptic time decay (Q, τ) was derived from the weights and time constants of the corresponding synapse models (Geminiani et al., 2019a).
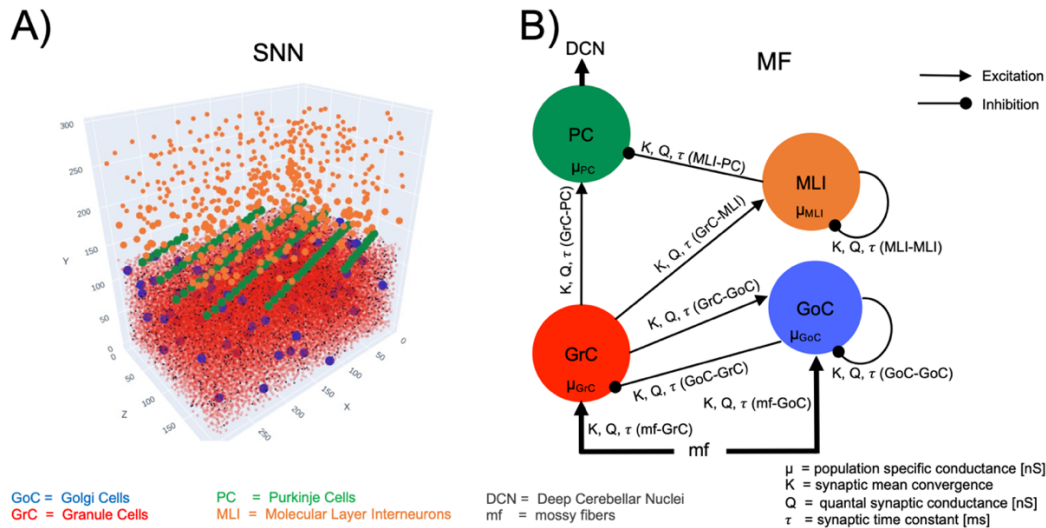
Figure 3. 2) Multi-layer MF architecture and parameters. A: Spiking Neural Network model (SNN). The cerebellar cortical volume (length = 300, width = 200, height = 295 µm3) contained a total of 29230 neurons including 28615 GrC, 70 GoC, 446 MLI and 99 PC. **B**: Multi-layer MF architecture with neuronal populations connected according to anatomical knowledge. The main cerebellar neuron types are included: GrC and GoC, receiving input from mossy fibers, MLI and PC, which are the sole output of the cerebellar cortex. Each population receive excitatory and/or inhibitory input activity v from presynaptic populations, depending on their specific conductance µ and on the synaptic properties of each connection (convergence, synaptic conductance, and time constant).

Table 3. 2) Presynaptic parameters

Presynaptic connection	K	Q [nS]	τ [ms]	E_{rev} [V]
mf-GrC	4.00	0.230	1.9	0
GoC-GrC	3.50	0.240	4.5	-80
mf-GoC	57.10	0.240	5.0	0
GrC-GoC	501.98	0.437	1.25	0
GoC-GoC	2592.00	0.007	5.0	-80
GrC-MLI	243.96	0.154	0.64	0
MLI-MLI	1418.69	0.005	2.0	-80
GrC-PC	489.16	0.510	1.1	0
MLI-PC	10.28	1.244	2.8	-80

Parameters used to set up the inter-population connectivity of the multi-layer MF cerebellar network. The parameters were extracted from the spiking neural network simulating the cerebellar cortex spiking activity (Geminiani et al., 2019b). Mf = mossy fibers, GrC = Granule Cells, GoC = Golgi Cells, MLI = Molecular Layer Interneurons (Basket cells and Stellate cells). K = pre-synaptic connectivity resulting by weighting the mean synaptic convergence with the number of synapses; Q = quantal synaptic conductance in nS; τ = synaptic decay time constant; E_{rev} = reversal potential that is 0 V for excitatory synaptic connections and -80 V for inhibitory synaptic connections.

TF Computation

The TF is defined for each population as a mathematical construct that takes the activity of the presynaptic population (v_s) as input and provides an average population activity signal as output (v_{out}) (Kuhn et al., 2004).

A purely analytic derivation of the TF (using approximations and stochastic calculus, e.g. Brunel & Amit, 1997) was not possible given the relative complexity of the neuronal (E-GLIF) and synaptic (alpha-waveform) models considered here. Therefore, the TFs presented here relied on a semi-analytical approach that couples an approximate analytical estimate with an optimization step to capture the firing response of analytically intractable models (Zerlaut et al., 2016, see also Brunel & Sergi, 1998 for a similar approach). More details can be found in Zerlaut et al. (2016) but we summarize the approach below.

The analytical template for the TF (indicated with F in the equations for sake of simplicity) of all neuron types is derived from the probability to be above threshold in the fluctuation-driven regime (Kuhn et al., 2004):

$$v_{out} = F_p(v_s) = \alpha \; \frac{1}{2\tau_V} erfc(\frac{V_{thre}^{eff} - \mu_V}{\sqrt{2}\sigma_V})$$

(34)

where *erfc* is the error function while μ_V, $\sigma_V{}^2$ and τ_V are the average, variance and autocorrelation time respectively of the membrane potential fluctuations. Two phenomenological terms were introduced: V_{thre}^{eff}, an effective firing threshold to capture the impact of single cell non-linearities on firing response (Zerlaut et al., 2016) and α, a multiplicative factor to adapt the equations also to high input frequency regimes (Carlu et al., 2020). Those two terms were optimized for each neuron type (steps *d* and *e* respectively) from single neuron simulations of input-output transformation in terms of firing rate (i.e., the numerical TF, see step b). The TF depends on the statistical properties of the subthreshold membrane voltage dynamics (mean = μ_V, standard deviation = $\sigma_V{}^2$ and autocorrelation time τ_V, calculated in step *c*). These in turns depend on the average population conductances that are computed with the biologically-grounded functional parameters derived from SNN models at single neuron resolution (step *a*), bringing the physiological properties into the MF mathematical construct.**Errore. Il segnalibro non è definito.**

a) Equations of Population-specific conductance. For each neuronal population, the average conductance was defined as a function of the presynaptic inputs, according to the topology described in **section 3.2.2** (Figure 3.2.):

$$\mu_p =. \sum_s K_{s-p}\tau_{s-p}Q_{s-p}v_s$$

(35)

where, for each population p (p = GrC, GoC, MLI, PC), K_{s-p}, τ_{s-p}, Q_{s-p} are the connection probabilities, synaptic decay times and quantal conductances of the connection for each presynaptic population s (e.g., for p = GrC, s-p is mossy fiber-GrC and GoC-GrC), ν_s is the presynaptic population activity in Hz computed as explained in (b).

b) Numerical TF. The reference functional target was the neuronal spiking activity obtained in SNN simulations (*in vivo* conditions) as described in **section 3.2.1**. The activity of GrC, GoC, MLI and PC embedded in the SNN was simulated for different input amplitudes (ν_{drive}) in the range 0-80 Hz, with input spikes generated from a Poisson distribution. For each ν_{drive}, the simulation lasted 5 seconds with a time resolution of 0.1 ms. The working frequencies of each population were extracted by averaging the spiking neuron firing rates. For each population, the outcome of numerical TF computation was a template of dimension equal to the number of presynaptic populations, resulting in 2D numerical TFs for GrC, MLI and PC and 3D numerical TF for GoC (Figure 3.3A).

The 2D numerical TF of each population was computed as the population firing rate when receiving the firing rates of the presynaptic populations, given a certain ν_{drive} : for example, for the numerical TF numerical template of PC, the average firing rates of MLI and GrC were computed for each ν_{drive} in the range 0-80 Hz. Then, these quantities were used as presynaptic signals to stimulate PC and a numerical template was obtained from the resulting PC firing rate, for each combination of presynaptic activities). The 3D TF numerical template of GoC was computed following the same strategy but considering 3 presynaptic signals (GrC, GoC, mossy fibers). GrC excitation and GoC self-inhibition were extracted from SNN simulations and the mossy fibers excitation corresponded to ν_{drive}.

c) Statistical moments of the MF. The statistical moments included in the MF are μ_V, σ_V and τ_V. Starting from the conductances of the presynaptic populations, the average conductance μ_G of the target population reads:

$$\mu_G(\nu_s) = \sum_s \mu_{Gs} + g_L$$

(36)

Where μ_{Gs} is the presynaptic population conductance (equation (35)) and g_L is the leak conductance of the target population (Table 3.1). Then, the effective membrane time constant of the target population is computed from μ_G as:

$$\tau_m^{eff}(\nu_s) = \frac{C_m}{\mu_G}$$

(37)

Where C_m is the membrane capacitance (Table 3.1).

The first statistical moment, i.e., the average of membrane potential fluctuation μ_V reads:

$$\mu_V(\nu_s) = e\,\frac{\sum_s \mu_{Gs}\,E_s + g_L E_L}{\mu_G}$$

(38)

With E_s = reversal potential of the presynaptic connection (0 mV for the presynaptic excitatory populations and -80 mV for the presynaptic inhibitory populations), E_L = rest potential of the target population (Table 3.1).

This expression is adapted from Zerlaut et al. 2018 to model the alpha synapses consistently with the models used in the SNN (equations (30), (31), and (32)). Consequently, the variance and the autocorrelation time of membrane fluctuations result in:

$$\sigma_V(\nu_s) = \sqrt{\sum_s (2\tau_m^{eff} + \tau_{s-p})\left(\frac{eU_{s-p}\tau_{s-p}}{2(\tau_m^{eff} + \tau_{s-p})}\right)^2 K_{s-p}\nu_{s-p}}$$

(39)

$$\tau_V(\nu_s) = \frac{1}{2}\,\frac{\sum_s K_{p-s}\nu_s (eU_{p-s}\tau_{p-s})^2}{\sum_s (2\tau_m^{eff} + \tau_{p-s})\left(\frac{eU_{p-s}\tau_{p-s}}{2(\tau_{p-s} + \tau_m^{eff})}\right)^2 K_{p-s}\nu_s}$$

(40)

With $U_s = \frac{Q_{s-p}}{\mu_G}(E_s - \mu_V)$.

d) Phenomenological threshold. The ability of the analytical template (34) to capture different firing behavior is given by the introduction of 5 parameters in the phenomelogical threshold term. The phenomenological threshold is expressed as a linear combination of the V_m fluctuations properties whose coefficients are linearly fitted to the numerical TF data (Zerlaut et al., 2016):

$$V_{thre}^{eff}(\mu_V, \sigma_V, \tau_V) = P_0 + P_{\mu V}\frac{\mu_V - \mu_V^0}{\partial \mu_V^0} + P_{\sigma V}\frac{\sigma_V - \sigma_V^0}{\partial \sigma_V^0} + P_{\tau V}\frac{\tau_V^N - \tau_V^{N0}}{\partial \tau_V^{N0}} + P_{\mu G}\ln\left(\frac{\mu_G}{g_L}\right)$$

(41)

Where τ_V^N is τ_V adjusted with the ratio between membrane capacitance and leak conductance ($\frac{C_m}{g_L}$), and $\mu_V^0, \sigma_V^0, \tau_V^{N0}, \partial\mu_V^0, \partial\sigma_V^0, \partial\tau_V^{N0}$ are rescaling constants to normalize the contribution of each term

(Zerlaut et al., 2018). P are the polynomial coefficients which are the target of the fitting procedure to compute the analytical TF as explained in e) (see Table 3.3).

e) *Analytical TF.* The statistical moments in equations (38), (39), (40) and the phenomenological threshold in equation (41) were plugged into equation (44) and the phenomenological threshold is computed through a fitting procedure described in Zerlaut et al. 2016. The TFs specific for the cerebellar populations are reported in Figure 3.3B.

The parameter alpha (equation (34)) was set to an optimal value for each population to fit both low and high frequencies (Carlu et al., 2020). The analytical TF, together with the statistical moments μ_V, σ_V, and τ_V defined the cerebellar MF equations.

Multi-layer equations

The multi-layer MF was developed as a set of equations capturing the interdependence of the population-specific TFs, tailoring the isocortical MF described in (El Boustani and Destexhe, 2009) for excitatory-inhibitory networks to the cerebellar network. This formalism describes the network activity at a time resolution T which is set to ensure a Markovian dynamic of the network: T should be large enough to ensure memoryless activity (e.g., it cannot be much lower than the refractory period, which would introduce memory effects) and small enough so that each neuron fires statistically less than once per time-bin T. The choice of T is quite crucial and here it was tailored to account for cerebellar dynamics as explained in **section Timing Optimization**.

The model describes the dynamics of the first and the second moments of the population activity for each population. The cerebellar network was build up with four interconnected populations (GrC, GoC, MLI, PC) receiving external input from mossy fibers (mf) (Figure 3.2), thus resulting in twenty differential equations: the four population activities ($\nu_{GrC}(t)$, $\nu_{GoC}(t)$, $\nu_{MLI}(t)$, $\nu_{PC}(t)$) and the driving input ($\nu_{mf}(t) = \nu_{drive}(t)$), the four variances of the population activities ($c_{GrC\text{-}GrC}(t)$, $c_{GoC\text{-}GoC}(t)$, $c_{MLI\text{-}MLI}(t)$, $c_{PC\text{-}PC}(t)$) and the one of the driving input from mossy fibers ($c_{mf\text{-}mf}(t)$), the six covariances among population activities ($c_{GrC\text{-}GoC}(t)$, $c_{GrC\text{-}PC}(t)$, $c_{GrC\text{-}MLI}(t)$, $c_{GoC\text{-}MLI}(t)$, $c_{GoC\text{-}PC}(t)$, $c_{MLI\text{-}PC}(t)$) and the four covariances between population activities and the driving input ($c_{GrC\text{-}mf}(t)$, $c_{GoC\text{-}mf}(t)$, $c_{MLI\text{-}mf}(t)$, $c_{PC\text{-}mf}(t)$). Einstein's notation was used to report the differential system in a concise form:

$$\begin{cases} T\dfrac{d\nu_\mu}{dt} = \left(F_\mu - \nu_\mu\right) + \dfrac{1}{2}c_{\lambda\eta}\dfrac{\partial F_\mu}{\partial \nu_\lambda \partial \nu_\eta} \\[2em] T\dfrac{dc_{\lambda\eta}}{dt} = \delta_{\lambda\eta}\dfrac{F_\lambda\left(\frac{1}{T} - F_\eta\right)}{N_\lambda} + (F_\lambda - \nu_\lambda)(F_\eta - \nu_\eta) + \dfrac{\partial F_\lambda}{\partial \nu_\mu}c_{\eta\mu} + \dfrac{\partial F_\eta}{\partial \nu_\mu}c_{\lambda\mu} - 2c_{\lambda\eta} \end{cases}$$

$$(42)$$

Where ν_μ is the activity of population μ; $c_{\lambda\eta}$ is the (co)variance between population λ and η; N is the number of cell included in population λ. According to Einstein's notation, a repeated index in a product implies a summation over the whole range of values. TF dependencies on the firing rate of presynaptic populations are omitted yielding F_μ instead of $F_\mu(\nu_s)$ with $\mu = \{GrC, GoC, MLI, PC\}$ and s is the presynaptic population (e.g. $F_{GoC} = F_{GoC}(\nu_{drive}, \nu_{GrC}, \nu_{GoC})$). The model equations (42) were numerically solved using forward Euler method with an integration step of 0.1 ms.

Timing Optimisation

The MF time-constant T was optimised by comparing the model prediction with experimental data of the cerebellar Granular layer (Figure 3.4). The simulated average activity was interpolated with the experimental Local Field Potential (LFP) measured with high-density microelectrode arrays (HD-MEA) in the granular layer of acute mouse cerebellar slices (Mapelli and D'Angelo, 2007)

LFP data were recorded at 37 °C. The external stimulus consisted in a pulse train of 5 stimuli of 50 Hz amplitude. This stimulation protocol was repeated nine times changing the HD-MEA recording channels across each experiment (Figure 3.4A). The LFP signals recorded were averaged across the nine experiments resulting in five values that represented the average of each pulse of the input trains. These average records were normalised on the amplitude of the signal recorded after the first stimulus.

The cerebellar MF simulation protocol was configured with a ν_{drive} = 50 Hz for 100 ms, reproducing the experimental protocol (Figure 3.4B). A range of plausible T values was evaluated according to literature (El Boustani and Destexhe, 2009; Zerlaut et al., 2016, 2018; Carlu et al., 2020). MF simulations were performed with a systematic change of T value and the granular layer average activity was calculated by a weighted-mean of GrC and GoC activity. The weight of GrC and of GoC was computed as the ratio of the spiking surfaces (GoC/GrC) resulting in 0.13 (Mapelli and D'Angelo, 2007). The granular layer average activity was normalised on the maximum peak, and it was interpolated with LFP recordings (Figure 3.4C). For each simulation the mean absolute error was computed to select the T value that minimised the discrepancy with the LFP signals. Since the granular layer is the driving layer of the network, the optimal T value was extended to the molecular and Purkinje layers.

3.2.3 Constructive and Functional validity

For constructive and *functional validity*, the cerebellar MF was tested using stimulation protocols designed to assess its ability in reproducing proper cerebellar dynamics and stimulus-response patterns.

Four different stimulation protocols were defined, each lasting 500 ms:

i) ν_{drive} = Step function. A square wave with steps of amplitude 50 Hz, and lasting 250 ms to reproduce a conditioned stimulus (e.g., a sound)

ii) ν_{drive} = Theta-band sinusoid. A sinusoidal input with rate amplitude set at 20 Hz and frequency at 6Hz (theta band) to simulate the whisker movements experimental conditions.

iii) ν_{drive} = Combination of alpha, theta, and gamma band sinusoid. A combination of 3 sinusoidal inputs, with fixed rate amplitude at 40 Hz and frequency at 1Hz, 15Hz and 30Hz respectively reproducing a EEG-like pattern.

iv) ν_{drive} = Step function plus multi-band sinusoid. Summation of the step function described in (i) with amplitude of 20 Hz and sinusoidal function including alpha, theta and gamma band with the same frequency of (iii) and amplitude of 7.5 Hz to simulate a more complex input like a conditioned stimulus overlapped to a realistic basal activity

Population activities predicted by the MF were overlayed to the Peristimulus Time Histogram (PSTH) with bin = 15 ms, computed from spiking activities of the SNN in NEST simulations of the same stimulation protocols. Then, the PC activity, i.e., the output of the cerebellar cortex, was quantified as mean ± standard deviation of the firing rate for both MF and SNN simulation. Boxplots were shown to quantitively compare MF and SNN outcomes, and the computational efficiency of each model was measured as computational time in seconds required for each simulation performed with MF and with NEST.

3.2.4 Predictive Validity

For predictive validity, MF parameters were tuned to explore the MF sensitivity to modifications of local mechanisms. These modifications were derived from experimental studies on neural correlates of behavior in functional or dysfunctional conditions, focusing on inhibitory control and long term plasticity on PCs (Wulff et al., 2009; ten Brinke et al., 2015)

MLI feed forward inhibition modulation

Feedforward inhibition from molecular layer interneurons regulates adaptation of PCs. Impact of MLI-PC conductance on PC activity was explored by defining different values of MLI-PC synaptic strength w_{MLI-PC} = [5, 30, 100, 150, 200, 250] %, where w_{MLI-PC} = 100% represents the standard condition, rates lower than 100% model disinhibited activity, while rates higher than 100% extra-inhibition.

w_{MLI-PC} was added to the Analytical TF_{PC} as a modulatory parameter of the presynaptic input ν_{MLI}, resulting in a modulation of MLI contribution in PC population conductance (35) defined as follows

$$\mu_{PC} = K_{MLI-PC}Q_{MLI-PC}\tau_{MLI-PC}\nu_{MLI}w_{MLI-PC} + K_{GrC-PC}Q_{GrC-PC}\tau_{GrC-PC}\nu_{GrC}$$

(43)

Each simulation lasted 500 ms with a 50Hz driving input of 250 ms after 125 ms of resting.

The Area Under Curve (AUC) of PC activity, PC peak and the depth of the pause were computed as quantitative scores for each w_{MLI-PC} value AUCs and PC peaks were normalised on the respective values corresponding to the standard condition defined as w_{MLI-PC} = 100%.

PC Learning

Long term potentiation and depression (LTP and LTD) are forms of synaptic plasticity at the basis of brain learning processes (Bliss and Cooke, 2011). In the cerebellum, motor learning is driven by PC activity modulation, regulated by the plasticity of the synapses between parallel fibers (pfs – from GrC) and PC, resulting in a reduction of PC activity due to LTD and in an increase of PC activity due to LTP (Mittmann and Häusser, 2007; Prestori et al., 2013). To simulate pf-PC plasticity, the following synaptic strengths (w_{pf-PC}) were explored to investigate the consequent PC modulation: [5, 20, 35, 50, 65, 80, 100, 120, 135, 150, 165, 180, 200, 235, 250, 265] % where 65% corresponds to the decrease of pf-PC strength during motor learning according to animal experiments value (ten Brinke et al., 2015), and the others were defined to capture the trend of pf-PC plasticity mechanism. The values minor than 100% means LTD occurred, while the values higher than 100% represent LTP occurrence. The strategy applied was analogous to equation (43).

PC AUC and PC peak were computed for each $w_{\text{pf-PC}}$ value as quantitative score to correlate the amount of LTD and LTP with the output activity of the cerebellar cortex.

3.2.5 Hardware and software

The SNN was built with the BSB release 3.0 (https://bsb.readthedocs.io/en/v3-last) and the numerical simulations were performed with NEST version 2.18 (https://zenodo.org/record/2605422).

The MF design, the timing optimisation, the MF validation, and the MF predictive simulations were implemented in Python 3.8. Functions packages written for the present work are available on *https://github.com/RobertaMLo/CRBL_MF_Model.*

All optimisation procedures and simulations were run on a Desktop PC provided with AMD Ryzen 7 2700X CPU @ 2.16GHz with 32 GB RAM in Ubuntu 16.04.7 LTS (OS).

3.3 Results

3.3.1 The cerebellar MF

The workflow for reconstructing the cerebellar MF is shown in Figure 3.1 leading to a condensed representation using 4 neuronal populations for GrC, GoC, PC, MLI neurons (Figure 3.2). The MF was designed based on structural and functional parameters extracted from SNN simulations and the time constant was optimized LFP experimental data. The MF working frequencies were extracted from NEST simulations of the cerebellar SNN exploring multiple ν_{drive} from 4 to 80 Hz. Then these frequency ranges were used to set different plausible presynaptic signals in defining the Numerical TFs of each population (Figure 3.3A). The ranges were [0.42, 24.17] Hz for GrCs, [3.63, 183.15] Hz for GoCs, and [3.27, 41.66] Hz for MLIs. Note that PC working frequencies were not computed since PC activity is only projected forward to the cerebral cortex, therefore PCs never play the role of presynaptic population in this cortical cerebellar microcircuit. The α parameters that maximised the fitting performance for each population were α $_{\text{GrC}}$ = 2, α $_{\text{GoC}}$ = 1.3, α $_{\text{MLI}}$ = 5 and α $_{\text{PC}}$ = 5. The fitted coefficients P are reported in Table 3.3

2D Analytical TFs show a sigmoidal trend in relation with excitatory inputs (Figure 3.3B). GoC inhibition strongly affects the GrC Analytical TF; for ν_{GoC} higher than 100 Hz, GrC Analytical TF is almost 0 Hz. For low inhibition, e.g., ν_{GoC}= 13 Hz, GrC Analytical TF is almost linear. MLI Analytical TF presents a well-defined sigmoidal trend depending on ν_{GrC} and modulated by the auto-inhibition, with resulting activity frequency spanning from 0 Hz up to 200 Hz. PC Analytical TF presents an increasing trend ranging from 0 to 100 Hz in relation to ν_{GrC} from 0 to 25 Hz, with the modulation due to the inhibitory control from MLIs. 3D Analytical TF of GoC shows a linear trend both for low and high ν_{drive}.

The cerebellar MF resulted in a set of 20 second order differential equations including the specific population TFs, where 4 equations described the time variation of population activity, and the remaining 16 equations modelled the covariances of the interconnected populations. Figure 3.4 shows the result of T optimisation: for T = 3.5 ms the average granular layer activity (purple line) interpolates the experimental LFPs (red dots) with a mean absolute error of 3%.
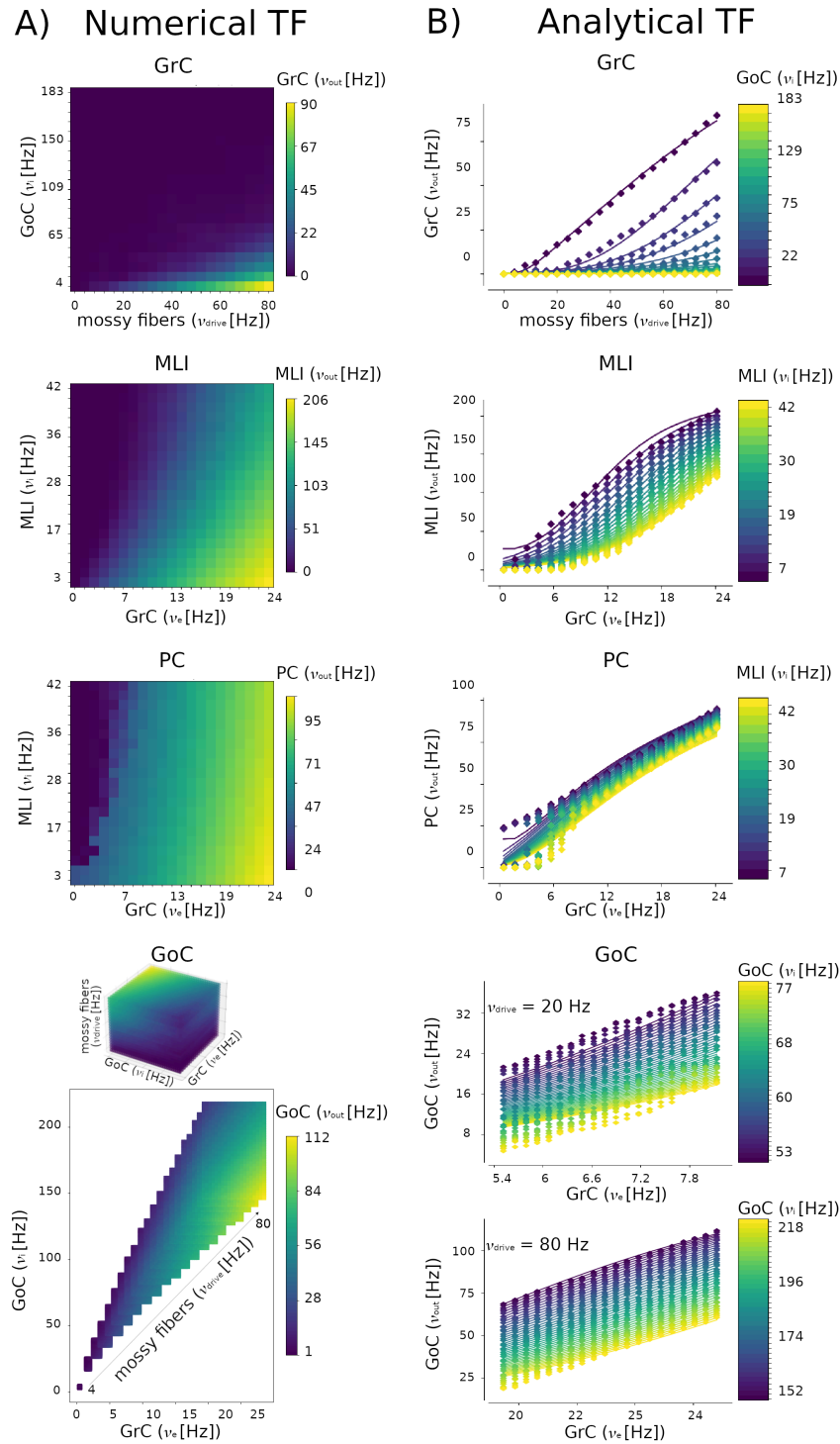
Figure 3. 3) Numerical TFs and the corresponding Analytical fitting. The simulation used to compute the numerical TFs last 5 seconds, with a time step = 0.1 ms. **A)** A 2D numerical TF template is reported for GrC, MLI and PC, which receive inputs from two presynaptic populations. A 3D numerical TF template is reported for GoC, which receive input from 3 presynaptic sources, i.e., mossy fibers, GrC and GoC. From the 3D domain of frequencies combination, only the physiological working frequencies of GrC and GoC are considered for mossy fibers inputs from 0 Hz to 80 Hz, as obtained in corresponding spiking neural network simulations and 3D numerical TF for GoC which receive three presynaptic inputs. **B)** The numerical TFs are used to fit the corresponding analytical TF. For each neuronal population, the average activity obtained in spiking neural network simulations is represented in color code, for each combination of input activity levels. The 2D analytical TF presents a non-linear trend, while the GoC Analytical TF shape is almost linear both for lower ν_{drive} = 20 Hz and higher ν_{drive} = 80 Hz.

Table 3. 3) Fitted coefficients of the Analytical TFs

Phenomenological threshold

$$V_{thre}^{eff}(\mu_V, \sigma_V, \tau_V)$$
$$= P_0 + P_{\mu V}\frac{\mu_V - \mu_V^0}{\partial \mu_V^0} + P_{\sigma V}\frac{\sigma_V - \sigma_V^0}{\partial \sigma_V^0} + P_{\tau V}\frac{\tau_V^N - \tau_V^{N0}}{\partial \tau_V^{N0}}$$
$$+ P_{\mu G}\ln\left(\frac{\mu_G}{g_L}\right)$$

Fitted coefficient P [V]

	P_0	$P_{\mu V}$	$P_{\sigma V}$	$P_{\tau V}$	$P_{\mu G}$
GrC	-0.426	0.007	0.023	0.482	0.216
GoC	-0.144	0.003	0.011	0.031	0.011
MLI	-0.128	-0.001	0.012	-0.093	-0.063
PC	-0.080	0.009	0.004	0.006	0.014

P coefficients computed with the fitting procedure explained in Zerlaut et al., 2016 and extended to E-GLIF neurons.
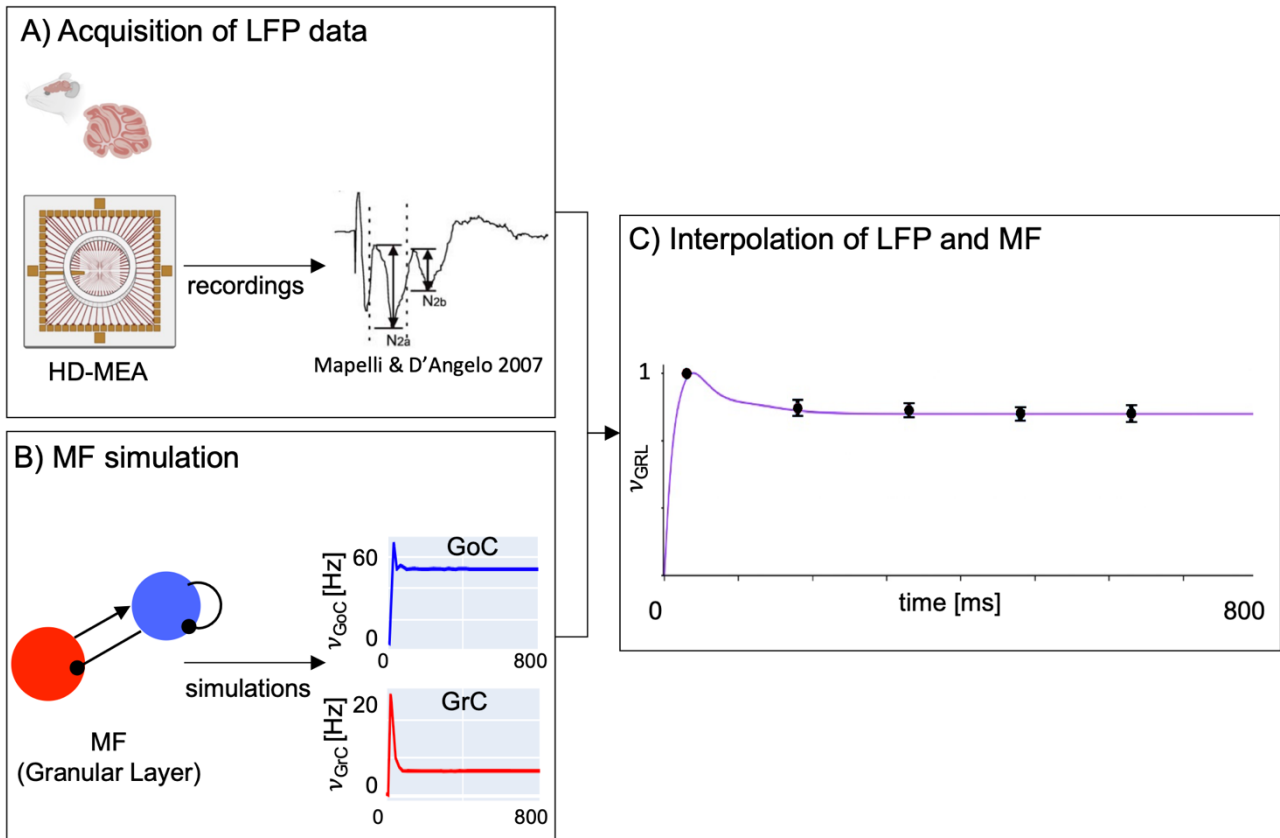
Figure 3. 4) The mean-field time constant. **A)** Experimental acquisition of LFP. LFP signals were acquired in the cerebellar granular layer of acute mice cerebellar para-sagittal slices using HD-MEA in response to five stimulation pulse trains of 50 Hz (Unpublished data, courtesy of Lisa Mapelli and Anita Monteverdi). **B)** MF simulation. The activity of the granular layer was simulated with the cerebellar MF using a stimulation protocol emulating experimental LFP recordings. **C)** Interpolation of LFP and MF. The weighted average of the predicted Granular Layer activity (ν_{GRL}, violet line) interpolates the LFP data (mean ± SD; dots and bars). The relative weights of GoC and GrC are 13% and 87%, respectively. The optimal T value is 3.5 ms ± 5%, (mean ± mean absolute error between ν_{GRL} and LFP).

3.3.2 Constructive and functional validity

The validation of the cerebellar MF was obtained generating neuronal population dynamics with different stimulation protocols and comparing them with the corresponding SNN simulations (Figure. 3.5). For all the protocols, the simulation lasted 500 ms and was performed with the hardware and software specified in **section 3.2.5.**

Step function (i). The MF was tested with a 250 ms@50 Hz step function on the mossy fibers, simulating a conditioned stimulus (Figure 3.5A) (Jirenhed and Hesslow, 2011). GrC activity rapidly raised at the beginning of the step input, then strongly decreased due to inhibitory GoC activity. GoCs, after an initial small peak due to both the direct incoming input and the GrC excitation, maintained a steady-state activity for all the step duration. The dynamics of GrC-GoC interplay faithfully reproduced the feedback loop between GoCs and GrCs. GrC was the excitatory input for the molecular layer, and both MLI and PC activity arose in correspondence of the GrC initial peak. Thus, exploiting network di-synaptic delays, MLIs reduced PC activity soon after its maximum, generating the typical burst-pause pattern of these neurons. The PC pause is due to both the single neuron parameters and to inhibitory local connectivity in the microcircuit. After this rapid transient, the activity of MLIs and PCs reached a steady-state. In the MF, fast dynamics at the input step onset and at the steady-state matched SNN simulations for all neuronal populations.

Theta band sinusoid (ii). Simulated dynamics of all cerebellar populations showed oscillations driven by the input reproducing whisker movements (Figure 3.5B) (Popa et al., 2013). GrC activity projected to the molecular layer a sinusoidal-shaped signal at 0.05-5Hz, contributing to an oscillatory behaviour in GoCs, and causing an oscillation in MLI between at 23-41 Hz, and in PC activity at 42-69 Hz. Oscillations had comparable amplitude in MF and SNN simulations and occurred in the same frequency ranges (except for MLI activity that was slightly higher in MF that SNN).

Alpha, gamma and theta band sinusoid (iii). Combination of alpha, gamma and theta sinusoids (with EEG-like frequency (Del Percio et al., 2017) of 1 Hz, 15 Hz, 30 Hz, respectively) caused an irregular oscillation in the input carried by mossy fibers (2-47 Hz range) (Figure 3.5C) Oscillations had comparable amplitude in MF and SNN simulations and occurred in the same frequency ranges.

Step function plus multi-band sinusoid (iv). The summation of repeated step function (i) and multi-band sinusoid (iii) resulted in an irregular input (Figure 3.5D) depicting in-vivo noisy baseline activity with a conditioned stimulus superimposed. GrC activity faithfully transmitted the driving input, with peaks at ~21 Hz. In correspondence with the GrC excitatory peak, MLIs peaked at ~130 Hz and PCs at ~100 Hz.

The responses had comparable dynamics and amplitude in MF and SNN simulations.
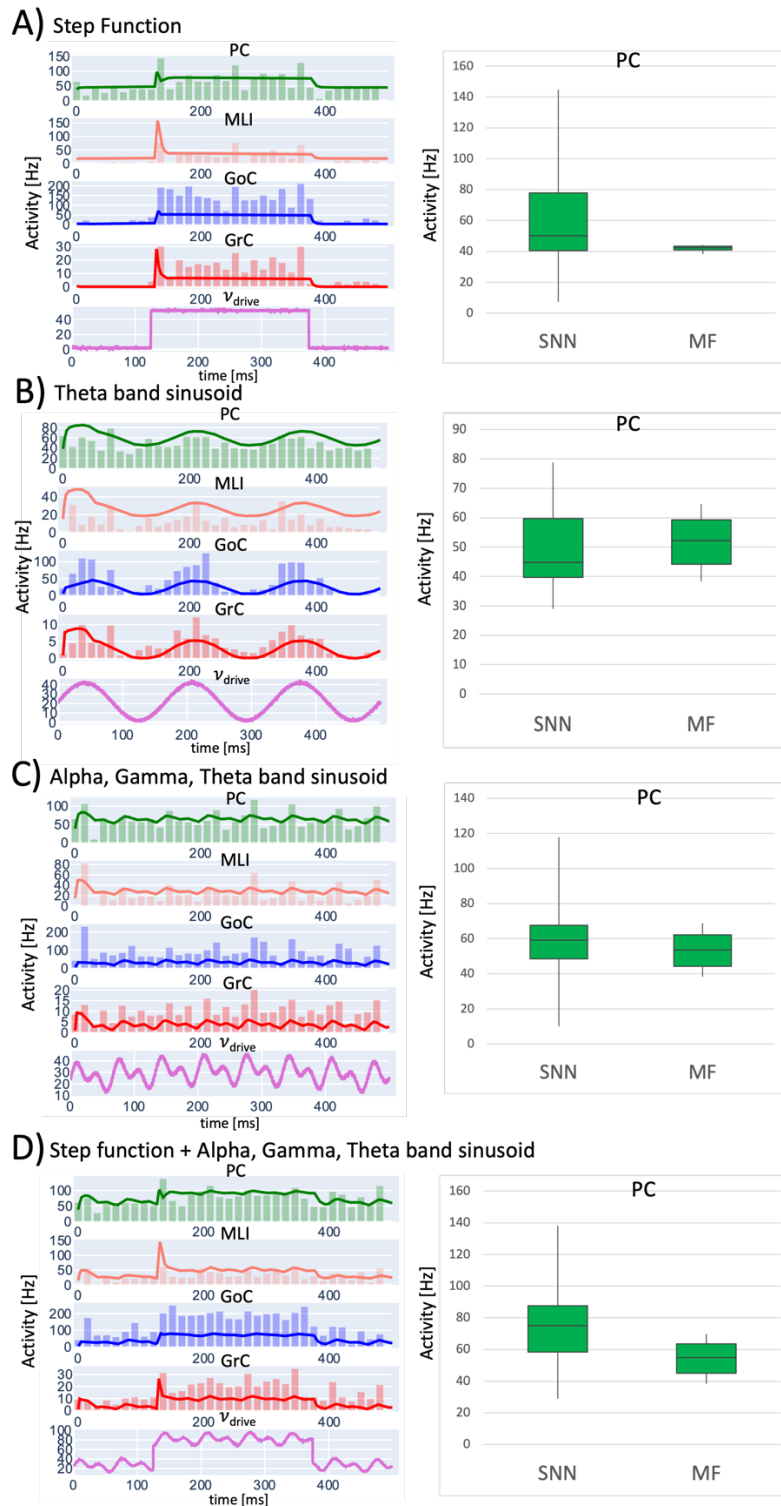
Figure 3. 5) Constructive and functional validity. Comparison of SNN and MF activity in cerebellar cortical populations in response to different driving input (ν_{drive}) patterns, lasting 500 ms with time resolution = 0.1 ms. **A)** step function (Conditioned stimulus-like); **B)** sinusoidal input in the theta band (whisker-like); **C)** multi-frequency sinusoidal function (EEG-like); **D)** combined stimulus summing (A) step function and (C) multi-frequency sinusoidal. The trace of MF activity is overlayed to the spiking activity, which is represented as a PSTH (time bins of 15ms). In all cases, MF activity is within physiological ranges, capturing also fast changes of activity due to instantaneous input changes in step-function input protocols. The boxplots of PC simulated activity with SNN and MF, shows that the MF is able to respond to the different stimulation patterns within the same frequency ranges of SNN.

3.3.3 Predictive validity

The PC response to a 50Hz step-stimulus was described by a peak at 97 Hz followed by a pause down to 68 Hz; then a steady-state of 78 Hz was attained. MLI-PC and pf-PC modulation (Figure 3.6) perturbed this reference condition.

MLI-PC feed forward inhibition

Inhibitory interneurons control the generation of burst-pause patterns in PC, which is fundamental for shaping the cerebellar output during motor learning (Casali et al., 2019; Kim and Augustine, 2021). For instance, knock-out of MLI inhibition on PC impacts on vestibulo-ocular reflex adaptation (Wulff et al., 2009). Here in MF simulations, when the MLI-PC conductance was reduced to 5% of the reference condition, the burst-pause dynamics of PC was lost, so that the PC firing settled directly back to baseline (which was elevated due to lack of inhibitory control). Conversely, when PCs were over-inhibited by the MLIs (MLI-PC conductance increased to 250% of reference condition), the pause was deeper. The PC overall activity (AUC), and PC Peak reveal an exponential trend that decays for higher MLI-PC conductances. The PC pause shows a decreasing sigmoidal trend for higher MLI-PC conductances (Figure 3.6A).

PC plasticity

Long Term Depression (LTD) and Long Term Potentiation (LTP) at pf-PC synapses are though to drive cerebellar adaptation and learning. The overall activity and the peak of PCs showed a linear and a sigmoidal trend, respectively, with the increase of pf-PC weight. With decreased pf-PC strength, the peak was reduced or disappeared, and the steady-state activity reached lower levels. With increased pf-PC strength, both the peak and steady-state values were increased (Figure 3.6B). During a typical cerebellum-driven behaviour, the eyeblink classical conditioning (EBCC), a level of suppression of about 15% has been reported and correlated with a stable generation of associative blink responses at the end of the learning process (ten Brinke et al., 2015). SNN simulation got the same result by setting AMPA-mediated pf-PC synapses = 35% (De Schepper et al., 2022). In MF simulations, for w_{pf-PC} = 65%, which corresponded to a reduction of pf-PC conductance of 35%, PC activity presented a 22% reduction of the peak and a 10% reduction of the AUC, falling into the experimental range of PC suppression (ten Brinke et al., 2015).
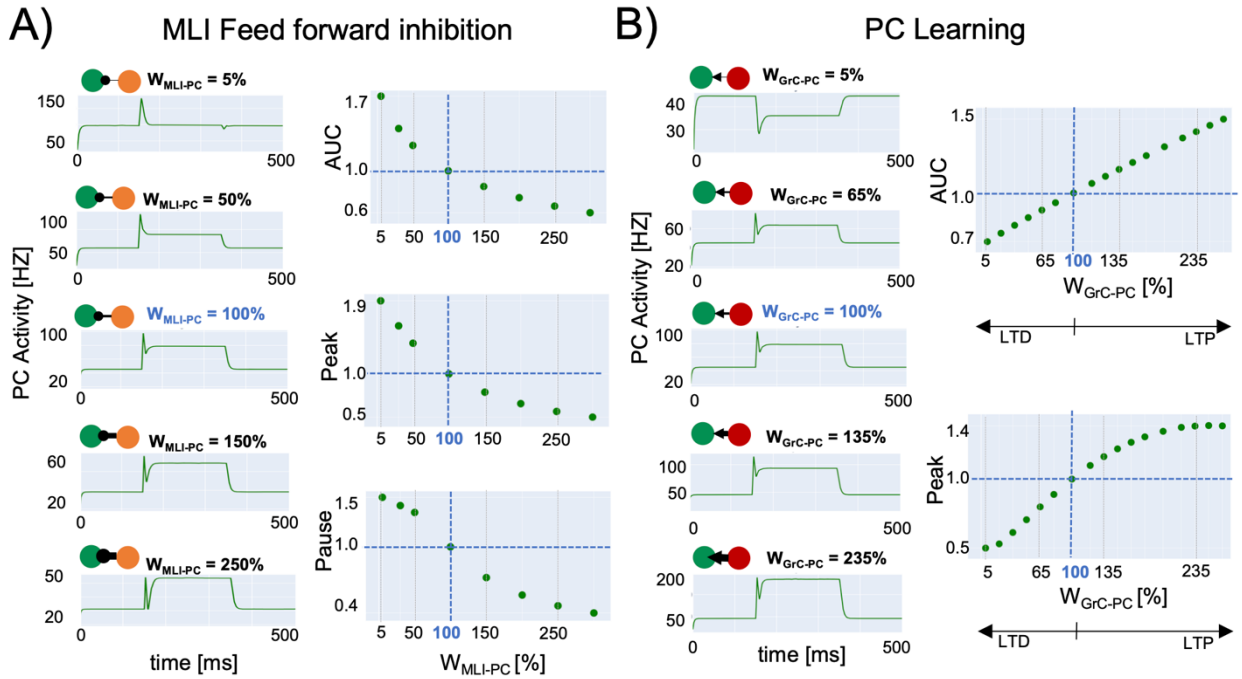
Figure 3. 6) Predictive validity. MF simulations using different strengths at PC connections. Simulations last 500 ms with a time resolution of 0.1 ms and νdrive is a step at 50 Hz lasting 250 ms starting at 125 ms. Quantitative score normalized to baseline (w = 100% in blue). **A) MLI-PC feed forward inhibition**. The change of total activity (measured as AUC) and the initial peak amplitude decrease exponentially with the MLI-PC strength. The amplitude of the pause after the peak response decreases with MLI-PC strength following an inverse sigmoidal function. **B) PC Learning** with different GrC-PC plasticity conditions (LTP and LTD). AUC linearly increases with the GrC-PC strength, matching the experimental values in experimental learning protocols. The initial peak caused by the step stimulus onset increases with GrC-PC until saturation, following a sigmoidal function.

3.4. Discussion

This work shows, for the first time, a MF of cerebellar cortex. According to its bottom-up nature, the MF transfers the microscopic properties of neurons (including GrC, GoC, MLI, and PC) and synapses of the cerebellar cortex into a condensed representation of neural activity through its two main statistical moments, mean and variance. The construction and validations strategies adopted here make the present MF an effective representation of the main physiological properties of a canonical cerebellar module (D'Angelo and Casali, 2013)

3.4.1 MF design and validation

The cerebellar network and TF formalism

The cerebellar cortex MF was based on the same general formalism previously developed for the isocortex MFs (Moran et al., 2013; Di Volo et al., 2019; Carlu et al., 2020; Huang and Lin, 2021). However, the cerebellar cortex MF benefitted of a previously validated SNN to precisely remap cellular and synaptic biophysical properties and network topology. Moreover, the electrophysiological properties of neurons were represented using non-linear EGLIF models and the synapses with alpha-based conductance functions. This resulted in three main advantages.

First, the parameters of population specific TFs were validated against biophysically detailed models of neurons and the connectome was derived from precise scaffold model reconstructions providing a direct link to the biological microcircuit (De Schepper et al., 2022).

Secondly, the equations of μ_V, σ_V and τ_V included in the TF formalism were adapted to model the alpha-shaped synapses and to maintain rise-times in synaptic dynamics. For comparison, previous MFs (Zerlaut et al., 2016, 2018) used exponential synapses, which provide a less realistic approximation due to their instantaneous rise time (Brette and Gerstner, 2005).

Finally, MF included 4 different species of neurons that were modelled using either 2D or 3D TFs to account for the multiplicity of their inputs (Figure 3.3). It is worth noting that the analysis of both 2D TFs of GrC, MLI and PC, and 3D TF of GoC were fitted considering only physiological input combinations computed from single-neuron computational models. In the fitting procedures, indeed, fine-tuned parameters were included to maintain a strong physiological correspondence. The 3D dimension of the GoC TF avoided to merge the excitatory input from GrC and mossy fibers (ν_{GrC} and ν_{drive}, respectively), enabling us to investigate distinct excitatory input contributions to granular layer dynamics and to the whole cerebellar MF. By fixing the excitatory mossy fibers driving input, we assessed the power of the Analytical TF in simulating spiking network activity for inputs at both low and high frequency (e.g., see Figure 3.4 with ν_{drive}= 20 Hz and = ν_{drive}= 80 Hz).

A technical issue incurred while fitting the numerical TF. The TF formalism models the difference between phenomenological threshold (V_{thre}^{eff}) and population average responses (μ_V) through the complementary error function (erfc in equation (34)), providing an immediate interpretation of how single neuron activity was related with statistics of population dynamics (μ_V, σ_V, τ_V). Since erfc is stiff and limited between -1 and 1, it may not accurately follow the numerical TF distribution at the boundaries, losing precision at high frequencies. This problem was circumvented by tuning the parameter alpha (Carlu et al., 2020), making the TF analytical expression reliable over the whole range of input working frequencies.

MF tuning

The inclusion of precise structural and functional parameters in the design of cerebellar MF (see Figure 3.2 and 3.3) generated a biology grounded model that could be validated at a higher scale with the prediction of cerebellar dynamics (multi-layer equation 42). The dynamics of the cerebellar cortex are several times faster compared to those of the cerebral cortex (D'Angelo, 2011), so that the MF time constant, T, must be optimized accordingly. The MF time constant was optimized using experimental LFP recordings from the cerebellar granular layer acquired on the same spatial scale of the MF. The best fitting was obtained by accounting for the smaller contribution of GoC than GrC activity (13% vs. 87% (Dieudonné, 1998; D'Angelo et al., 1999)) to LFPs (Mapelli and D'Angelo, 2007), revealing that the MF time constant of the cerebellar cortex is T=3.5 ms with mean absolute error of 3% (Figure 3.4). T is definitely smaller than in cerebral cortex MFs, which range up to 20 ms (Zerlaut et al., 2018; Di Volo et al., 2019; Carlu et al., 2020), and captures the peculiar high speed of cerebellar dynamics (D'Angelo, 2011). This result further confirms the need of a MF specifically tailored on the cerebellum functional and topological parameters.

The optimal T value was plugged into equation 42 resulting in a second order differential equation system of interdependent TFs capturing the dynamics of multiple cerebellar populations and their covariances. This rich pool of equations allowed our cerebellar MF to reproduce a variety of cerebellar dynamics in response to different inputs (see **section 3.2.3** and shown in Figure 3.5) which, by comparison with the equivalent SNN output, provided the benchmark for constructive and functional validity. A rapidly changing input like a step function reproduced a conditioned stimulus (Jirenhed and Hesslow, 2011) carried by the peripherical mossy fibers, causing rich dynamics in the cerebellar cortex including the typical PC burst-and-pause responses (Herzfeld et al., 2015). Adding a multi-sinusoidal input to the conditioned stimulus replicated a more physiological condition accounting for background activity. This resulted in rich PC dynamics, which still maintained burst-and-pause responses. A sinusoidal input was meant to emulate more complex experimental conditions, like those determined by whisker movement (Popa et al., 2013; Yamazaki and Igarashi, 2013; Antonietti et al., 2017; Masoli et al., 2020a; Gagliano et al., 2021, 2022). In particular, a multi-sinusoidal waveform (comprised of frequencies in the EEG spectrum) was used to emulate composite inputs from the cerebral cortex (Del Percio et al., 2017; Tzvi et al., 2022).

The cerebellar MF reproduced the known aspects of circuit physiology revealed experimentally. Indeed, GrCs respond to impulsive inputs with bursts curtailed by GoCs and are also able to follow slower input fluctuations (D'Angelo and De Zeeuw, 2009). The PCs generate burst-pause responses that are accentuated by MLIs (Masoli and D'Angelo, 2017; Rizza et al., 2021). The cerebellar MF quantitatively reproduced these patterns matching the corresponding SNN simulations, with the only exception of the maximal GoC responses, which did not increase as expected with rapidly changing inputs like the step function. This is a consequence of the lack of GoC heterogeneity in MF, in which all GoC are collapsed in a homogeneous population despite their biological heterogeneity (Galliano et al., 2010). Except for this, MF predicted with good approximation the SNN cerebellar output, i.e., the PC activity (Boxplot in Figure 3.5). The inclusion of probabilistic kernels addressing parameter heterogeneity could also help improving the MF fitness (Di Volo and Destexhe, 2021).

3.4.2 MF predictions

A critical step in model validation is to demonstrate its ability to predict functional states not used for model construction. The cerebellum is well known for the ability to change its network functioning because of synaptic and non-synaptic plasticity. However, different from SNN, the MF did not include plasticity mechanisms. Thus, we directly tested the MF ability to predict the effects of plasticity expression by mapping a set of precomputed synaptic changes on the MF itself. MF reproduced the impact of MLI-PC conductance confirming that, also in the cerebellar MF, the complex burst-pause behaviour of PC is tuned through the MLI-PC connectivity.

The cerebellar MF reproduced the experimental recordings in EBCC experiments on behaving mice (ten Brinke et al., 2015) pointed out a PC LTD of 10% in terms of overall activity and 22% for the peak (Figure 3.6 $w_{pf-PC} = 65\%$). This protocol corresponds to a reduction of 35% of AMPA-mediated pf-PC in SNN simulation, therefore our MF capability of capturing synaptic mechanism is further validated against in-vivo recordings.

In aggregate, the cerebellar MF, despite a lower level of detail than SNN, was able to reproduce complex physiological mechanisms and predict the activity changes caused by synaptic modulation (ten Brinke et al., 2015; De Schepper et al., 2022). Therefore, this MF is a flexible tool that can be

used to investigate advanced physiological or pathological properties by tuning the input of TF on a target population (TF$_{PC}$ in these simulations), without complicating neither the TF fitting procedure nor the model equations. The procedure of parameters tuning might pave the way for further manipulation to remap physiological and/or pathological features onto the MF. Identifying and extracting biophysical meaningful features from subject-specific data, like diffusion weighted imaging or spectroscopy, might allow the MF tailoring onto subject-specific characteristics and to combine functional simulations with (micro)structural information.

3.4.3 Performance vs. realism

The MF approximated a complex SNN of ~$3x10^4$ neurons and ~$1x10^6$ synapses (**section 3.2.1**) with 20 equations reducing the computational time by 60% with lower memory requirements. Nevertheless, TFs fitting could be improved replacing the procedure in **section 3.2.2 - TF computation** with a lookup table-based algorithm, which might yield to a gain in computational time up to an order of magnitude. This will represent a definite advantage when performing long-lasting simulations reflecting the acquisition time of *in vivo* recordings like EEG and fMRI or when simulating learning processes in closed-loop controllers. On the other hand, thanks to its bottom-up nature it was possible to maintain the biological realism in responses to various stimuli, including simulations of learning-induced firing rate changes and pathological conditions at the neuronal population level, obtaining a good balance between computational load and biological plausibility. This will allow to make predictions on the underlying neural bases of ensemble brain signals and to identify the elementary causes of signal alterations in pathology.

3.4.4 Conclusions and perspectives

In aggregate, the cerebellar cortex MF enforces a bottom-up approach tailored to the specific structural and functional interactions of the local neuronal populations and has a substantial constructive and functional validity. By accounting for a variety of representative patterns of discharge in cerebellar cortical neurons, the present MF can be considered as an effective proxy of the biological network. The internal model parameters inform about the average properties and variance of fundamental mechanisms in the circuit, namely intrinsic and synaptic excitation, and can therefore be used to remap biological properties onto the MF (Naskar et al., 2021). In future applications, this will allow to tune the MF toward specific functional or dysfunctional states that affect the cerebellum. Among these it is worth mentioning ataxias (Pedroso et al., 2019; Rosenthal, 2022), paroxysmal dyskinesia (Mendonça and Alves da Silva, 2021; Ekmen et al., 2022), dystonia (Mahajan et al., 2021; Morigaki et al., 2021), autistic spectrum disorders (Bruchhage et al., 2018; Kelly et al., 2020) as well as other pathologies like and multiple sclerosis (Tornes et al., 2014; Schreck et al., 2018), dementia (Monteverdi et al., 2022) and Parkinson disease (Wu and Hallett, 2013; Shen et al., 2020), in which a cerebellum involvement has been reported. The cerebellar MF could be applied to whole-brain simulators using TVB and DCM, as much as it has been done before for the isocortical MF in TVB (Pinotsis et al., 2012; Goldman et al., 2019; Sadeghi et al., 2020; Ruffini and Deco, 2021). Considering the specificity of signal processing in different brain regions, this approach represents a definite step ahead compared to the classical one adopting generic neural masses for all brain regions. This is a promising active field in theoretical neuroscience and clinics, indeed applications of specific MF to Parkinson disease have been already implemented by reconstructing a

model specifically tailored on basal-ganglia and connected with thalamocortical circuit (BGTCS MF), accurately reproducing parkinsonian state (van Albada and Robinson, 2009; van Wijk et al., 2018). Integrating BGTCS and cerebellar MF, and in general MF specifics of brain regions embedded into the motor circuit, would remarkably improve the simulation of brain dynamics, allowing to compare dysfunctional oscillations with physiological activity.

On the theoretical side, TVB simulations using classical neural masses (Wong and Wang, 2006) for all brain nodes (Palesi et al., 2020; Monteverdi et al., 2022) can now be compared to those using the cerebellum MF. At the other extreme of the spectrum, TVB with embedded cerebellar MF can be compared to TVB-NEST co-simulations (Meier et al., 2022), in which spiking neurons are represented explicitly (Geminiani et al., 2018, 2019b, 2019a; De Schepper et al., 2022). These comparisons will inform us about the impact of populations, neurons, and spikes on ensemble brain dynamics and whole brain computations (D'Angelo and Jirsa, 2022).

In conclusion, the cerebellar MF represents the first step toward a new generation of models capable of bearing biological properties into virtual brains that will allow to simulate the healthy and pathological brain towards the overarching aim of a personalized brain representation and ultimately personalized medicine and the technology of brain digital twins (Amunts et al., 2022).

Take the stock: possible improvements and future perspectives

Mean Field theory presented in **Chapter 2** is a reliable formalism for direct simulation of mesoscale data as LFPs, and calcium imaging but also macroscale recordings such as BOLD signal by using interconnected MFs integrated into whole-brain simulators. The MF approach has been already tested to reproduce mesoscale cerebral cortical data and it has been extended to achieve an improved biological reliability (Di Volo et al., 2019). Nevertheless, this formalism presents some limitations that the extension to a more complex multi-layer network doesn't overcome. The aim of this chapter is to take the stock of the present thesis, discussing potential limits and improvements (**section 4.1**). Furthermore, it provides an overview of ongoing works and future developments of the multi-layer cerebellar model in the perspective of its integration in brain dynamic simulators (**section 4.2**).

4.1 Limits and model improvements

MF is an approximation of the real physiological context of neural circuits and even if the multi-layer network design depicts the biological structure of the cerebellar cortex, some simplifications have been performed. As an example, to define the average membrane potential μ_V only the leakage current (E_{LgL}) was considered while the dynamics of other currents, such as the sodium one, were neglected. This assumption is generally acceptable but when the neuron firing rate increases, e.g., due to a high external stimulus, this could become a poor assumption (Carlu et al., 2020). Furthermore, the present multi-layer cerebellar MF doesn't include an equation to model complex phenomena such as adaptation, whose contribution would significantly improve the predicted activity for GoC and PC.

As mentioned in **section 2.3.2**, the choice of T is a crucial part of the formalism. In the multi-layer cerebellar MF presented here T was optimized on neuronal and microcircuital experimental recordings, strictly linking the multi-layer cerebellar MF to biological data. However, these experimental data were available only for the granular layer, therefore T was optimized only for this layer and then assumed to be equal also for molecular and Purkinje layer. The granular layer is known to be the driving part of the circuit so it was plausible to extend the optimal T also to the other layers, however it is not possible to exclude that the integration of data from molecular and/or Purkinje layer would modify the optimal T value. Furthermore, the optimization was performed interpolating the granular layer MF activity with the mean of LFP signals amplitude recorded from different channels, but it would be incredibly interesting to generate LFP data directly form the MF model and compare them with the experimental ones, to obtain a stronger validation of T.

The SNN of the cerebellar cortex is build up with 29230 neurons. Each neurons dynamics is reproduced with three EGLIF equations, along with other equations for the alpha synaptic conductances (**section 3.2.1**), resulting in more than 90000 equations. Although the MF presented here reduced the SNN complexity to 20 differential equations (**section 3.4.3**), its computational efficiency could be further improved. Two step fitting procedure of TFs (**section 3.2.2**) yielded to a population-specific TF analytical expressions that captures the different activity of each neuronal population, such as linear behavior of GoC and almost sigmoidal trend of GrC TFs (**section 3.3.1**). On the other hand, the error function computation embedded into the analytical TF expression could be time-consuming. TVB already integrated an efficient lookup-table based formalism, thus in the perspective of integrating the cerebellar MF into TVB and connecting it with other cortical MFs, replacing the two-step fitting procedure with the lookup-table would significantly speed up the computational time of simulation.

4.2 Ongoing studies and future perspective

The work presented in this thesis could trigger future studies focusing on different aspects such as investigating the impact of cerebellar on cortical dynamics to predicting functional and dysfunctional mesoscale mechanisms. The role of the cerebellum in brain dynamics was investigated both in resting condition with TVB and during complex task performance with DCM (**section 4.2.1**). Our results demonstrated that its inclusion in resting state dynamics simulation improved the accuracy of simulated functional dynamics, and its activity modulated the complex response in cortical areas recorded by fMRI. Moreover, an explorative study to assess whether the model can reproduce also pathological and altered pattern is ongoing with promising outcomes to further explore the possibility to tune the cerebellar MF on parameters specific to model pathologies (**section 4.2.2**). These results are promising thanks to a sophisticate and deeply biology grounded network which can be further improve by adding more components (i.e., layers) such as the Deep Cerebellar Nuclei (**section 4.2.3**)

4.2.1 Why multi-layer cerebellar MF should be integrated in whole-brain dynamics simulators?

One might wonder whether the integration of the multi-layer cerebellar MF in TVB and DCM is a merely theoretical exercise or could improve the accuracy of whole-brain dynamics simulation, representing a tangible step ahead in personalized medicine. The present section aims to provide an answer to this query by presenting two studies that investigate the role of the cerebellum in whole-brain dynamics.

Firstly, we published a study that is pioneering in including cerebellar nodes for simulating whole-brain dynamics (Palesi et al., 2020):

The Importance of Cerebellar Connectivity on Simulated Brain Dynamics

F. Palesi[1,2], R.M. Lorenzi[1], C. Casellato[1], P. Ritter[3,4], V. Jirsa[5], C.A.M. Gandini Wheeler-Kingshott[1,2,6] and E. D'Angelo[1,2]

1 Department of Brain and Behavioral Sciences, University of Pavia, Pavia, Italy
2 Brain Connectivity Center, IRCCS Mondino Foundation, Pavia, Italy
3 Brain Simulation Section, Department of Neurology with Experimental Neurology, Charité –Universitätsmedizin Berlin and Berlin Institute of Health, Berlin, Germany
4 Bernstein Center for Computational Neuroscience, Berlin, Germany
5 Institut de Neurosciences des Systèmes – Inserm UMR1106, Aix-Marseille Université,Marseille, France
6 NMR Research Unit, Queen Square MS Centre, Department of Neuroinflammation, UCL Institute
of Neurology, London, United Kingdom

TVB takes in input experimental recordings such as EEG or fMRI specific of several distinct brain regions (i.e. nodes) and provides as output the simulated functional activity for all nodes, from which functional connectivity between pairs of nodes is derived. The best simulations are obtained by optimizing model parameters through an iterative procedure that maximize a similarity measure between simulated and empirical functional connectivity (**section 1.2.3**). To perform this study, fMRI experimental recordings from the free available Human Connectome Project database (https://db.humanconnectome.org/) were provided as input to TVB. The brain cortex was parcellated into 93 regions and 33 cerebellar nodes were added. The structural connectome was defined based on whole-brain tractography and corrected for the cerebro-cerebellar connections explored in a previous work (Palesi et al., 2017). The empirical functional connectivity was computed by extracting the average time-course of the BOLD signal per node, and Pearson correlation coefficient (PCC) of the BOLD was computed between pairs of nodes.

To assess the impact of cerebellum on cerebral dynamics, three different networks were considered:

1. Whole-brain network with 126 nodes (cerebral and cerebellar regions together) (Figure 4.1 A- red).
2. Cerebral subnetwork with only the 93 cerebral nodes (Figure 4.1 A - light blue).
3. Embedded cerebro-cerebellar subnetwork, evaluating the simulated functional connectivity as discrepancy between the simulated functional connectivity computed in 1 and 2 (Figure 4.1 A – orange)

The functional connectivity was simulated for each of the three networks and correlated with the empirical functional connectivity.

Our findings revealed an improvement in simulated functional dynamics of the cerebral cortex when the cerebellar nodes were included, thus the simulation protocol described in 3. maximized the similarity between empirical and simulated functional connectivity (Figure 4.1 B). These promising outcomes demonstrated that the impact of the cerebellum on cerebral cortex dynamics couldn't be neglected anymore to achieve an increasing realism in large-scale functional simulations. Furthermore, the accuracy of the cerebellar impact on whole-brain dynamics can be improved by replacing general MF models with a cerebellar specific MF model.

A - Functional networks

Whole-brain network

Cerebral subnetwork

Embedded cerebro-cerebellar subnetwork
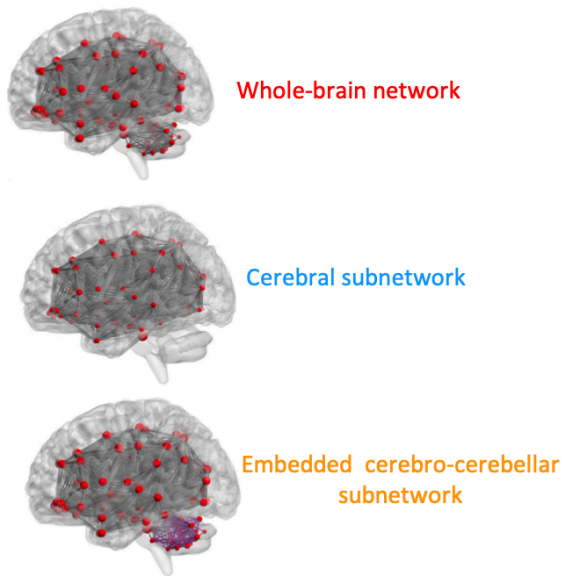
B - PCC between empirical FC and simulated FC
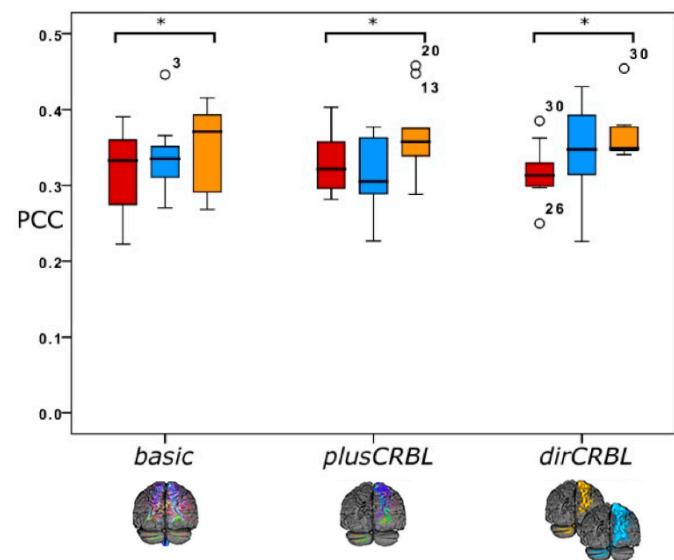
Figure 4. 1) TVB study: The impact of the Cerebellum on whole-brain dynamics. **A)** <u>Functional networks</u>. Three functional networks were defined: Whole-brain network (red), Cerebral subnetwork (light blue), Embedded cerebro-cerebellar subnetwork (orange). **B)** <u>Statistical analysis.</u> Simulated functional connectivity (FC) was correlated with the empirical FC through PCC, considering three different structural connectivity (SC) extracted from tractography: basic = SC with spurious cerebro-cerebellar tracts; plusCRBL= SC with only contralateral cerebro-cerebellar tracts; dirCRBL = SC with directional contralateral cerebro-cerebellar tracts. Embedded cerebro-cerebellar subnetwork shows a significant higher PCC with respect to whole-brain network in basic, plusCRBL and dirCRBL cases. Adapted from Palesi et al., 2020.

In addition to this work (Palesi et al., 2020), we performed a DCM-based study (**section 1.2.3**) to investigate whether the cerebellum acts both as a predictor and a modulator of the activity of cortical regions. Specifically, the modulation of complex BOLD response in cortical regions during action execution was investigated. Below the pipeline and the outcomes of the DCM analysis are presented.

The cerebellum modulates non-linear behavior of motor planning areas in variable grip force visuomotor task

Roberta Maria Lorenzi[1], Gokce Korkmaz[1], Adnan Alahmadi[2,3], Letizia Casiraghi[4], Anita Monteverdi[5], Egidio D'Angelo[1,5], Fulvia Palesi[1], Claudia A.M. Gandini Wheeler-Kingshott[1,3,5]

[1]Department of Brain and Behavioural Sciences, University of Pavia, Pavia, Italy
[2]Department of Diagnostic Radiology, College of Applied medical sciences, King Abdulaziz University, Jeddah, Saudi Arabia
[3]NMR Research Unit, Queen Square Multiple Sclerosis Centre, Department of Neuroinflammation, UCL Queen Square Institute of Neurology, UCL, London, UK
[4]Department of Mental Health and Dependence, ASST of Pavia, Pavia, Italy
[5]Brain Connectivity Center IRCCS Mondino Foundation, Pavia, Italy

Introduction. Dynamic Causal Modelling (DCM) is a framework stablishing causal relationships between interconnected brain regions by estimating the direct influences (effective connectivity) and the hierarchical activations of different brain regions (Friston et al., 2003). DCM relies on Bayesian inference that estimates the connectivity parameters combining priors with the observed Blood Oxygenation Level Dependent (BOLD) signals. Here, DCM was used to investigate the causal influence of the cerebellum onto the cerebral regions embedded in a cerebro-cerebellar loop activated by a visuomotor task.

Material and Methods. High-resolution anatomical T13D and fMRI images of twenty-three right-handed healthy volunteers were analyzed. Subjects performed with their right hand a dynamic power grip task, using a squeeze-ball, controlled by a visual cue (Alahmadi et al., 2016; Casiraghi et al., 2019) A standard fMRI pre-processing steps were applied to optimize the experimental data. The visuomotor network included the right cerebellum, bilateral primary visual cortex, left primary motor cortex, left supplementary motor area, left premotor cortex, left cingulate cortex, and left superior parietal lobule. Different DCM models were specified and estimated to assess with which cerebral regions the cerebellum is connected and how it modulates cortical activity.

Results. The winning model, i.e., the model that maximized the likelihood with BOLD, demonstrated that the cerebellum linearly modulated the primary motor cortex, while a quadratic modulation was found with supplementary motor area, both results with a probability higher than 90%.

Discussion and conclusion. For the first time the cerebellum was included in a visuomotor network, and it was not consider as merely connected with the other cerebral regions, but it was supposed to have a strong influence on responses recorded in the cerebral regions. Our findings showed that the cerebellum was not only effectively connected with cerebral motor area as expected, but it also modulated the complex activation in supplementary motor area, suggesting that the cerebellum activates before than this cortical area during action prediction (Figure 4.2). Further investigations could explore whether the cerebellum modulates the activity also of cingulate cortex and superior parietal lobule, which are involved in action selection and visual attention respectively (Serences, 2008; Bueichekú et al., 2020). Needless to say, this overview on the hierarchical activation of cerebro-cerebellar functional links could be of great interest for understanding BOLD variation in neurological diseases involving these regions. To further improve these results and to achieve a framework enough reliable both for research and for clinics, specific model tailored on specific regions should be included. Compared to novel promising techniques to quantify the effective

connectivity, (Gilson et al., 2019; Hahn et al., 2019; Prando et al., 2020), DCM provides reliable results for a limited number of regions. On the other hand, first attempts to include model specific for subcortical cerebral structure as the thalamus and basal ganglia have been done to investigate altered effective connectivity in Parkinson disease but a cerebellar-specific model is still missing, limiting the specificity of the outcomes for pathologies that deeply affect the cerebellum. For this reason, the multi-layer cerebellar MF presented here would be a promising tool to improve DCM power in studying the effective connectivity and consequently the hierarchy within cerebro-cerebellar loops.
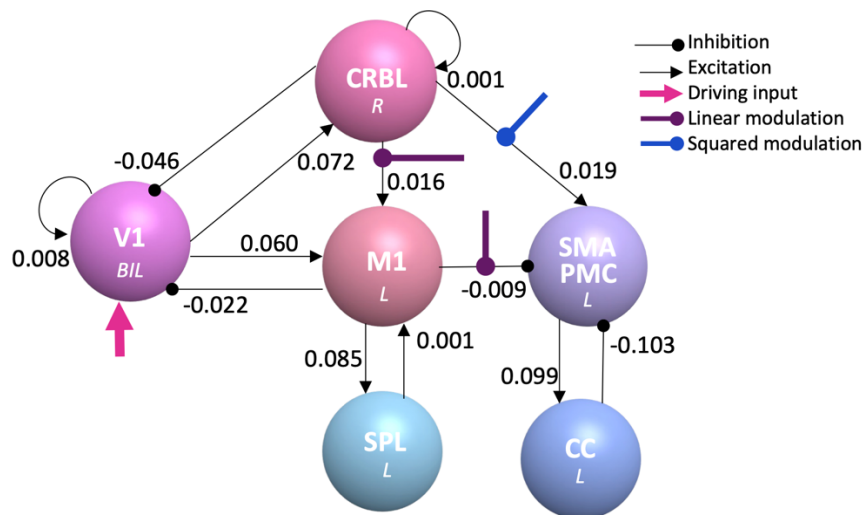
Figure 4. 2) DCM study: Cerebellum as a modulator of a visuomotor network. Visuomotor network with effective connectivity. For each subject, Bayesian model inversion quantified the posterior value for each connection, then the values of the effective connectivity were averaged to get group-wise effective connectivity. Cerebellum (CRBL - pink) modulates the activity of the primary motor cortex (M1 - salmon) with a linear relation (e.g., CRBL activity increases and then also M1 activity increases), and the activity of the supplementary motor area and of the premotor cortex (SMA-PMC - violet), demonstrating to act as a predictor both for action execution (CRBL-to-M1) and action planning (CRBL-to-SMA PMC). BIL= Bilateral, R = Right, L = Left., V1 = primary visual cortex (driving region), SPL = superior parietal lobule, CC = cingulate cortex.

4.2.2 Pathological MF: the dystonic cerebellum

One of the most relevant applications of the multi-layer cerebellar MF might be the simulation of altered activity due to pathologies that deeply involve the cerebellum, such as cerebellar ataxia, autism, and dystonia. In this context, a preliminary investigation to test whether the multi-layer cerebellar MF can reproduce an altered pattern without modifying its own parameters was carried out. A dystonic input was simulated with the same protocol already used to validate SNN of the cerebellar cortex, which was used here as functional reference. This perspective study is presented in the abstract below, showing the preliminary results and underlining future developments.

Multi-layer cerebellar mean-field model reproduces altered dystonia-like patterns of activity

R.M. Lorenzi*[1], A. Geminiani[1], C.A.M Gandini Wheeler Kingshott[1,2,3], F. Palesi[1], C. Casellato[1] and E. D'Angelo[1,3]

[1] Department of Brain and Behavioral Sciences, University of Pavia, Pavia, Italy
[2] NMR Research Unit, Queen Square Multiple Sclerosis Centre, Department of Neuroinflammation, UCL Queen Square Institute of Neurology, UCL, London, UK
[3] Brain Connectivity Center, IRCCS Mondino Foundation, Pavia, Italy

In preparation

Introduction. Dystonia is a disorder characterized by sustained or intermittent muscle contractions causing abnormal movements, postures, or both. Traditionally, dystonia related to basal ganglia dysfunction but recent evidence found also cerebellar abnormalities correlated with dystonia (Pizoli et al., 2002; Fremont et al., 2017; Washburn et al., 2019). PC burst-firing with excessive and repetitive complex spike firing was observed in cerebellum-specific IP3R1 knock-out dystonic mice, which also exhibited increased Inferior Olive (IO) activity (LeDoux and Lorden, 2002). A recent study of spiking cerebellar cortex suggested that only certain types of alteration in olivocerebellar input are compatible with changes observed in dystonia, indicating that some cerebellar lesions can have a causative role in the pathogenesis of symptoms (Geminiani et al., 2022). Thus, in this work the power of the cerebellar MF model was tested in reproducing pathological pattern of activity by modelling a dystonic lesion.

Material and Methods. The stimulation protocol was implemented to provide the typical stimuli of Eye-Blink Classical Conditioning (EBCC), where a spiking cerebellar cortex was used to simulate dystonia during EBCC. The conditioned stimulus (CS), e.g., a sound, was simulated as a non-recurrent 40-Hz spike train conveyed by mossy fibers lasting 280 ms. In the MF simulation, the CS and US input were similarly implemented. The unconditioned stimulus (US), e.g., an Air-Puff, was carried by the climbing fibers from the IO to the PC and in the MF model was introduced in TF_{PC} as an extra excitatory contribution summed to the ν_{GrC} to model the IO-PC synaptic convergence from the spiking neural network (SNN). TF_{PC} dependencies resulted:

$$TF_{PC}(\nu_{GrC} + US \cdot K_{io-PC}, \nu_{MLI})$$

The US pattern was simulated as a 500-Hz burst lasting 30 ms and co-terminating with the CS. One CS-US repetition was simulated, followed by a 620 ms baseline period as physiological reference. This was reproduced as a 20-ms spike train with 40 ms pauses in IO neurons (Geminiani et al., 2022). Dystonic stimulus was simulated with the same protocol with an additionally 20-ms spike train with 40 ms pauses in IO neurons (Geminiani et al., 2022) pathological input. PC activity was plotted both for physiological and pathological protocol.

Results. Cerebellar MF model predictions for EBCC-like stimulation showed the physiological case with ν_{drive} implemented as the CS+US In physiological conditions, PC emitted a burst following the US with an increase in the activity up to 300 Hz (Figure 4.3A). Dystonia-like simulation showed the dystonic burst-firing pattern of PC induced by dysfunctional IO-bursting (Figure 4.3B). With the inclusion of altered patterns, multi-layer MF simulated an increased PC activity (bursts) also during baseline and CS intervals, The activity of GrC, GoC and MLI (not reported in 4.3) didn't change between control case and dystonic protocol because the lesion concerned signals impinging only on PC.

Discussion and Conclusion. Cerebellum involvement in several brain pathologies, such as ataxia, autism and dystonia has been extensively demonstrated (Pizoli et al., 2002; D'Angelo and Casali, 2012; Geminiani et al., 2022). Aberrant burst-firing pattern from IO cells provoked an altered PC activity observed in mouse models of dystonia (LeDoux and Lorden, 2002; Hisatsune et al., 2013; Fremont et al., 2017; Washburn et al., 2019) and simulated with a spiking cerebellar cortex model showing a PC burst-firing characterized by an excessive and repetitive increase of PC firing rate as observed in experiments (LeDoux and Lorden, 2002) and in Spiking Neural Network Simulation (Geminiani et al., 2022). Figure 4.3 shows the activity simulated with a first attempt of dystonic cerebellar MF model, which is in line with the outcomes of the spiking cerebellar cortex, showing patterns of repetitive increased activity up to 300 Hz. The alteration was induced by adding a further excitatory contribution to the excitatory input of TF_{PC}, enabling us to simulate an altered dynamics without performing again the entire fitting procedure (**section 3.2.2 "Transfer Function Computation"**).

This preliminary exploration assessed that multi-layer MF can reproduce pathological patterns by modulating the TF of the affected population(s), and this would impact on the plasticity mechanisms once embedded.

It would be interesting to simulate also dystonic pattern as aberrant PC firing rate provoked by an altered PC endogenous current (I_e, see Table 3.1 for the complete parameters list). A dystonic TF_{PC} would be recomputed to consider this alteration at single cell level, and it would be interesting to compare the *physiological* TF_{PC} with a *dystonic* TF_{PC} to study how single cell alterations are modeled by the TF formalism. Although altered patterns were properly reproduced, dystonic learning curves couldn't be simulated with our MF model without the inclusion of deep cerebellar nuclei and long-term plasticity rules. However, the fact that our MF properly simulated altered dynamics paves the way for the integration of these alterations at the level of connectivity parameters, to fit the model on pathological parameters configurations, empowering the study of the cerebellar causal role in dystonia. Importantly, this approach will allow us to feed our multi-layer cerebellar MF with patient-specific pathological features acquired with non-invasive *in vivo* techniques, as fMRI and EEG, enabling to simulate a patient-specific pathologic cerebellum, opening new frontiers in personalized medicine (D'Angelo and Jirsa, 2022).

A - Physiological MF simulation
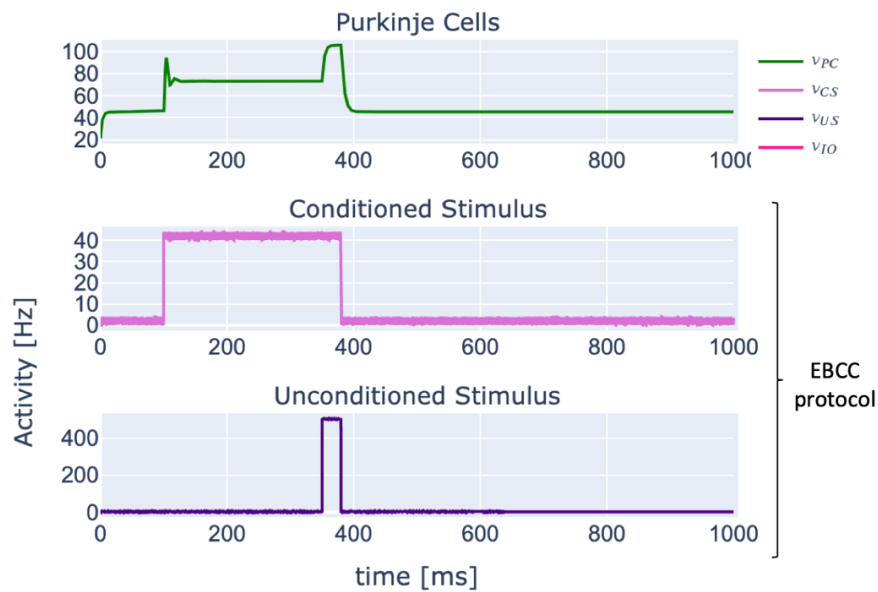
B - Dystonic-like MF simulation
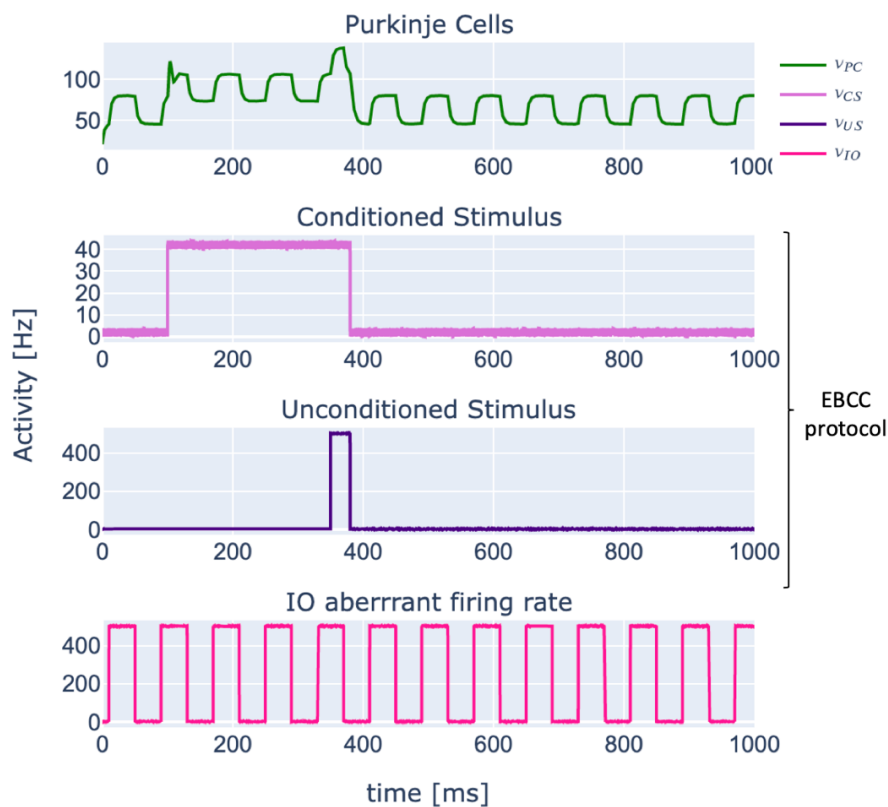
Figure 4. 3) Simulation of altered activity: Dystonia case. **A)** Physiological simulated response of Purkinje cells (PC) with an Eye Blink Conditioned Control (EBCC) protocol. Simulation length: 1000 ms, Conditioned stimulus (CS): 40 Hz for 280 ms, Unconditioned stimulus (US): 500 Hz for 30 ms. **B)** Dystonia-like simulated response of PCs. Aberrant activity of Inferior Olive (IO) cells modelled as a step function representing a non-recurrent 40-Hz spike train. Mean field simulated PC activity shows patterns of repetitive increased activity up to 300 Hz

77

4.2.3 Expanding the layers to Deep Cerebellar Nuclei

The multi-layer cerebellar MF relies on a modular design where the layers are stack up like *Lego bricks* ensuring flexibility of construction. Indeed, this design not only reproduces the multi-layer quasi crystalline organization of the cerebellar cortex but achieves to investigate separately the specific activity of each layer. As an example, MLI-PC feed-forward inhibition was investigated by modifying the strength of the inhibitory conductance only between MLI and PC to simulate extra inhibition (i.e., assumption of inhibitory drugs) as well as disinhibited situations (e.g., in drunken or anesthetized state). The same strategy was used to investigate long term potentiation (LTP), and long term depression (LTD) mechanisms recorded in PC activity, where only the granular layer *brick* was changed by modifying the strength between GrC-PC excitatory synapses. GrC represents the excitatory input for all the other layers, but the modular *Lego bricks* design allows to change the GrC-PC synaptic strength without affecting neither the parameters that regulate granular layer connectivity (GrC-GoC synaptic parameters) nor the MLI-GrC connections.

The modular design can be exploited also for adding Deep Cerebellar Nuclei (DCN) as new *brick* (i.e., layer) and, if a feedback loop is not included, without re-fitting the Transfer Functions. The expansion of the multi-layer cerebellar MF by including subcortical cerebellar structures will improve the biological realism of the network because it will be possible to integrate further excitatory and inhibitory mechanisms through mossy fibers-DCN excitation and PC-DCN inhibition connections, enriching the dynamics of the multi-layer cerebellar MF. Furthermore, DCN are important not only to bring information to the cerebellum but also to vehicle the cerebellar output towards the cerebral cortex. Therefore, the integration of DCN parameters with their specific TF could represent a definitive step ahead in the perspective of the integration into a whole-brain dynamics simulator.

This evidence discussed so far highlights the crucial role played by the cerebellum in whole-brain dynamics. Indeed, the inclusion of the cerebellum in a whole-brain network led to an improvement in the correlation between experimental and simulated functional dynamics (Palesi et al., 2020). Embedded in a visuomotor network, it demonstrated to exert a direct causal influence on the complex activity recorded in cerebral cortical areas activated in motor planning. Given the relevance of these outcomes and the specific structural and functional organization of the cerebellum, the lack of a specific cerebellar model clearly emerges in simulators that pretend to be reliable tools for both research and clinics. Furthermore, the involvement of the cerebellum has been indeed confirmed at multi-scale level in several neurodegenerative pathologies, like ataxia (Marchese et al., 2021), dementia (Monteverdi et al., 2022) and the distonia (Geminiani et al., 2022), thus a specific cerebellar model could improve the accuracy of simulated brain activity, representing a concrete step ahead towards reliable personalized medicine. For this reason, our multi-layer cerebellar MF model was developed as a flexible framework not only in terms of adding new layers (section 5.2.1) but also in the computationally perspective to be integrated into whole-brain dynamics simulators with different purposes such as the DCM and the TVB.

4.2.4 Cerebellar MF will get social: integration into brain dynamics simulators

Cerebellar MF presented in Chapter 3 would be part of a pool of new generation models developed accounting for region-specific structural and functional features. Attempts to develop specific model of the cortical regions have been developed over the past years confirming the need of region-specific models to improve brain dynamics simulation. These models have been integrated into DCM to

investigate the between-regions direct causal influences linking the hemodynamic macroscale recordings to underlying microscale neuronal properties specific for the regions considered. Model of basal ganglia-thalamocortical circuit is already part of this framework and it is already used to quantify the differences of cerebral effective connectivity in Parkinson disease with respect to healthy controls. Furthermore, a MF specific for basal ganglia-thalamocortical system is currently under development following the same MF approximation adopted for the cerebellar MF presented here, potentially providing a region-specific pool of models consistently developed and ready to be integrated in TVB. Cerebellar MF could be integrated in this framework (Figure 4.4), expanding the brain network involved in Parkinson disease and in general to all the neurodegenerative disease affecting the motor circuit such as dystonia and ataxia.
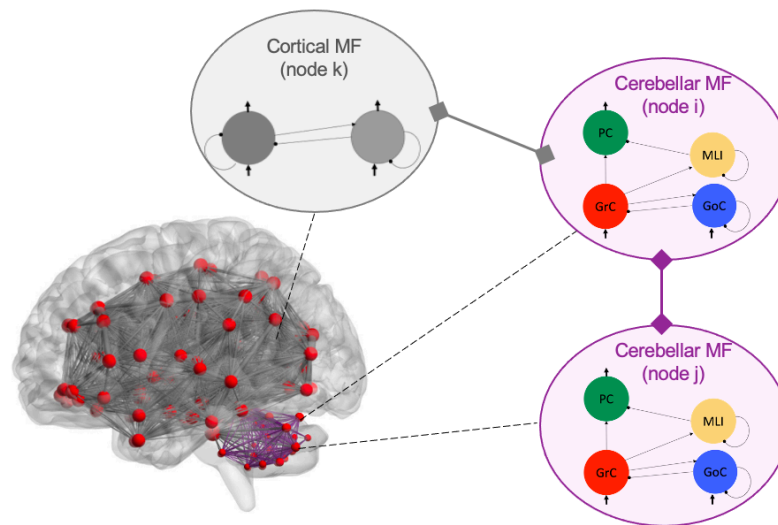
Figure 4. 4) Next step: Cerebellar mean-field integration into whole-brain simulation. Conceptualization of cerebellar mean-field integration in a whole-brain network for whole-brain dynamics simulations. Different modules of cerebellar MF should be considered (violet panel) and connected each other (violet arrows) introducing functional and structural intra-cerebellar coupling parameters. Additionally, the connection with cortical MFs (gray panel and gray bold arrows) could be set considering structural parameters extracted from large-scale connectome (e.g. tract length) and functional parameters related to the speed of signal propagation (e.g. the myelin thickness computed with quantitative score like g-ratio).

Conclusions

Studying the activity of the brain is an ongoing and remarkable challenge due to its multiscale organization. Its multifaceted dynamics could be addressed with bottom-up and/or top-down approaches, with different models integrated in different simulators. Which approach is the best is an ill-posed quest because it depends on the target of simulation, which can range from a single neuron to brain network activity. Therefore, the focus shouldn't be finding out the best approach and the best model ever but integrating biology grounded bottom-up models into top-down whole-brain dynamics simulators to link macroscale predictions to physiological microscale properties. In this context, MF models represent an effective mesoscale formalism to bridge the gap between micro and macroscale. The rationale of MF formalism is to approximate the interactions between the elements of the system with the interactions between an element and the average activity of the others included in the system. Therefore, MF theory has a widespread application in cross-cutting fields, whenever an effective approximation of a complex system is needed. It is used to predict the evolution of financial markets as well as the evolution of COVID-19 outbreaks. Applied to neuroscience, MF modelling allows to reproduce the dynamics of a mesoscale network of spiking neurons as a continuous signal in the same time domain of the experimental recordings, as local field potentials.

A heuristic approach to the master equation describing the time evolution of the neuronal activity expressed in terms of probability to spike endows a simple definition of MF model through the fitting of a transfer function, which is a mathematical construct linking single cell properties to the statistical moments (mean, standard deviation, and autocorrelation) of the network activity. Generally, this approach demonstrated to be effective to model a generic cortical MF model of one excitatory and one inhibitory population. For the first time, here this formalism was extended to implement a multi-layer MF model of the cerebellum including the main neuronal population of the cerebellar cortex (Granule cells, Golgi cells, Molecular Layer Interneurons, and Purkinje cells), resulting in biology grounded mesoscale model implemented with a bottom-up approach.

The implementation of a multi-layer cerebellar MF model finds its roots in the need of a model specifically tailored on the cerebellum to provide a deep insight into its functions. On top of that, a framework to develop an advanced MF with a multi-layer modular structure is presented. This framework can be tuned on parameters of a specific brain regions that require a multi-layer design without collapsing the neurons features in an excitatory and inhibitory population. Maintaining the physiological salient features of each type of neuron is one of the strength points of this formalism and the reason why it can define it "biology grounded".

Models tuned for a specific region and the link between model parameters and physiological features are essential aspects in the perspective to build up reliable *virtual brains*. In a reality where the word *metaverse* and the concept associated has become of common use, opening to new virtual experiences, like buy NFT (non-fungible token) art or travel around the world with more and more realistic simulators, the ambitious project to build up subject-specific *virtual brain* - a digital twin - starts to take a hold. *Digital brain twin* can be implemented as the simulation of subject-specific brain dynamics representing a real step ahead in both research and clinics. Indeed, it can be used to compare subject-specific features to shed light on unveiling aspects of the brain dynamics and it can be also used to tailored pharmacological treatment making them more effective. It is clear that to achieve this ambitious goal, increasingly accurate models of the brain regions are required in order to link neurons

underlying activity with recorded brain signals. MF models tuned on single cell specific features can provide an effective way of modeling brain regions bridging the gap between spiking neurons and whole-brain dynamics. Multi-layer cerebellar MF enriches the pool of region-specific models, playing a main role for the implementation of a digital twin. It allows to virtualize subject specific physiological dynamic as well as pathological activity, enabling to build up a meta-brain with a strong impact on the real-world challenges such as an accessible ultimately personalized medicine.

Extended generalized leaky integrate-and-fire model: an insight into the MF functional reference

This section provides an insight into the extended generalized leaky integrate-and-fire (E-GLIF) neuron model detailed in previously published works (Geminiani et al., 2018, 2019a), aiming at clarifying the reason why E-GLIF was chosen as functional reference for the cerebellar MF.

E-GLIF is a point neuron model derived from the leaky-integrate-and-fire model family (LIF), maintaining the limited computational load typical of a linear low-dimensional system and admitting analytical solutions. E-GLIF computes the membrane potential dynamic with a set of three interconnected equations (**section 3.3.1** equation 30), explicitly accounting for the time evolution of adaptation and depolarization currents. E-GLIF model was developed integrating conductance-base synapses, reproducing the synaptic dynamic with a higher level of realism than current-based models (Cavallari et al., 2014) (**section 1.2.2**). Furthermore, the synaptic activation of interconnected neurons were modeled with alpha function (**section 3.3.1** equation 31) (Roth and van Rossum, 2013) which accounts for a short transient before the decay (Figure A1), increasing the realism of synaptic mechanisms respect to the instantaneous decay of the exponential synapses.
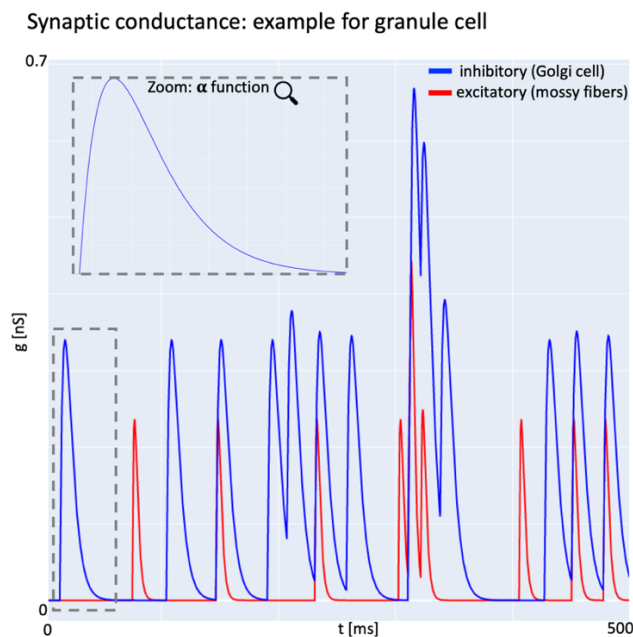
Figure A. 1) Alpha-based synaptic conductance. Example for a granule cell. Simulation last 500 ms. Inhibitory conductance is shown in blue while excitatory in red. In the gray panel, a zoom on alpha-conductance trend was reported to highlight the transient typical of the alpha-function.

Moreover, E-GLIF equations were designed and specifically optimized for the neurons of the cerebellar cortex (GrC, GoC, MLI and PC, **section 1.1.1**), in order to account for the rich variety of electroresponsive properties of cerebellar neural populations which have a crucial role in cerebellar functioning and processing (D'Angelo et al., 2016) (**section 1.1.4**). These microscale properties, thus, impact considerably on the meso and macroscale, contributing to shape the cerebellar activity and the dynamics of the cerebro-cerebellar loop (**section 1.1.5**). E-GLIF equations demonstrated to capture the single neuron specific feature and their predictive power was tested reproducing GoC behavior (Geminiani et al., 2018), and then, extended to the other neurons of cerebellar cortex (GrC, MLI, and PC) (Geminiani et al., 2019a). For each neuron type, E-GLIF neurophysiological parameters such as membrane conductance, membrane time constant, reversal potential, refractory time constant, threshold potential and reset potential, were derived from in in vitro experiments (D'Angelo et al., 1999; Solinas et al., 2007; Lennon et al., 2014). The remaining parameters, which don't directly represent a physiological quantity but model functional properties, were derived through an optimization procedure based on a desired input-output relationship, targeting the electroresponsive phenotype of the neural population. Specifically, the optimization procedure was designed considering four different current steps (excitatory (exc) current I_{stim} = exc1 < exc2 < exc3 and inhibitory (inh) current) as the input and spike times as the output (Geminiani et al., 2018). Gradient-descent algorithm was used to optimize the spike times in sub-intervals (Δt_1, Δt_2, Δt_{ss}) of the exc current-step stimulation protocol (I_{stim}= (i) = [0, exc$_1$, exc$_2$, exc$_3$] pA) and in the interval following the inhibition phase, to reproduce electrophysiological input-output patterns. The target cost function was defined as:

$$c\_fun = \frac{\sqrt{\sum error_{(i)} + error_{(inh)}}}{6}$$

$$error_{(i)} = \frac{1}{3} \cdot \left[\left(error\_\Delta t_1^{(i)} \right)^2 + \left(error\_\Delta t_2^{(i)} \right)^2 + \left(error\_\Delta t_{SS}^{(i)} \right)^2 \right]$$

$$error_{(inh)} = \left(error\_burst\_\Delta t_1^{(i)} \right)^2 + \left(error\_burst\_\Delta t_2^{(i)} \right)^2$$

With error$_{(i)}$ computed as the error for each current step value ([0, exc$_1$, exc$_2$, exc$_3$]), considering each one of the three sub-intervals (Δt_1 = time to the first spike, Δt_2 = time between first and second spike, Δt_{SS} = time between two steady-state spikes); error$_{(inh)}$ defined as the error in first two sub-intervals (Δt_1, Δt_2) of a I_{stim} = 0 phase, following a hyperpolarizing I_{stim}. This latter expression was written in order to evaluate the neuronal complex properties of rebound bursting in the optimization protocol.

Combining prior knowledge based on literature and optimization techniques provided a set of physiological and functional parameters specific for each neuron type of the cerebellar cortex. The parameters value are reported in Table 3.1.

As a result, a whole set of dynamic properties were reproduced, namely pacemaking, adaptation, bursting, post-inhibitory rebound excitation, subthreshold oscillations, resonance, capturing the whole set of electroresponsive patterns in cerebellar neurons (Figure A2).
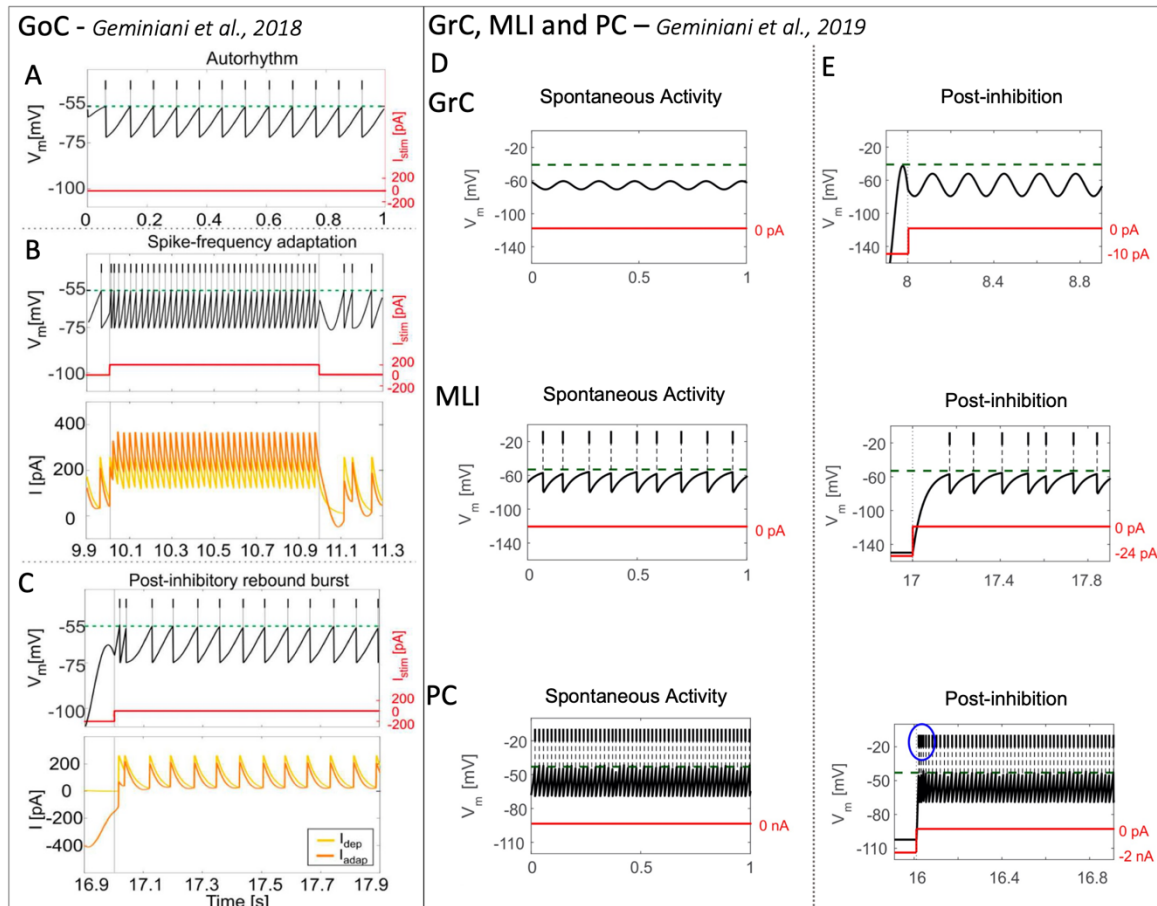
Figure A. 2) E-GLIF simulations for the cerebellar cortex neuron. **Left column: GoC**. Membrane potential (black), spike events (black lines in the upper part), and the input current (red). **(A)** Autorhythmic phase with zero-stimulation current; **(B)** Depolarization-induced excitation and spike-frequency. Depolarization current (I_{dep}) is faster and contributes to bursting mechanisms, while adaptation current (I_{adap} - with lower update rate) generates spike-frequency adaptation reaching its steady-state value after the first 2 spikes following depolarization have already occurred. **(C)** Rebound doublet after an inhibitory current step followed by a short quiescent period before returning to tonic firing. **Right column: GrC, MLI, PC**: responses to zero-input current **(D)** and following a hyperpolarizing current step **(E)**. Zero-current inputs cause subthreshold oscillation in GrC, and autorhythmic in the others. Post-inhibitory rebound excitation (burst or spike) is present in PC (blue circle)

E-GLIF point-neuron models integrated into cerebellar SNN demonstrated to be an effective tool to evaluate the impact of microscale complex properties at the mesoscale circuits, up to macroscale network with TVB co-simulation to evaluate the effects of deep brain stimulations (Meier et al., 2022). Compared to the generic cortical MF (Zerlaut et al., 2018; Di Volo et al., 2019), which relied on Adaptive Exponential (AdEx) point neurons, the cerebellar MF adopted E-GLIF equations which are linear and were specifically tailored and tuned on each cerebellar cortex neuron type, translating microscale physiological and functional characteristics into the MF formalism. Furthermore, compared to LIF version of cerebellar neurons, E-GLIF SNN demonstrated to model rich population dynamics such as the burst-pause response of Purkinje cells as recorded *in vivo* (Geminiani et al., 2019b).

In the present work, E-GLIF model has a ground role to translate microscale *in vivo* properties into mesoscale approximations (Figure. A3). A cerebellar spiking cortex module, built up as a E-GLIF SNN, constituted the functional reference used to extract the actual working frequencies for each cerebellar neuronal population, by averaging the point neurons firing rate. The population firing rate was used as input to compute the Transfer Function (TF) numerical template of the interconnected neuronal population (e.g., population working frequencies of GrC and MLI were used to as input to compute TF_{PC}). The same SNN demonstrated also the constructive, functional and predictive validity of the cerebellar MF, proving that the choice of EGLIF as functional reference endowed a real biology grounded MF tailored ad-hoc on features specifics for the cerebellar cortex neurons.
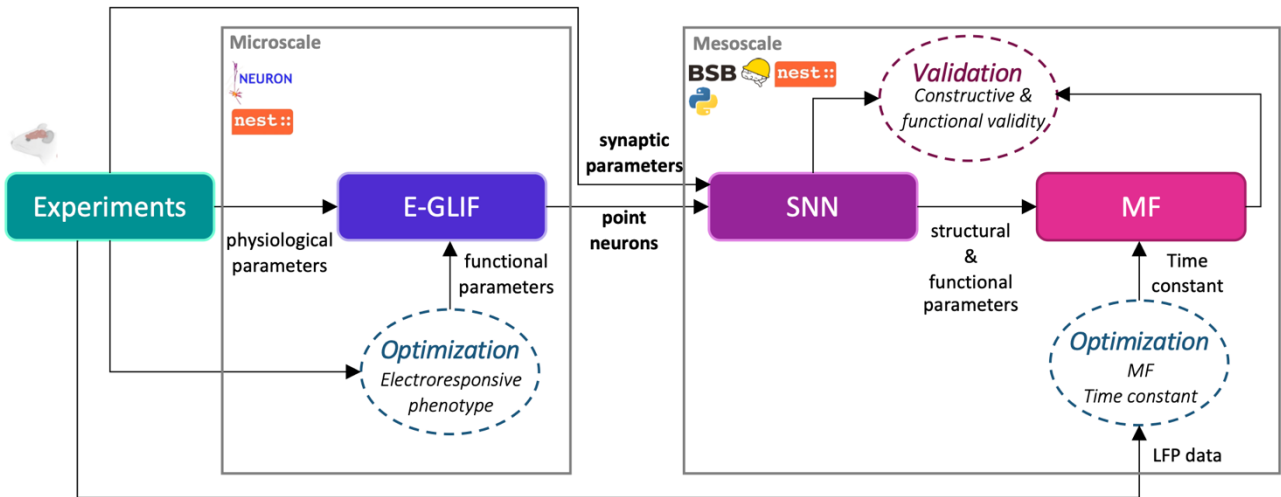
Figure A. 3) E-GLIF embedded into the mean-field pipeline. The block schema shows the cross-cutting scale the pipeline. E-GLIF equations bridge the gap between microscale parameters extracted from in-vivo single cell experiments and mesoscale network. SNN collects about 30000 interconnected single point neurons, resulting in about 1 million equations. The structural and functional parameters extracted from SNN to build up MF convey the in-vivo recorded information form single neuron. Furthermore, MF considers also LFP data to optimize the model time constant, including also mesoscale in-vivo recordings.

Acknowledgments

References

Achdou, Y., Camilli, F., and Capuzzo-Dolcetta, I. (2012). Mean field games: Numerical methods for the planning problem. *SIAM J. Control Optim.* 50, 77–109. doi:10.1137/100790069.

Akar, N. A., Cumming, B., Karakasis, V., Küsters, A., Klijn, W., Peyser, A., et al. (2019). Arbor - A Morphologically-Detailed Neural Network Simulation Library for Contemporary High-Performance Computing Architectures. *Proc. - 27th Euromicro Int. Conf. Parallel, Distrib. Network-Based Process. PDP 2019*, 274–282. doi:10.1109/EMPDP.2019.8671560.

Alahmadi, A. A. S., Samson, R. S., Gasston, D., Pardini, M., Friston, K. J., D'Angelo, E., et al. (2016). Complex motor task associated with non-linear BOLD responses in cerebro-cortical areas and cerebellum. *Brain Struct. Funct.* 221, 2443–2458. doi:10.1007/s00429-015-1048-1.

Amit, D. J., and Brunel, N. (1997). Model of global spontaneous activity and local structured activity during delay periods in the cerebral cortex. *Cereb. Cortex* 7, 237–252. doi:10.1093/cercor/7.3.237.

Amunts, K., DeFelipe, J., Pennartz, C., Destexhe, A., Migliore, M., Ryvlin, P., et al. (2022). Linking Brain Structure, Activity, and Cognitive Function through Computation. *eNeuro* 9. doi:10.1523/ENEURO.0316-21.2022.

Amunts, K., Lepage, C., Borgeat, L., Mohlberg, H., Dickscheid, T., Rousseau, M. É., et al. (2013). BigBrain: An ultrahigh-resolution 3D human brain model. *Science (80-.).* 340, 1472–1475. doi:10.1126/science.1235381.

Andersen, L. M., Jerbi, K., and Dalal, S. S. (2020). Can EEG and MEG detect signals from the human cerebellum? *Neuroimage* 215, 116817. doi:10.1016/j.neuroimage.2020.116817.

Antonietti, A., Casellato, C., D'Angelo, E., and Pedrocchi, A. (2017). Model-driven analysis of eyeblink classical conditioning reveals the underlying structure of cerebellar plasticity and neuronal activity. *IEEE Trans. Neural Networks Learn. Syst.* 28, 2748–2762. doi:10.1109/TNNLS.2016.2598190.

Aspart, F., Ladenbauer, J., and Obermayer, K. (2016). Extending Integrate-and-Fire Model Neurons to Account for the Effects of Weak Electric Fields and Input Filtering Mediated by the Dendrite. *PLoS Comput. Biol.* 12, 1–29. doi:10.1371/journal.pcbi.1005206.

Auksztulewicz, R., and Friston, K. (2015). Attentional enhancement of auditory mismatch responses: A DCM/MEG study. *Cereb. Cortex* 25, 4273–4283. doi:10.1093/cercor/bhu323.

Barmack, N. H., and Yakhnitsa, V. (2013). "Vestibulocerebellar Connections BT - Handbook of the Cerebellum and Cerebellar Disorders," in, eds. M. Manto, J. D. Schmahmann, F. Rossi, D. L. Gruol, and N. Koibuchi (Dordrecht: Springer Netherlands), 357–375. doi:10.1007/978-94-007-1333-8_18.

Barreiro-Gomez, J., and Tembine, H. (2019). Blockchain Token Economics: A Mean-Field-Type Game Perspective. *IEEE Access* 7, 64603–64613. doi:10.1109/ACCESS.2019.2917517.

Bastos, A. M., Usrey, W. M., Adams, R. A., Mangun, G. R., Fries, P., and Friston, K. J. (2012). Canonical Microcircuits for Predictive Coding. *Neuron* 76, 695–711.

References

doi:10.1016/j.neuron.2012.10.038.

Bick, C., Goodfellow, M., Laing, C. R., and Martens, E. A. (2020). Understanding the dynamics of biological and neural oscillator networks through exact mean-field reductions: a review. *J. Math. Neurosci.* 10. doi:10.1186/s13408-020-00086-9.

Bliss, T. V. P., and Cooke, S. F. (2011). Long-term potentiation and long-term depression: A clinical perspective. *Clinics* 66, 3–17. doi:10.1590/S1807-59322011001300002.

Booth, J. R., Wood, L., Lu, D., Houk, J. C., and Bitan, T. (2007). The role of the basal ganglia and cerebellum in language processing. *Brain Res.* 1133, 136–144. doi:10.1016/j.brainres.2006.11.074.

Bostan, A. C., Dum, R. P., and Strick, P. L. (2010). The basal ganglia communicate with the cerebellum. *Proc. Natl. Acad. Sci. U. S. A.* 107, 8452–8456. doi:10.1073/pnas.1000496107.

Bottou, L. (2012). Stochastic gradient descent tricks. *Lect. Notes Comput. Sci. (including Subser. Lect. Notes Artif. Intell. Lect. Notes Bioinformatics)* 7700 LECTU, 421–436. doi:10.1007/978-3-642-35289-8_25.

Bower, J. M., and Beeman, D. (1998). *The Book of GENESIS: Exploring Realistic Neural Models with the GEneral NEural SImulation System.* Springer New York.

Brette, R., and Gerstner, W. (2005). Adaptive exponential integrate-and-fire model as an effective description of neuronal activity. *J. Neurophysiol.* 94, 3637–3642. doi:10.1152/jn.00686.2005.

Brown, A. (2022). The Hodgkin and Huxley papers: still inspiring after all these years. *J. Physiol.* 600, 173–174. doi:https://doi.org/10.1113/JP282700.

Bruchhage, M. M. K., Bucci, M.-P., and Becker, E. B. E. (2018). Cerebellar involvement in autism and ADHD. *Handb. Clin. Neurol.* 155, 61–72. doi:10.1016/B978-0-444-64189-2.00004-4.

Brunel, N., and Sergi, S. (1998). Firing frequency of integrate-and-fire neurons with finite synaptic time constants. *J Theor Biol* 195, 87–95. Available at: https://ac.els-cdn.com/S0022519398907822/1-s2.0-S0022519398907822-main.pdf?_tid=331cafda-44da-429c-bf68-ac5202229016&acdnat=1523470850_55b12946e4f5f0d44c99ffb01f231fd0%0Ahttp://www.ncbi.nlm.nih.gov/entrez/query.fcgi?cmd=Retrieve&db=PubMed&dopt=Citation&li.

Bueichekú, E., Miró-Padilla, A., and Ávila, C. (2020). Functional connectivity at rest captures individual differences in visual search. *Brain Struct. Funct.* 225, 537–549. doi:10.1007/s00429-019-02008-2.

Byrne, Á., Ross, J., Nicks, R., and Coombes, S. (2022). Mean-Field Models for EEG/MEG: From Oscillations to Waves. *Brain Topogr.* 35, 36–53. doi:10.1007/s10548-021-00842-4.

Cakan, C., and Obermayer, K. (2020a). Biophysically grounded mean-field models of neural populations under electrical stimulation. *PLoS Comput. Biol.* 16, 1–40. doi:10.1371/journal.pcbi.1007822.

Cakan, C., and Obermayer, K. (2020b). Biophysically grounded mean-field models of neural populations under electrical stimulation. *PLoS Comput. Biol.* 16, 1–30. doi:10.1371/journal.pcbi.1007822.

Capone, C., Volo, M. di, Romagnoni, A., Mattia, M., and Destexhe, A. (2019). A state-dependent

mean-field formalism to model different activity states in conductance based networks of spiking neurons. *bioRxiv*, 1–14. doi:10.1101/565127.

Cardaliaguet, P., and Porretta, A. (2020). "An Introduction to Mean Field Game Theory," in, eds. Y. Achdou, P. Cardaliaguet, F. Delarue, A. Porretta, F. Santambrogio, P. Cardaliaguet, et al. (Cham: Springer International Publishing), 1–158. doi:10.1007/978-3-030-59837-2_1.

Carlu, M., Chehab, O., Dalla Porta, X. L., Depannemaecker, D., Héricé, X. C., Jedynak, M., et al. (2020). A mean-field approach to the dynamics of networks of complex neurons, from nonlinear Integrate-and-Fire to Hodgkin-Huxley models. *J. Neurophysiol.* 123, 1042–1051. doi:10.1152/JN.00399.2019.

Carmona, R. (2021). Applications of Mean Field Games in financial engineering and economic theory. 165–219. doi:10.1090/psapm/078/05.

Carnevale, T., and Hines, M. (2006). *The NEURON book*. Cambridge, UK: Cambridhe University Press doi:10.1017/CBO9780511541612.

Casali, S., Marenzi, E., Medini, C., Casellato, C., and D'Angelo, E. (2019). Reconstruction and simulation of a scaffold model of the cerebellar network. *Front. Neuroinform.* 13, 1–19. doi:10.3389/fninf.2019.00037.

Casali, S., Tognolina, M., Gandolfi, D., Mapelli, J., and D'Angelo, E. (2020). Cellular-resolution mapping uncovers spatial adaptive filtering at the rat cerebellum input stage. *Commun. Biol.* 3, 635. doi:10.1038/s42003-020-01360-y.

Casiraghi, L., Alahmadi, A. A. S., Monteverdi, A., Palesi, F., Castellazzi, G., Savini, G., et al. (2019). I See Your Effort: Force-Related BOLD Effects in an Extended Action Execution–Observation Network Involving the Cerebellum. *Cereb. Cortex* 29, 1351–1368.

Castellazzi, G., Bruno, S. D., Toosy, A. T., Casiraghi, L., Palesi, F., Savini, G., et al. (2018). Prominent Changes in Cerebro-Cerebellar Functional Connectivity During Continuous Cognitive Processing . *Front. Cell. Neurosci.* 12, 331. Available at: https://www.frontiersin.org/article/10.3389/fncel.2018.00331.

Castellazzi, G., Palesi, F., Casali, S., Vitali, P., Wheeler-Kingshott, C. A. M., Sinforiani, E., et al. (2014). A comprehensive assessment of resting state networks: Bidirectional modification of functional integrity in cerebro-cerebellar networks in dementia. *Front. Neurosci.* 8, 1–18. doi:10.3389/fnins.2014.00223.

Cavallari, S., Panzeri, S., and Mazzoni, A. (2014). Comparison of the dynamics of neural interactions between current-based and conductance-based integrate-and-fire recurrent networks. *Front. Neural Circuits* 8, 1–23. doi:10.3389/fncir.2014.00012.

Cerminara, N. L., Lang, E. J., Sillitoe, R. V., and Apps, R. (2015). Redefining the cerebellar cortex as an assembly of non-uniform Purkinje cell microcircuits. *Nat. Rev. Neurosci.* 16, 79–93. doi:10.1038/nrn3886.

Clower, D. M., Dum, R. P., and Strick, P. L. (2005). Basal Ganglia and Cerebellar Inputs to 'AIP.' *Cereb. Cortex* 15, 913–920. doi:10.1093/cercor/bhh190.

Coombes, S., and Byrne, Á. (2019). "Next Generation Neural Mass Models BT - Nonlinear Dynamics in Computational Neuroscience," in, eds. F. Corinto and A. Torcini (Cham: Springer

International Publishing), 1–16. doi:10.1007/978-3-319-71048-8_1.

D'Angelo, E., and Casali, S. (2013). Seeking a unified framework for cerebellar function and dysfunction: from circuit operations to cognition . *Front. Neural Circuits* 6. Available at: https://www.frontiersin.org/articles/10.3389/fncir.2012.00116.

D'Angelo, E. (2011). Neural circuits of the cerebellum: hypothesis for function. *J. Integr. Neurosci.* 10, 317–352. doi:10.1142/S0219635211002762.

D'Angelo, E. (2018). *Physiology of the cerebellum.* 1st ed. Elsevier B.V. doi:10.1016/B978-0-444-63956-1.00006-0.

D'Angelo, E. (2019). The cerebellum gets social. *Science (80-.).* 363, 229. doi:10.1126/science.aaw2571.

D'Angelo, E., Antonietti, A., Casali, S., Casellato, C., Garrido, J. A., Luque, N. R., et al. (2016). Modeling the cerebellar microcircuit: New strategies for a long-standing issue. *Front. Cell. Neurosci.* 10, 1–29. doi:10.3389/fncel.2016.00176.

D'Angelo, E., and Casali, S. (2012). Seeking a unified framework for cerebellar function and dysfunction: from circuit operations to cognition. *Front. Neural Circuits* 6, 116. doi:10.3389/fncir.2012.00116.

D'Angelo, E., and De Zeeuw, C. I. (2009). Timing and plasticity in the cerebellum: focus on the granular layer. *Trends Neurosci.* 32, 30–40. doi:https://doi.org/10.1016/j.tins.2008.09.007.

D'Angelo, E., and Jirsa, V. (2022). Neurosciences The quest for multiscale brain modeling. *Trends Neurosci.* xx, 1–14. doi:10.1016/j.tins.2022.06.007.

D'Angelo, E., Nieus, T., Maffei, A., Armano, S., Rossi, P., Taglietti, V., et al. (2001). Theta-frequency bursting and resonance in cerebellar granule cells: experimental evidence and modeling of a slow k+-dependent mechanism. *J. Neurosci. Off. J. Soc. Neurosci.* 21, 759–770. doi:10.1523/JNEUROSCI.21-03-00759.2001.

D'Angelo, E., Rossi, P., Armano, S., and Taglietti, V. (1999). Evidence for NMDA and mGLU receptor-dependent long-term potentiation of mossy fiber-granule cell transmission in rat cerebellum. *J. Neurophysiol.* 81, 277–287. doi:10.1152/jn.1999.81.1.277.

D'Angelo, E., Solinas, S., Mapelli, J., Gandolfi, D., Mapelli, L., and Prestori, F. (2013). The cerebellar Golgi cell and spatiotemporal organization of granular layer activity. *Front. Neural Circuits* 7, 1–21. doi:10.3389/fncir.2013.00093.

D'Mello, A. M., and Stoodley, C. J. (2015). Cerebro-cerebellar circuits in autism spectrum disorder. *Front. Neurosci.* 9. doi:10.3389/fnins.2015.00408.

De Schepper, R., Geminiani, A., Masoli, S., Rizza, M. F., Antonietti, A., Casellato, C., et al. (2022). Model simulations unveil the structure-function-dynamics relationship of the cerebellar cortical microcircuit. *Commun Biol*. doi:https://doi.org/10.1038/s42003-022-04213-y.

Deco, G., Jirsa, V. K., Robinson, P. A., Breakspear, M., and Friston, K. (2008). The dynamic brain: From spiking neurons to neural masses and cortical fields. *PLoS Comput. Biol.* 4. doi:10.1371/journal.pcbi.1000092.

Deco, G., McIntosh, A. R., Shen, K., Hutchison, R. M., Menon, R. S., Everling, S., et al. (2014a). Identification of optimal structural connectivity using functional connectivity and neural

modeling. *J. Neurosci. Off. J. Soc. Neurosci.* 34, 7910–7916. doi:10.1523/JNEUROSCI.4423-13.2014.

Deco, G., Ponce-Alvarez, A., Hagmann, P., Romani, G. L., Mantini, D., and Corbetta, M. (2014b). How local excitation-inhibition ratio impacts the whole brain dynamics. *J. Neurosci.* 34, 7886–7898. doi:10.1523/JNEUROSCI.5068-13.2014.

Deco, G., Ponce-Alvarez, A., Mantini, D., Romani, G. L., Hagmann, P., and Corbetta, M. (2013). Resting-state functional connectivity emerges from structurally and dynamically shaped slow linear fluctuations. *J. Neurosci.* 33, 11239–11252. doi:10.1523/JNEUROSCI.1091-13.2013.

Del Percio, C., Drinkenburg, W., Lopez, S., Infarinato, F., Bastlund, J. F., Laursen, B., et al. (2017). On-going electroencephalographic rhythms related to cortical arousal in wild-type mice: the effect of aging. *Neurobiol. Aging* 49, 20–30. doi:https://doi.org/10.1016/j.neurobiolaging.2016.09.004.

Depannemaecker, D., Gorski, T., Destexhe, A., Depannemaecker, D., Gorski, T., Destexhe, A., et al. (2020). Conductance-based Adaptive Exponential integrate-and-fire model To cite this version : HAL Id : hal-02507596 Conductance-based Adaptive Exponential integrate-and-fire model.

Destexhe, A., Rudolph, M., and Paré, D. (2003). The high-conductance state of neocortical neurons in vivo. *Nat. Rev. Neurosci.* 4, 739–751. doi:10.1038/nrn1198.

Destexhe, A., and Sejnowski, T. J. (2009). The Wilson-Cowan model, 36 years later. *Biol. Cybern.* 101, 1–2. doi:10.1007/s00422-009-0328-3.

Devalle, F., Roxin, A., and Montbrió, E. (2017). Firing rate equations require a spike synchrony mechanism to correctly describe fast oscillations in inhibitory networks. *PLOS Comput. Biol.* 13, e1005881. Available at: https://doi.org/10.1371/journal.pcbi.1005881.

Di Volo, M., and Destexhe, A. (2021). Optimal responsiveness and information flow in networks of heterogeneous neurons. *Sci. Rep.* 11, 1–11. doi:10.1038/s41598-021-96745-2.

Di Volo, M., Romagnoni, A., Capone, C., and Destexhe, A. (2019). Biologically Realistic Mena-Field Models of Conductance-Based Networks of Spiking Neurons with Adaptation. *Neural Comput.* 31, 653–680. doi:10.1162/neco_a_01173.

Dieudonné, S. (1998). Submillisecond kinetics and low efficacy of parallel fibre-Golgi cell synaptic currents in the rat cerebellum. *J. Physiol.* 510, 845–866. doi:10.1111/j.1469-7793.1998.845bj.x.

Doron, K. W., Funk, C. M., and Glickstein, M. (2010). Fronto-cerebellar circuits and eye movement control: a diffusion imaging tractography study of human cortico-pontine projections. *Brain Res.* 1307, 63–71. doi:10.1016/j.brainres.2009.10.029.

du Boisgueheneuc, F., Levy, R., Volle, E., Seassau, M., Duffau, H., Kinkingnehun, S., et al. (2006). Functions of the left superior frontal gyrus in humans: a lesion study. *Brain* 129, 3315–3328. doi:10.1093/brain/awl244.

Dum, R. P., and Strick, P. L. (2003). An unfolded map of the cerebellar dentate nucleus and its projections to the cerebral cortex. *J. Neurophysiol.* 89, 634–639. doi:10.1152/jn.00626.2002.

Ekmen, A., Meneret, A., Valabregue, R., Beranger, B., Worbe, Y., Lamy, J.-C., et al. (2022). Cerebellum Dysfunction in Patients With PRRT2-Related Paroxysmal Dyskinesia. *Neurology*

References

98, e1077–e1089. doi:10.1212/WNL.0000000000200060.

El Boustani, S., and Destexhe, A. (2009). A master equation formalism for macroscopic modeling of asynchronous irregular activity states. *Neural Comput.* 21, 46–100. doi:10.1162/neco.2009.02-08-710.

El Houssaini, K., Bernard, C., and Jirsa, V. K. (2020). The Epileptor Model: A Systematic Mathematical Analysis Linked to the Dynamics of Seizures, Refractory Status Epilepticus, and Depolarization Block. *eNeuro* 7. doi:10.1523/ENEURO.0485-18.2019.

Ferrari, C., Fiori, F., Suchan, B., Plow, E. B., and Cattaneo, Z. (2021). TMS over the posterior cerebellum modulates motor cortical excitability in response to facial emotional expressions. *Eur. J. Neurosci.* 53, 1029–1039. doi:https://doi.org/10.1111/ejn.14953.

Fremont, R., Tewari, A., Angueyra, C., and Khodakhah, K. (2017). A role for cerebellum in the hereditary dystonia DYT1. *Elife* 6, e22775. doi:10.7554/eLife.22775.

Friston, K. J., Harrison, L., and Penny, W. (2003). Dynamic causal modelling. *Neuroimage* 19, 1273–1302. doi:10.1016/S1053-8119(03)00202-7.

Friston, K. J., Kahan, J., Biswal, B., and Razi, A. (2014). A DCM for resting state fMRI. *Neuroimage* 94, 396–407. doi:10.1016/j.neuroimage.2013.12.009.

Friston, K. J., Preller, K. H., Mathys, C., Cagnan, H., Heinzle, J., Razi, A., et al. (2019). Dynamic causal modelling revisited. *Neuroimage* 199, 730–744. doi:10.1016/j.neuroimage.2017.02.045.

Friston, K. J., and Stephan, K. E. (2007). Free-energy and the brain. *Synthese* 159, 417–458. doi:10.1007/s11229-007-9237-y.

Friston, K., Mattout, J., Trujillo-Barreto, N., Ashburner, J., and Penny, W. (2007). Variational free energy and the Laplace approximation. *Neuroimage* 34, 220–234. doi:10.1016/j.neuroimage.2006.08.035.

Gabrié, M. (2020). Mean-field inference methods for neural networks. *J. Phys. A Math. Theor.* 53. doi:10.1088/1751-8121/ab7f65.

Gagliano, G., Monteverdi, A., Casali, S., Laforenza, U., Gandini Wheeler-Kingshott, C. A. M., D'Angelo, E., et al. (2022). Non-Linear Frequency Dependence of Neurovascular Coupling in the Cerebellar Cortex Implies Vasodilation–Vasoconstriction Competition. *Cells* 11. doi:10.3390/cells11061047.

Gagliano, G., Monteverdi, A., Casali, S., Laforenza, U., Wheeler-Kingshott, C. A. M. G., D'Angelo, E., et al. (2021). Non-linear frequency-dependence of neurovascular coupling in the cerebellar cortex implies vasodilation-vasoconstriction competition. *bioRxiv*, 2021.07.30.454430. Available at: https://www.biorxiv.org/content/10.1101/2021.07.30.454430v1%0Ahttps://www.biorxiv.org/content/10.1101/2021.07.30.454430v1.abstract.

Galliano, E., Gao, Z., Schonewille, M., Todorov, B., Simons, E., Pop, A. S., et al. (2013). Silencing the Majority of Cerebellar Granule Cells Uncovers Their Essential Role in Motor Learning and Consolidation. *Cell Rep.* 3, 1239–1251. doi:10.1016/j.celrep.2013.03.023.

Galliano, E., Mazzarello, P., and D'Angelo, E. (2010). Discovery and rediscoveries of Golgi cells. *J. Physiol.* 588, 3639–3655. doi:10.1113/jphysiol.2010.189605.

Gao, H., Li, W., Pan, M., Han, Z., and Poor, H. V (2021). Modeling COVID-19 with mean field evolutionary dynamics: Social distancing and seasonality. *J. Commun. Networks* 23, 314–325. doi:10.23919/JCN.2021.000032.

Geminiani, A., Casellato, C., D'Angelo, E., and Pedrocchi, A. (2019a). Complex Electroresponsive Dynamics in Olivocerebellar Neurons Represented With Extended-Generalized Leaky Integrate and Fire Models. *Front. Comput. Neurosci.* 13, 1–12. doi:10.3389/fncom.2019.00035.

Geminiani, A., Casellato, C., Locatelli, F., Prestori, F., Pedrocchi, A., and D'Angelo, E. (2018). Complex dynamics in simplified neuronal models: Reproducing golgi cell electroresponsiveness. *Front. Neuroinform.* 12, 1–19. doi:10.3389/fninf.2018.00088.

Geminiani, A., Mockevičius, A., D'Angelo, E., and Casellato, C. (2022). Cerebellum Involvement in Dystonia During Associative Motor Learning: Insights From a Data-Driven Spiking Network Model. *Front. Syst. Neurosci.* 16, 1–15. doi:10.3389/fnsys.2022.919761.

Geminiani, A., Pedrocchi, A., D'Angelo, E., and Casellato, C. (2019b). Response Dynamics in an Olivocerebellar Spiking Neural Network With Non-linear Neuron Properties. *Front. Comput. Neurosci.* 13, 1–15. doi:10.3389/fncom.2019.00068.

Giannari, A. G., and Astolfi, A. (2022). Model design for networks of heterogeneous Hodgkin–Huxley neurons. *Neurocomputing* 496, 147–157. doi:https://doi.org/10.1016/j.neucom.2022.04.115.

Gilson, M., Zamora-López, G., Pallarés, V., Adhikari, M. H., Senden, M., Campo, A. T., et al. (2019). Model-based whole-brain effective connectivity to study distributed cognition in health and disease. *Netw. Neurosci.* 4, 338–373. doi:10.1162/netn_a_00117.

Glomb, K., Ponce-Alvarez, A., Gilson, M., Ritter, P., and Deco, G. (2017). Resting state networks in empirical and simulated dynamic functional connectivity. *Neuroimage* 159, 388–402. doi:10.1016/j.neuroimage.2017.07.065.

Goldman, J. S., Kusch, L., Hazal Yalç inkaya, B., Nghiem, T.-A. E., Jirsa, V., and Destexhe, A. (2021). A comprehensive neural simulation of slow-wave 1 sleep and highly responsive wakefulness dynamics 2. *bioRxiv*, 2021.08.31.458365. Available at: https://www.biorxiv.org/content/10.1101/2021.08.31.458365v1%0Ahttps://www.biorxiv.org/content/10.1101/2021.08.31.458365v1.abstract%0Ahttps://doi.org/10.1101/2021.08.31.458365.

Goldman, J. S., Kusch, L., Yalcinkaya, B. H., Depannemaecker, D., Nghiem, T.-A. E., Jirsa, V., et al. (2020). Brain-scale emergence of slow-wave synchrony and highly responsive asynchronous states based on biologically realistic population models simulated in The Virtual Brain. *bioRxiv*, 2020.12.28.424574. Available at: https://www.biorxiv.org/content/10.1101/2020.12.28.424574v1%0Ahttps://www.biorxiv.org/content/10.1101/2020.12.28.424574v1.abstract.

Goldman, J. S., Tort-Colet, N., di Volo, M., Susin, E., Bouté, J., Dali, M., et al. (2019). Bridging Single Neuron Dynamics to Global Brain States. *Front. Syst. Neurosci.* 13, 1–9. doi:10.3389/fnsys.2019.00075.

Grefkes, C., Ritzl, A., Zilles, K., and Fink, G. R. (2004). Human medial intraparietal cortex subserves visuomotor coordinate transformation. *Neuroimage* 23, 1494–1506. doi:10.1016/j.neuroimage.2004.08.031.

References

Grefkes, C., Weiss, P. H., Zilles, K., and Fink, G. R. (2002). Crossmodal processing of object features in human anterior intraparietal cortex: an fMRI study implies equivalencies between humans and monkeys. *Neuron* 35, 173–184. doi:10.1016/s0896-6273(02)00741-9.

Greif, A. (2010). A Primer in Game Theory. *Institutions Path to Mod. Econ.*, 407–420. doi:10.1017/cbo9780511791307.017.

Hahn, G., Skeide, M. A., Mantini, D., Ganzetti, M., Destexhe, A., Friederici, A. D., et al. (2019). A new computational approach to estimate whole-brain effective connectivity from functional and structural MRI, applied to language development. *Sci Rep* 9, 1–13. doi:10.1038/s41598-019-44909-6.

Havlicek, M., Roebroeck, A., Friston, K. J., Gardumi, A., Ivanov, D., and Uludag, K. (2017). On the importance of modeling fMRI transients when estimating effective connectivity: A dynamic causal modeling study using ASL data. *Neuroimage* 155, 217–233. doi:10.1016/j.neuroimage.2017.03.017.

Herculano-Houzel, S. (2009). The human brain in numbers: A linearly scaled-up primate brain. *Front. Hum. Neurosci.* 3, 1–11. doi:10.3389/neuro.09.031.2009.

Herculano-Houzel, S. (2010). Coordinated scaling of cortical and cerebellar numbers of neurons. *Front. Neuroanat.* 4, 1–8. doi:10.3389/fnana.2010.00012.

Herzfeld, D. J., Kojima, Y., Soetedjo, R., and Shadmehr, R. (2015). Encoding of action by the Purkinje cells of the cerebellum. *Nature* 526, 439–442. doi:10.1038/nature15693.

Hines, M. L., and Carnevale, N. T. (1997). The NEURON simulation environment. *Neural Comput.* 9, 1179–1209. doi:10.1162/neco.1997.9.6.1179.

Hisatsune, C., Miyamoto, H., Hirono, M., Yamaguchi, N., Sugawara, T., Ogawa, N., et al. (2013). IP3R1 deficiency in the cerebellum/brainstem causes basal ganglia-independent dystonia by triggering tonic Purkinje cell firings in mice. *Front. Neural Circuits* 7, 1–13. doi:10.3389/fncir.2013.00156.

Hodgkin, A. L., and Huxley, A. F. (1952). A quantitative description of membrane current and its application to conduction and excitation in nerve. *J. Physiol.* 117, 500–544.

Houssaini, K. El, Bernard, C., and Jirsa, V. K. (2020). The epileptor model: A systematic mathematical analysis linked to the dynamics of seizures, refractory status epilepticus, and depolarization block. *eNeuro* 7. doi:10.1523/ENEURO.0485-18.2019.

Huang, C. H., and Lin, C. C. K. (2021). A novel density-based neural mass model for simulating neuronal network dynamics with conductance-based synapses and membrane current adaptation. *Neural Networks* 143, 183–197. doi:10.1016/j.neunet.2021.06.009.

Ito, M. B. T.-R. M. in B. S. (2014). "Cerebellar Microcircuitry☆," in (Elsevier). doi:https://doi.org/10.1016/B978-0-12-801238-3.04544-X.

Jansen, B. H., and Rit, V. G. (1995). Electroencephalogram and visual evoked potential generation in a mathematical model of coupled cortical columns. *Biol. Cybern.* 73, 357–366. doi:10.1007/BF00199471.

Jirenhed, D. A., and Hesslow, G. (2011). Time course of classically conditioned purkinje cell response is determined by initial part of conditioned stimulus. *J. Neurosci.* 31, 9070–9074. doi:10.1523/JNEUROSCI.1653-11.2011.

Jirsa, V. K., Proix, T., Perdikis, D., Woodman, M. M., Wang, H., Bernard, C., et al. (2017). The Virtual Epileptic Patient: Individualized whole-brain models of epilepsy spread. *Neuroimage* 145, 377–388. doi:10.1016/j.neuroimage.2016.04.049.

Jordan, J., Mørk, H., Vennemo, S. B., Terhorst, D., Peyser, A., Ippen, T., et al. (2019). NEST 2.18.0. doi:10.5281/ZENODO.2605422.

Kadanoff, L. P. (2009). More is the Same; Phase Transitions and Mean Field Theories. *J. Stat. Phys.* 137, 777. doi:10.1007/s10955-009-9814-1.

Kandel, E. R., Schwartz, J. H., Jessel, T. M., Siegelbaum, S. A., Hudspeth, A. J., and Mack, S. (2013). *Principle on neural science.* , ed. McGraw-Hill New York, NY: Education LLC.

Kapalka, G. M. (2010). "Chapter 3 - Pharmacodynamics," in *Practical Resources for the Mental Health Professional*, ed. G. M. B. T.-N. and H. T. for C. and A. Kapalka (San Diego: Academic Press), 47–70. doi:https://doi.org/10.1016/B978-0-12-374927-7.00003-0.

Kelly, E., Meng, F., Fujita, H., Morgado, F., Kazemi, Y., Rice, L. C., et al. (2020). Regulation of autism-relevant behaviors by cerebellar-prefrontal cortical circuits. *Nat. Neurosci.* 23, 1102–1110. doi:10.1038/s41593-020-0665-z.

Kelly, R. M., and Strick, P. L. (2003). Cerebellar loops with motor cortex and prefrontal cortex of a nonhuman primate. *J. Neurosci. Off. J. Soc. Neurosci.* 23, 8432–8444. doi:10.1523/JNEUROSCI.23-23-08432.2003.

Kim, J.-A., Sekerková, G., Mugnaini, E., and Martina, M. (2012). Electrophysiological, morphological, and topological properties of two histochemically distinct subpopulations of cerebellar unipolar brush cells. *Cerebellum* 11, 1012–1025. doi:10.1007/s12311-012-0380-8.

Kim, J., and Augustine, G. J. (2021). Molecular Layer Interneurons: Key Elements of Cerebellar Network Computation and Behavior. *Neuroscience* 462, 22–35. doi:https://doi.org/10.1016/j.neuroscience.2020.10.008.

Klein, A. P., Ulmer, J. L., Quinet, S. A., Mathews, V., and Mark, L. P. (2016). Nonmotor Functions of the Cerebellum: An Introduction. *AJNR. Am. J. Neuroradiol.* 37, 1005–1009. doi:10.3174/ajnr.a4720.

Knight, J. C., Komissarov, A., and Nowotny, T. (2021). PyGeNN: a Python library for GPU-enhanced neural networks. *Front. Neuroinform.* 15, 659005.

Krienen, F. M., and Buckner, R. L. (2009). Segregated fronto-cerebellar circuits revealed by intrinsic functional connectivity. *Cereb. Cortex* 19, 2485–2497. doi:10.1093/cercor/bhp135.

Kuhn, A., Aertsen, A., and Rotter, S. (2004). Neuronal Integration of Synaptic Input in the Fluctuation-Driven Regime. *J. Neurosci.* 24, 2345–2356. doi:10.1523/JNEUROSCI.3349-03.2004.

Kumar, A., Schrader, S., Aertsen, A., and Rotter, S. (2008). The High-Conductance State of Cortical Networks. *Neural Comput.* 20, 1–43. doi:10.1162/neco.2008.20.1.1.

Kumbhar, P., Hines, M., Fouriaux, J., Ovcharenko, A., King, J., Delalondre, F., et al. (2019). CoreNEURON : An Optimized Compute Engine for the NEURON Simulator . *Front. Neuroinformatics* 13. Available at:

References

https://www.frontiersin.org/articles/10.3389/fninf.2019.00063.

Lachamp, P. M., Liu, Y., and Liu, S. J. (2009). Glutamatergic Modulation of Cerebellar Interneuron Activity Is Mediated by an Enhancement of GABA Release and Requires Protein Kinase A/RIM1α Signaling. *J. Neurosci.* 29, 381 LP – 392. doi:10.1523/JNEUROSCI.2354-08.2009.

Lackey, E. P., Heck, D. H., and Sillitoe, R. V (2018). Recent advances in understanding the mechanisms of cerebellar granule cell development and function and their contribution to behavior. *F1000Research* 7. doi:10.12688/f1000research.15021.1.

Lainé, J., and Axelrad, H. (1998). Lugaro cells target basket and stellate cells in the cerebellar cortex. *Neuroreport* 9, 2399–2403. doi:10.1097/00001756-199807130-00045.

LeDoux, M. S., and Lorden, J. F. (2002). Abnormal spontaneous and harmaline-stimulated Purkinje cell activity in the awake genetically dystonic rat. *Exp. brain Res.* 145, 457–467. doi:10.1007/s00221-002-1127-4.

Lee, W., Liu, S., Li, W., and Osher, S. (2022). *Mean field control problems for vaccine distribution*. Springer International Publishing doi:10.1007/s40687-022-00350-2.

Lee, W., Liu, S., Tembine, H., Li, W., and Osher, S. (2021). Controlling propagation of epidemics via mean-field control. *SIAM J. Appl. Math.* 81, 190–207. doi:10.1137/20M1342690.

Lennon, W., Hecht-Nielsen, R., and Yamazaki, T. (2014). A spiking network model of cerebellar Purkinje cells and molecular layer interneurons exhibiting irregular firing. *Front. Comput. Neurosci.* 8, 157. doi:10.3389/fncom.2014.00157.

Levenstein, D., Buzsáki, G., and Rinzel, J. (2019). NREM sleep in the rodent neocortex and hippocampus reflects excitable dynamics. *Nat. Commun.* 10, 1–12. doi:10.1038/s41467-019-10327-5.

Li, P., Gu, H., Xu, J., Zhang, Z., Li, F., Feng, M., et al. (2019). Purkinje cells of vestibulocerebellum play an important role in acute vestibular migraine. *J. Integr. Neurosci.* 18, 409–414. doi:10.31083/j.jin.2019.04.1168.

Luft, A. R., Manto, M.-U., and Oulad Ben Taib, N. (2005). Modulation of motor cortex excitability by sustained peripheral stimulation: The interaction between the motor cortex and the cerebellum. *The Cerebellum* 4, 90–96. doi:10.1080/14734220410019084.

Magkanaris, I., Mcdougal, R. A., Newton, A. J. H., Pereira, F., Alexandru, S., Carnevale, N. T., et al. (2022). M ODERNIZING THE NEURON S IMULATOR FOR.

Mahajan, A., Gupta, P., Jacobs, J., Marsili, L., Sturchio, A., Jinnah, H. A., et al. (2021). Impaired Saccade Adaptation in Tremor-Dominant Cervical Dystonia-Evidence for Maladaptive Cerebellum. *Cerebellum* 20, 678–686. doi:10.1007/s12311-020-01104-y.

Mapelli, J., and D'Angelo, E. (2007). The spatial organization of long-term synaptic plasticity at the input stage of cerebellum. *J. Neurosci.* 27, 1285–1296. doi:10.1523/JNEUROSCI.4873-06.2007.

Marchese, S. M., Palesi, F., Monteverdi, A., Bruzzone, M., Nigri, A., D'Arrigo, S., et al. (2021). Whole-brain dynamics in patients with cerebellar ataxia. in *Modelling the brain: Elementaty components to explain ensemble functions*, ed. Erice School Camillo Golgi (Erice: in press).

Marreiros, A. C., Kiebel, S. J., and Friston, K. J. (2008). Dynamic causal modelling for fMRI: A two-

state model. *Neuroimage* 39, 269–278. doi:10.1016/j.neuroimage.2007.08.019.

Marsden, J. F. (2018). Cerebellar ataxia. *Handb. Clin. Neurol.* 159, 261–281. doi:10.1016/B978-0-444-63916-5.00017-3.

Masoli, S., and D'Angelo, E. (2017). Synaptic activation of a detailed Purkinje cell model predicts voltage-dependent control of burst-pause responses in active dendrites. *Front. Cell. Neurosci.* 11, 1–18. doi:10.3389/fncel.2017.00278.

Masoli, S., Ottaviani, A., Casali, S., and D'Angelo, E. (2020a). Cerebellar Golgi cell models predict dendritic processing and mechanisms of synaptic plasticity. *PLoS Comput. Biol.* 16, e1007937. doi:10.1371/journal.pcbi.1007937.

Masoli, S., Rizza, M. F., Sgritta, M., Van Geit, W., Schürmann, F., and D'Angelo, E. (2017). Single Neuron Optimization as a Basis for Accurate Biophysical Modeling: The Case of Cerebellar Granule Cells . *Front. Cell. Neurosci.* 11. Available at: https://www.frontiersin.org/articles/10.3389/fncel.2017.00071.

Masoli, S., Solinas, S., and D'Angelo, E. (2015). Action potential processing in a detailed Purkinje cell model reveals a critical role for axonal compartmentalization. *Front. Cell. Neurosci.* 9, 47. doi:10.3389/fncel.2015.00047.

Masoli, S., Tognolina, M., Laforenza, U., Moccia, F., and D'Angelo, E. (2020b). Parameter tuning differentiates granule cell subtypes enriching transmission properties at the cerebellum input stage. *Commun. Biol.* 3, 222. doi:10.1038/s42003-020-0953-x.

McKay, B. E., and Turner, R. W. (2005). Physiological and morphological development of the rat cerebellar Purkinje cell. *J. Physiol.* 567, 829–850. doi:10.1113/jphysiol.2005.089383.

Mei, S., Misiakiewicz, T., and Montanari, A. (2019). Mean-field theory of two-layers neural networks: dimension-free bounds and kernel limit. Available at: http://arxiv.org/abs/1902.06015.

Mei, S., Montanari, A., and Nguyen, P.-M. (2018). A mean field view of the landscape of two-layer neural networks. *Proc. Natl. Acad. Sci.* 115, E7665–E7671. doi:10.1073/pnas.1806579115.

Meier, J. M., Perdikis, D., Blickensdörfer, A., Stefanovski, L., Liu, Q., Maith, O., et al. (2022). Virtual deep brain stimulation: Multiscale co-simulation of a spiking basal ganglia model and a whole-brain mean-field model with The Virtual Brain. *Exp. Neurol.* 354. doi:10.1016/j.expneurol.2022.114111.

Melik-Musyan, A. B., and Fanardzhyan, V. V (2004). Morphological Characteristics of Lugaro Cells in the Cerebellar Cortex. *Neurosci. Behav. Physiol.* 34, 633–638. doi:10.1023/B:NEAB.0000028297.30474.f9.

Mendonça, M. D., and Alves da Silva, J. (2021). A Cerebellar Wave for Paroxysmal Dyskinesia. *Mov. Disord.* 36, 2767. doi:10.1002/mds.28848.

Middleton, F. A., and Strick, P. L. (2001). Cerebellar projections to the prefrontal cortex of the primate. *J. Neurosci. Off. J. Soc. Neurosci.* 21, 700–712. doi:10.1523/JNEUROSCI.21-02-00700.2001.

Mittmann, W., and Häusser, M. (2007). Linking synaptic plasticity and spike output at excitatory and

inhibitory synapses onto cerebellar Purkinje cells. *J. Neurosci.* 27, 5559–5570. doi:10.1523/JNEUROSCI.5117-06.2007.

Molineux, M. L., McRory, J. E., McKay, B. E., Hamid, J., Mehaffey, W. H., Rehak, R., et al. (2006). Specific T-type calcium channel isoforms are associated with distinct burst phenotypes in deep cerebellar nuclear neurons. *Proc. Natl. Acad. Sci. U. S. A.* 103, 5555–5560. doi:10.1073/pnas.0601261103.

Montbrió, E., Pazó, D., and Roxin, A. (2015). Macroscopic description for networks of spiking neurons. *Phys. Rev. X* 5, 1–15. doi:10.1103/PhysRevX.5.021028.

Monteverdi, A., Palesi, F., Costa, A., Vitali, P., Pichiecchio, A., Ramusino, M. C., et al. (2022). Subject-specific features of excitation / inhibition profiles in neurodegenerative diseases. 1–17. doi:10.3389/fnagi.2022.868342.

Moran, R. J., Mallet, N., Litvak, V., Dolan, R. J., Magill, P. J., Friston, K. J., et al. (2011). Alterations in brain connectivity underlying beta oscillations in parkinsonism. *PLoS Comput. Biol.* 7. doi:10.1371/journal.pcbi.1002124.

Moran, R., Pinotsis, D. A., and Friston, K. (2013). Neural masses and fields in dynamic causal modelling. *Front. Comput. Neurosci.* 7, 1–12. doi:10.3389/fncom.2013.00057.

Morigaki, R., Miyamoto, R., Matsuda, T., Miyake, K., Yamamoto, N., and Takagi, Y. (2021). Dystonia and cerebellum: From bench to bedside. *Life* 11. doi:10.3390/life11080776.

Mugnaini, E., and Floris, A. (1994). The unipolar brush cell: A neglected neuron of the mammalian cerebellar cortex. *J. Comp. Neurol.* 339, 174–180. doi:https://doi.org/10.1002/cne.903390203.

Mugnaini, E., Sekerková, G., and Martina, M. (2011). The unipolar brush cell: A remarkable neuron finally receiving deserved attention. *Brain Res. Rev.* 66, 220–245. doi:https://doi.org/10.1016/j.brainresrev.2010.10.001.

Murta, T., Leal, A., Garrido, M. I., and Figueiredo, P. (2012). Dynamic Causal Modelling of epileptic seizure propagation pathways: A combined EEG-fMRI study. *Neuroimage* 62, 1634–1642. doi:10.1016/j.neuroimage.2012.05.053.

Naskar, A., Vattikonda, A., Deco, G., Roy, D., and Banerjee, A. (2021). Multiscale dynamic mean field (MDMF) model relates resting-state brain dynamics with local cortical excitatory-inhibitory neurotransmitter homeostasis. *Netw. Neurosci. (Cambridge, Mass.)* 5, 757–782. doi:10.1162/netn_a_00197.

Nordlie, E., Tetzlaff, T., and Einevoll, G. T. (2010). Rate dynamics of leaky integrate-and-fire neurons with strong synapses. *Front. Comput. Neurosci.* 4, 1–13. doi:10.3389/fncom.2010.00149.

Nourian, M., and Caines, P. E. (2013). Epsilon-Nash Mean Field Game Theory for Nonlinear Stochastic Dynamical Systems with Major and Minor Agents. *SIAM J. Control Optim.* 51, 3302–3331. doi:10.1137/120889496.

Olmez, S. Y., Aggarwal, S., Kim, J. W., Miehling, E., Başar, T., West, M., et al. (2022). Modeling Presymptomatic Spread in Epidemics via Mean-Field Games. in *2022 American Control Conference (ACC)*, 3648–3655. doi:10.23919/ACC53348.2022.9867547.

Palay, S. L., and Chan-Palay, V. (1974a). "Granule Cells," in *Cerebellar Cortex: Cytology and Organization*, eds. S. L. Palay and V. Chan-Palay (Berlin, Heidelberg: Springer Berlin

Heidelberg), 63–99. doi:10.1007/978-3-642-65581-4_3.

Palay, S. L., and Chan-Palay, V. (1974b). "The Basket Cell," in *Cerebellar Cortex: Cytology and Organization* (Berlin, Heidelberg: Springer Berlin Heidelberg), 180–215. doi:10.1007/978-3-642-65581-4_7.

Palay, S. L., and Chan-Palay, V. (1974c). "The Golgi Cells," in *Cerebellar Cortex: Cytology and Organization* (Berlin, Heidelberg: Springer Berlin Heidelberg), 100–132. doi:10.1007/978-3-642-65581-4_4.

Palay, S. L., and Chan-Palay, V. (1974d). "The Lugaro Cell," in *Cerebellar Cortex: Cytology and Organization*, eds. S. L. Palay and V. Chan-Palay (Berlin, Heidelberg: Springer Berlin Heidelberg), 133–141. doi:10.1007/978-3-642-65581-4_5.

Palay, S. L., and Chan-Palay, V. (1974e). "The Purkinje Cell," in *Cerebellar Cortex: Cytology and Organization*, eds. S. L. Palay and V. Chan-Palay (Berlin, Heidelberg: Springer Berlin Heidelberg), 11–62. doi:10.1007/978-3-642-65581-4_2.

Palay, S. L., and Chan-Palay, V. (1974f). "The Stellate Cell," in *Cerebellar Cortex: Cytology and Organization* (Berlin, Heidelberg: Springer Berlin Heidelberg), 216–233. doi:10.1007/978-3-642-65581-4_8.

Palesi, F., Lorenzi, R. M., Casellato, C., Ritter, P., Jirsa, V., Gandini Wheeler-Kingshott, C. A. M., et al. (2020). The Importance of Cerebellar Connectivity on Simulated Brain Dynamics. *Front. Cell. Neurosci.* 14, 1–11. doi:10.3389/fncel.2020.00240.

Palesi, F., Rinaldis, A. De, Castellazzi, G., Calamante, F., Chard, D., Tournier, J. D., et al. (2017). Contralateral cortico-ponto- cerebellar pathways reconstruction in humans in vivo : implications for reciprocal cerebro-cerebellar structural connectivity in motor and non-motor areas. 1–13. doi:10.1038/s41598-017-13079-8.

Palesi, F., Tournier, J.-D., Calamante, F., Muhlert, N., Castellazzi, G., Chard, D., et al. (2015). Contralateral cerebello-thalamo-cortical pathways with prominent involvement of associative areas in humans in vivo. *Brain Struct. Funct.* 220, 3369–3384. doi:10.1007/s00429-014-0861-2.

Parr, T., Sajid, N., and Friston, K. J. (2020). Modules or mean-fields? *Entropy* 22, 1–25. doi:10.3390/E22050552.

Pedroso, J. L., Vale, T. C., Braga-Neto, P., Dutra, L. A., França, M. C. J., Teive, H. A. G., et al. (2019). Acute cerebellar ataxia: differential diagnosis and clinical approach. *Arq. Neuropsiquiatr.* 77, 184–193. doi:10.1590/0004-282X20190020.

Peterson, A. D., Mareels, I. M., Meffin, H., Grayden, D. B., Cook, M. J., and Burkitt, A. N. (2015). The neurodynamics of epilepsy: a homotopy analysis between current-based and conductance-based synapses in a neural field model of epilepsy. *BMC Neurosci.* 16. doi:10.1186/1471-2202-16-s1-p23.

Peterson, C., and Hartman, E. (1989). Explorations of the mean field theory learning algorithm. *Neural Networks* 2, 475–494. doi:https://doi.org/10.1016/0893-6080(89)90045-2.

Petrakova, V., and Krivorotko, O. (2022). Mean field game for modeling of COVID-19 spread. *J. Math. Anal. Appl.* 514, 126271. doi:10.1016/j.jmaa.2022.126271.

References

Petrosjan, L. A., and Zenkevich, N. A. (1996). *Game Theory*. World Scientific Publishing Co. Pte. Ltd.

Pettersen, K. H., Lindén, H., Tetzlaff, T., and Einevoll, G. T. (2011). The ball and stick neuron model accounts both for microscopic and macroscopic power laws. *BMC Neurosci.* 12, P91. doi:10.1186/1471-2202-12-s1-p91.

Pinotsis, D. A., Moran, R. J., and Friston, K. J. (2012). Dynamic causal modeling with neural fields. *Neuroimage* 59, 1261–1274. doi:10.1016/j.neuroimage.2011.08.020.

Pizoli, C. E., Jinnah, H. A., Billingsley, M. L., and Hess, E. J. (2002). Abnormal cerebellar signaling induces dystonia in mice. *J. Neurosci.* 22, 7825–7833. doi:10.1523/jneurosci.22-17-07825.2002.

Pizzarotti, B., Palesi, F., Vitali, P., Castellazzi, G., Anzalone, N., Alvisi, E., et al. (2020). Frontal and Cerebellar Atrophy Supports FTSD-ALS Clinical Continuum. *Front. Aging Neurosci.* 12, 593526. doi:10.3389/fnagi.2020.593526.

Plesser, H. E., Diesmann, M., Gewaltig, M.-O., and Morrison, A. (2015). "NEST: the Neural Simulation Tool BT - Encyclopedia of Computational Neuroscience," in, eds. D. Jaeger and R. Jung (New York, NY: Springer New York), 1849–1852. doi:10.1007/978-1-4614-6675-8_258.

Pochon, J. B., Levy, R., Poline, J. B., Crozier, S., Lehéricy, S., Pillon, B., et al. (2001). The role of dorsolateral prefrontal cortex in the preparation of forthcoming actions: an fMRI study. *Cereb. Cortex* 11, 260–266. doi:10.1093/cercor/11.3.260.

Popa, D., Spolidoro, M., Proville, R. D., Guyon, N., Belliveau, L., and Léna, C. (2013). Functional role of the cerebellum in gamma-band synchronization of the sensory and motor cortices. *J. Neurosci.* 33, 6552–6556. doi:10.1523/JNEUROSCI.5521-12.2013.

Prando, G., Zorzi, M., Bertoldo, A., Corbetta, M., Zorzi, M., and Chiuso, A. (2020). Sparse DCM for whole-brain effective connectivity from resting-state fMRI data. *Neuroimage* 208, 116367. doi:10.1016/j.neuroimage.2019.116367.

Prestori, F., Bonardi, C., Mapelli, L., Lombardo, P., Goselink, R., De Stefano, M. E., et al. (2013). Gating of Long-Term Potentiation by Nicotinic Acetylcholine Receptors at the Cerebellum Input Stage. *PLoS One* 8. doi:10.1371/journal.pone.0064828.

Prestori, F., Mapelli, L., and Angelo, E. D. (2019). Diverse Neuron Properties and Complex Network Dynamics in the Cerebellar Cortical Inhibitory Circuit. 12, 1–23. doi:10.3389/fnmol.2019.00267.

Prestori, F., and Person, A. L. (2013). The cerebellar Golgi cell and spatiotemporal organization of granular layer activity. 7, 1–21. doi:10.3389/fncir.2013.00093.

Prevosto, V., Graf, W., and Ugolini, G. (2010). Cerebellar inputs to intraparietal cortex areas LIP and MIP: functional frameworks for adaptive control of eye movements, reaching, and arm/eye/head movement coordination. *Cereb. Cortex* 20, 214–228. doi:10.1093/cercor/bhp091.

Ramnani, N., Behrens, T. E. J., Johansen-Berg, H., Richter, M. C., Pinsk, M. A., Andersson, J. L. R., et al. (2006). The evolution of prefrontal inputs to the cortico-pontine system: diffusion imaging evidence from Macaque monkeys and humans. *Cereb. Cortex* 16, 811–818. doi:10.1093/cercor/bhj024.

Rizza, M. F., Locatelli, F., Masoli, S., Sánchez-Ponce, D., Muñoz, A., Prestori, F., et al. (2021).

Stellate cell computational modeling predicts signal filtering in the molecular layer circuit of cerebellum. *Sci. Rep.* 11, 1–18. doi:10.1038/s41598-021-83209-w.

Rogers, T. D., Dickson, P. E., Heck, D. H., Goldowitz, D., Mittleman, G., and Blaha, C. D. (2011). Connecting the dots of the cerebro-cerebellar role in cognitive function: Neuronal pathways for cerebellar modulation of dopamine release in the prefrontal cortex. *Synapse* 65, 1204–1212. doi:https://doi.org/10.1002/syn.20960.

Roostaei, T., Nazeri, A., Sahraian, M. A., and Minagar, A. (2014). The human cerebellum: A review of physiologic neuroanatomy. *Neurol. Clin.* 32, 859–869. doi:10.1016/j.ncl.2014.07.013.

Rosenthal, L. S. (2022). Neurodegenerative Cerebellar Ataxia. *Continuum (Minneap. Minn).* 28, 1409–1434. doi:10.1212/CON.0000000000001180.

Roth, A., and van Rossum, M. C. W. (2013). Modeling Synapses. *Comput. Model. Methods Neurosci.*, 139–160. doi:10.7551/mitpress/9780262013277.003.0007.

Rothkirch, I., Granert, O., Knutzen, A., Wolff, S., Gövert, F., Pedersen, A., et al. (2018). Dynamic causal modeling revealed dysfunctional effective connectivity in both, the cortico-basal-ganglia and the cerebello-cortical motor network in writers' cramp. *NeuroImage Clin.* 18, 149–159. doi:10.1016/j.nicl.2018.01.015.

Rouiller, E. M., Liang, F., Babalian, A., Moret, V., and Wiesendanger, M. (1994). Cerebellothalamocortical and pallidothalamocortical projections to the primary and supplementary motor cortical areas: a multiple tracing study in macaque monkeys. *J. Comp. Neurol.* 345, 185–213. doi:10.1002/cne.903450204.

Ruffini, G., and Deco, G. (2021). The 2D Ising model , criticality and AIT.

Sadeghi, S., Mier, D., Gerchen, M. F., Schmidt, S. N. L., and Hass, J. (2020). Dynamic Causal Modeling for fMRI With Wilson-Cowan-Based Neuronal Equations. *Front. Neurosci.* 14. doi:10.3389/fnins.2020.593867.

Saggar, M., Zanesco, A. P., King, B. G., Bridwell, D. A., MacLean, K. A., Aichele, S. R., et al. (2015). Mean-field thalamocortical modeling of longitudinal EEG acquired during intensive meditation training. *Neuroimage* 114, 88–104. doi:10.1016/j.neuroimage.2015.03.073.

Sanz-Leon, P., Knock, S. A., Spiegler, A., and Jirsa, V. K. (2015). Mathematical framework for large-scale brain network modeling in The Virtual Brain. *Neuroimage* 111, 385–430. doi:10.1016/j.neuroimage.2015.01.002.

Sanz Leon, P., Knock, S. A., Woodman, M. M., Domide, L., Mersmann, J., Mcintosh, A. R., et al. (2013). The virtual brain: A simulator of primate brain network dynamics. *Front. Neuroinform.* 7. doi:10.3389/fninf.2013.00010.

Schaub, M. T., and Schultz, S. R. (2012). The Ising decoder: Reading out the activity of large neural ensembles. *J. Comput. Neurosci.* 32, 101–118. doi:10.1007/s10827-011-0342-z.

Schirner, M., Rothmeier, S., Jirsa, V. K., McIntosh, A. R., and Ritter, P. (2015). An automated pipeline for constructing personalized virtual brains from multimodal neuroimaging data. *Neuroimage* 117, 343–357. doi:10.1016/j.neuroimage.2015.03.055.

Schreck, L., Ryan, S., and Monaghan, P. (2018). Cerebellum and cognition in multiple sclerosis. *J.*

References

Neurophysiol. 120, 2707–2709. doi:10.1152/jn.00245.2018.

Schutter, D. J. L. G., and van Honk, J. (2006). An electrophysiological link between the cerebellum, cognition and emotion: Frontal theta EEG activity to single-pulse cerebellar TMS. *Neuroimage* 33, 1227–1231. doi:https://doi.org/10.1016/j.neuroimage.2006.06.055.

Serences, J. T. (2008). Value-based modulations in human visual cortex. *Neuron* 60, 1169–1181. doi:10.1016/j.neuron.2008.10.051.

Shen, B., Pan, Y., Jiang, X., Wu, Z., Zhu, J., Dong, J., et al. (2020). Altered putamen and cerebellum connectivity among different subtypes of Parkinson's disease. *CNS Neurosci. Ther.* 26, 207–214. doi:10.1111/cns.13259.

Simões de Souza, F. M., and De Schutter, E. (2011). Robustness effect of gap junctions between Golgi cells on cerebellar cortex oscillations. *Neural Syst. Circuits* 1, 7. doi:10.1186/2042-1001-1-7.

Solinas, S., Forti, L., Cesana, E., Mapelli, J., De Schutter, E., and D'Angelo, E. (2007). Computational reconstruction of pacemaking and intrinsic electroresponsiveness in cerebellar Golgi cells. *Front. Cell. Neurosci.* 1, 2. doi:10.3389/neuro.03.002.2007.

Solinas, S., Nieus, T., Angelo, E. D., and Bower, J. M. (2010). A realistic large-scale model of the cerebellum granular layer predicts circuit spatio-temporal fi ltering properties. 4, 1–17. doi:10.3389/fncel.2010.00012.

Spreemann, G., Dunn, B., Botnan, M. B., and Baas, N. A. (2018). Using persistent homology to reveal hidden covariates in systems governed by the kinetic Ising model. *Phys. Rev. E* 97, 32313. doi:10.1103/PhysRevE.97.032313.

Stimberg, M., Brette, R., and Goodman, D. F. M. (2019). Brian 2, an intuitive and efficient neural simulator. *Elife* 8, 1–41. doi:10.7554/eLife.47314.

Stoodley, C. J. (2012). The cerebellum and cognition: evidence from functional imaging studies. *Cerebellum* 11, 352–365. doi:10.1007/s12311-011-0260-7.

Szoboszlay, M., Lőrincz, A., Lanore, F., Vervaeke, K., Silver, R. A., and Nusser, Z. (2016). Functional Properties of Dendritic Gap Junctions in Cerebellar Golgi Cells. *Neuron* 90, 1043–1056. doi:10.1016/j.neuron.2016.03.029.

Tembine, H. (2020). Covid-19: Data-driven mean-field-type game perspective. *Games* 11, 1–107. doi:10.3390/g11040051.

ten Brinke, M. M., Boele, H. J., Spanke, J. K., Potters, J. W., Kornysheva, K., Wulff, P., et al. (2015). Evolving Models of Pavlovian Conditioning: Cerebellar Cortical Dynamics in Awake Behaving Mice. *Cell Rep.* 13, 1977–1988. doi:10.1016/j.celrep.2015.10.057.

Tkacik, G., Schneidman, E., Berry, M. J., and Bialek, W. (2006). Ising models for networks of real neurons. Available at: http://arxiv.org/abs/q-bio/0611072.

Tornes, L., Conway, B., and Sheremata, W. (2014). Multiple sclerosis and the cerebellum. *Neurol. Clin.* 32, 957–977. doi:10.1016/j.ncl.2014.08.001.

Tunik, E., Frey, S. H., and Grafton, S. T. (2005). Virtual lesions of the anterior intraparietal area disrupt goal-dependent on-line adjustments of grasp. *Nat. Neurosci.* 8, 505–511. doi:10.1038/nn1430.

Tzvi, E., Gajiyeva, L., Bindel, L., Hartwigsen, G., and Classen, J. (2022). Coherent theta oscillations in the cerebellum and supplementary motor area mediate visuomotor adaptation. *Neuroimage* 251, 118985. doi:10.1016/j.neuroimage.2022.118985.

van Albada, S. J., and Robinson, P. A. (2009). Mean-field modeling of the basal ganglia-thalamocortical system. I. Firing rates in healthy and parkinsonian states. *J. Theor. Biol.* 257, 642–663. doi:10.1016/j.jtbi.2008.12.018.

Van Overwalle, F., Van de Steen, F., van Dun, K., and Heleven, E. (2020). Connectivity between the cerebrum and cerebellum during social and non-social sequencing using dynamic causal modelling. *Neuroimage* 206, 116326. doi:10.1016/j.neuroimage.2019.116326.

van Wijk, B. C. M., Cagnan, H., Litvak, V., Kühn, A. A., and Friston, K. J. (2018). Generic dynamic causal modelling: An illustrative application to Parkinson's disease. *Neuroimage* 181, 818–830. doi:10.1016/j.neuroimage.2018.08.039.

Washburn, S. G., Fremont, R., Moreno, M. C., Angueyra, C., and Khodakhah, K. (2019). Acute cerebellar knockdown of sgce reproduces salient features of myoclonus-dystonia (DYT11) in mice. *Elife* 8, 1–21. doi:10.7554/eLife.52101.

Watson, T., Jones, M., and Apps, R. (2009). Electrophysiological mapping of novel prefrontal - cerebellar pathways . *Front. Integr. Neurosci.* 3. Available at: https://www.frontiersin.org/articles/10.3389/neuro.07.018.2009.

Wilson, H. R., and Cowan, J. D. (1972). Excitatory and Inhibitory Interactions in Localized Populations of Model Neurons. *Biophys. J.* 12, 1–24. doi:https://doi.org/10.1016/S0006-3495(72)86068-5.

Wojtowytsch, S., and E, W. (2021). Can Shallow Neural Networks Beat the Curse of Dimensionality? A Mean Field Training Perspective. *IEEE Trans. Artif. Intell.* 1, 121–129. doi:10.1109/tai.2021.3051357.

Wong, K. F., and Wang, X. J. (2006). A recurrent network mechanism of time integration in perceptual decisions. *J. Neurosci.* 26, 1314–1328. doi:10.1523/JNEUROSCI.3733-05.2006.

Wu, T., and Hallett, M. (2013). The cerebellum in Parkinson's disease. *Brain* 136, 696–709. doi:10.1093/brain/aws360.

Wulff, P., Schonewille, M., Renzi, M., Viltono, L., Sassoè-Pognetto, M., Badura, A., et al. (2009). Synaptic inhibition of Purkinje cells mediates consolidation of vestibulo-cerebellar motor learning. *Nat. Neurosci.* 12, 1042–1049. doi:10.1038/nn.2348.

Yamazaki, T., and Igarashi, J. (2013). Realtime cerebellum: a large-scale spiking network model of the cerebellum that runs in realtime using a graphics processing unit. *Neural networks Off. J. Int. Neural Netw. Soc.* 47, 103–111. doi:10.1016/j.neunet.2013.01.019.

Yavuz, E., Turner, J., and Nowotny, T. (2016). GeNN: a code generation framework for accelerated brain simulations. *Sci. Rep.* 6, 1–14.

Zerlaut, Y., Chemla, S., Chavane, F., and Destexhe, A. (2018). Modeling mesoscopic cortical dynamics using a mean-field model of conductance-based networks of adaptive exponential integrate-and-fire neurons. *J. Comput. Neurosci.* 44, 45–61. doi:10.1007/s10827-017-0668-2.

References

Zerlaut, Y., Teleńczuk, B., Deleuze, C., Bal, T., Ouanounou, G., and Destexhe, A. (2016). Heterogeneous firing rate response of mouse layer V pyramidal neurons in the fluctuation-driven regime. *J. Physiol.* 594, 3791–3808. doi:10.1113/JP272317.

Zhou, W., Liu, Z., Li, J., Xu, X., and Shen, L. (2021). Multi-target tracking for unmanned aerial vehicle swarms using deep reinforcement learning. *Neurocomputing* 466, 285–297. doi:10.1016/j.neucom.2021.09.044.

Zimmermann, J., Perry, A., Breakspear, M., Schirner, M., Sachdev, P., Wen, W., et al. (2018). Differentiation of Alzheimer's disease based on local and global parameters in personalized Virtual Brain models. *NeuroImage Clin.* 19, 240–251. doi:10.1016/j.nicl.2018.04.017.